

RESEARCH INSTITUTE FOR HIGH ENERGY PHYSICS

REPORT SERIES

HU - SEFT - 1991 - 09

Energy Measurement in Collider Experiments and the Search for Scalar Quarks in Z^0 Decays at LEP I

Reino Keränen

ISSN 0788-3587

UNIVERSITY OF HELSINKI
RESEARCH INSTITUTE FOR HIGH ENERGY PHYSICS
SILTAVUORENPENGER 20 C • SF - 00170 HELSINKI • FINLAND

Helsinki 1991
Yliopistopaino

Energy Measurement in Collider Experiments and the Search for Scalar Quarks in Z^0 Decays at LEP I

Reino Keränen

Research Institute for High Energy Physics
University of Helsinki
Helsinki, Finland

Dissertation for the degree of Doctor of Technology to be presented with due permission for public examination and debate in Auditorium F1 at Helsinki University of Technology (Espoo, Finland) on the 20th of September, 1991, at 12 o'clock noon.

Contents

ESIPUHE	iii
PREFACE	v
SUMMARY	1
1 INTRODUCTION	6
1.1 Theoretical basis	6
1.2 LEP physics goals	7
1.3 LEP, the Large Electron Positron Storage Ring	11
1.4 DELPHI, the Detector with Lepton, Photon and Hadron Identification	16
1.4.1 General Purpose Detector Systems	16
1.4.2 The DELPHI detector	18
2 ENERGY MEASUREMENT IN COLLIDER EXPERIMENTS	25
2.1 Review of the results of the combined beam test of the DEL- PHI Hadron Calorimeter, Forward Electromagnetic Calorime- ter and Barrel Muon Chambers	28
2.2 A software point of view	30
2.3 A first look on the combined reconstruction of real data in a general purpose detector	31
3 THE SEARCH FOR SCALAR QUARKS IN Z^0 DECAYS	32
3.1 Strongly interacting supersymmetric particles	32
3.2 Introduction to the squark search in Z^0 decays	38
3.3 The massive LSP as a kinematical effect on the missing energy signature	40
3.3.1 Acollinearity and missing transverse momentum . . .	41
3.3.2 Visible energy and acollinearity in decays of pairly produced heavy particles into massive invisible particles	43
3.3.3 Discussion	46
3.4 Comments on the executed search	48
3.4.1 Expected signature, model dependencies and the cor- respondence to the selected candidates	48
3.4.2 Evaluation of the trigger efficiency	53
3.4.3 Time dependent effects and the run selection	54

4 CONCLUSIONS	56
References	58

List of Figures

1	Elementary structure of matter and the gauge bosons.	8
2	The LEP collider and CERN accelerator complex	12
3	Example of a beam gas or wall interaction, recorded in the DELPHI detector.	15
4	The DELPHI detector.	19
5	Squark and gluino mass limits deduced by the UA2 experiment	34
6	Kinematics of the two body decays of massive particles produced in pairs in e^+e^- annihilation.	44
7	Distributions of the visible energy in two body decays of scalar quarks.	45
8	Distributions of the acollinearity in decays of scalar quarks. .	47
9	Example event in the selected squark candidate sample. . . .	51
10	Comparison of the real candidate events and expectations. . .	52
11	The efficiency of the DELPHI barrel track trigger as a function of the acollinearity	55

List of Tables

1	Combination of the trigger and selection efficiencies in the search for squarks and massive LSPs.	49
2	Coupling constants for the squark pair production and expected rates at the Z^0 peak	50

ESIPUHE

*Ihmiset uskovat sen minkä näkevät,
erityisesti suomalainen ei usko,
ennenkuin näkee.*

(mukaeltu suomalaisesta sananlas-
kusta)

Tähän väitöskirjaan liittyvä työ tehtiin Helsingin yliopiston Suurenergiafysiikan laitoksella sekä DELPHI-kokeessa, joka on toiminnassa LEP-törmäyttimellä CERNissä (Euroopan Hiukkastutkimuskeskus, Geneve).

Kokeellinen tutkimustyö suurenergiafysiikan alalla on johtanut laajoihin kansainvälisiin tutkimusryhmiin. Niiden organisaatioiden, laitteiden ja voimavarojen mittakaavat ovat nähtävissä neljässä hiukkaskokeessa, joita parhaillaan suoritetaan LEP-törmäyttimellä. Organisaatioina ne luovat maailmanlaajuisia yhteistyötä suurenergiafysiikan alan instituutioiden välille. Rakennetut laitteet edustavat modernin luonnontieteen edistyneintä instrumentointia.

Hiukkaskokeiden sadat fyysikot, erikoistuneet insinöörit ja teknikot luovat usein äärimmilleen motivoituneen ilmapiirin. Syntyy lukemattomia inhimillisiä kontakteja, joiden kautta jokaisen yksilön panostus välittömästi arvioidaan ja sovitetaan yhteiseen projektiin. Kyseessä on prosessi, joka tarjoaa inspiraation ja tieteellisen tyydytyksen hyvinkin erilaisia fysiikan osa-alueita korostaville lähestymistavoille. Erityisesti se tarjoaa opiskelijoille mahdollisuuden omaksua monipuolista asiantuntemusta useilta kokeellisen fysiikan osa-alueilta.

Olen syvästi kiitollinen dos. Risto Oravalle tilaisuudesta osallistua tähän prosessiin, johon hän johdatti meidät LEP-fysiikan ja -kokeiden puitteissa tavalla, joka samalla avasi ovet suomalaisen hiukkasfysiikan kokeelliselle tutkimukselle täysivaltaiseksi kansainvälisen tiedeyhteistyön osapuoleksi. Olen pysyvästi hämmästynyt hänen luovasta mielikuvituksestaan ja poikkitieteellisestä asiantuntemuksestaan toteuttaa suunnitelmia, jotka työllistävät yhä kasvavan joukon innostuneita työtovereita. Kiitän mahdollisuudesta omistautua kokopäivätoimisesti tutkimukselle. Arvostan suuresti hänen suo- maansa vapautta suunnata tutkimuskohteensa oman riskivastuun kantaen. Oli monta mahdollisuutta, ja meitä pyydettiin katsomaan niitä tarkasti. Uskon, että teimme niin.

Olen mieluisaa kiittää kaikkia kollegojani ja ystäviäni DELPHI-kollaboraatiossa jatkuvasta avusta, jota ilman työni ei olisi voinut edistyä, sekä kuluneista vuosista monimuotoisen yhteistyön merkeissä, joiden aikana

opin tuntemaan heidät ammattilaisina, fyysikoina ja ihmisinä; lähimpinä mielessäni Jean-Eudes Augustin, Yuri Belokopytov, Petros Beltran, Paolo Checchia, Jon Guy, Frank Harris, Ingo Herbst, Heiner Herr, Hans Jürgen Hilke, Per Olof Hulth, Michel Jonker, Stavros Katsanevas, Elias Katsoufis, Barry King, Nils Joerg Kjaer, Hans Klein, Bernd Korzen, Pierre Lutz, Rasmus Møller, Klaus Mönig, Vladimir Obraztsov, Teodora Papadopoulou, Maria Elena Pol, Alphonso Rademakers, Francois Richard, Ron Shellard, Tzanko Spasoff, Nick van Eijndhoven, Pedro Vaz, Wilbur Venus, Marc Winter, Guy Wormser ja Marco Zito, unohtamatta lukuisia muita käytävillä ja kontrollihuoneissa.

Erityisesti ilmaisen kunnioitukseni DELPHIn puhemies prof. Ugo Amalidia kohtaan, joka kiireisen LEP-koeohjelman keskellä kiinnitti huomionsa yksittäiseen analyysityöhön, josta sittemmin muodostui laaja osa tätä väitöskirjaa, tunnisti sen tieteellisen merkittävyyden ja arvioi suoritettua analyysin ja kannusti suorittamaan työni loppuun. Kiitän häntä hyödyllisistä huomioista ja neuvoista.

Samoin haluan ilmaista erityiset kiitokset tiiviistä yhteistyöstä, kotoisen inspiroivasta ja jännittävästä hengestä Helsingin DELPHI-ryhmälle ja kehitysprojekteille (Mika, Richard, Paula, Jounit, Kalevi, Iiro, Panu, Jorma, Mikot, Kirsti, Kari, Rauno, Petri, Marek, Jukka, Markus, Antti, Jari, Markku, Wolfram, Camilla, Heimo, Sandor, Tuomo, Tuure, Martti, Raimo ja Kenneth), joista on kasvanut kymmenien lahjakkaiden tutkijoiden tuotetias yhteisö. Kiitän myös Helsingin yliopiston Suurenergiafysiikanlaitosta ja Suurenergiafysiikan tutkimuslaitosta perinteikkäästä tiedeilmapiiiristä.

Esitän lämpimimmät kiitokseni prof. Eero Bycklingille Teknillisessä korkeakoulussa pitkäaikaisesta tuesta ja opintojeni ohjauksesta.

Kiitän Donald Smartia kieliasun perusteellisesta tarkastamisesta, sekä Anneli Varankaa ja Veikko Sinkkosta korvaamattomasta avusta kuvamateriaalin piirtämisessä.

Suomen Akatemian, Opetusministeriön ja Helsingin yliopiston merkittävä taloudellinen tuki ansaitsee kiitokseni.

Omistan tämän työn

vanhemmilleni, elämästäni;

opettajilleni, kaikesta mitä olen oppinut ja

Marille, ”*ajasta, jonka vietimme yhdessä*”.

Helsingissä, 4. elokuuta 1991.

Reino Keränen

PREFACE

*People believe in what they see,
particularly the Finnish do not
believe before they see.*

(adapted from Finnish folklore)

The work for this thesis was carried out at the Research Institute for High Energy Physics, University of Helsinki, and in the DELPHI experiment which is in operation at the LEP collider at CERN, European Laboratory for Particle Research, Geneva.

The experimental research in modern high energy physics has developed to large international collaborations. The scale of the organization, equipment, and resources in these projects are apparent in the four experiments at the LEP collider. As organizations they establish links between institutions in high energy physics globally. The devices constructed represent the most advanced instrumentation in modern science.

The hundreds of collaborating physicists, the dedicated engineers and technicians in the experiments often create an exhaustively motivated atmosphere. Numerous human contacts are established through which the individual contributions are immediately evaluated and adapted to the common project. It is a process of inspiration and scientific satisfaction for physicists emphasizing the many diversified aspects of physics. It particularly provides students with a unique opportunity to gain versatile expertise in the various branches of experimental physics.

I am deeply grateful to doc. Risto Orava for the opportunity to participate in this process, through his introduction to the LEP physics and experiments - in a manner which at the same time paved the Finnish way to the full participation in the international co-operation in high energy physics. I am permanently amazed of his creative imagination and cross-disciplinary knowledge in realizing the visions which occupy ever increasing group of excited colleagues. I wish to thank him for the opportunity to devote myself to the full time research. I am very appreciative the freedom he allows to choose research topics at own risk. Many events were possible, and we were asked to look for them carefully. I believe we did it.

With pleasure I express my gratitude to all the colleagues and friends within the DELPHI Collaboration for their continuous help, without which my work could not have proceeded, and for the past years of diversified co-operation during which I have learnt to appreciate them as professionals, physicists and humans, among the very closest: Jean-Eudes Augustin, Yuri

Belokopytov, Petros Beltran, Paolo Checchia, Jon Guy, Frank Harris, Ingo Herbst, Heiner Herr, Hans Jürgen Hilke, Per Olof Hulth, Michel Jonker, Stavros Katsanevas, Elias Katsoufis, Barry King, Nils Joerg Kjaer, Hans Klein, Bernd Korzen, Pierre Lutz, Rasmus Møller, Klaus Mönig, Vladimir Obraztsov, Teodora Papadopoulou, Maria Elena Pol, Alphonso Rademakers, Francois Richard, Ron Shellard, Tzanko Spassoff, Nick van Eijndhoven, Pedro Vaz, Wilbur Venus, Marc Winter, Guy Wormser and Marco Zito, not forgetting numerous others in the corridors and control rooms.

In particular, I wish to extend my respect to prof. Ugo Amaldi, the DELPHI spokesman, who in the middle of the heavy duties of LEP experimentation focussed his attention to an individual contribution in analysis which evolved to form a major part of this thesis, recognized its physical significance, evaluated the executed analysis and encouraged the completion of the work. I thank him for the useful comments and advice.

I wish to express my very special thanks to the Helsinki DELPHI group and the R&D teams (Mika, Rikhard, Paula, Jounis, Kalevi, Iiro, Panu, Jorma, Mikkos, Kirsti, Kari, Rauno, Petri, Marek, Jukka, Markus, Antti, Jari, Markku, Wolfram, Camilla, Heimo, Sandor, Tuomo, Tuure, Martti, Raimo and Kenneth) which are now matured to become a productive community of dozens of talented people, for the homelike inspiring and exciting atmosphere. I wish to thank the personnel of the Department of the High Energy Physics at University of Helsinki and the Research Institute for High Energy Physics for the scientific atmosphere full of traditions.

I am greatly indebted to prof. Eero Byckling at Helsinki University of Technology for the long term support and supervision of my studies.

I wish to thank Donald Smart for his thoroughful language revision, and Anneli Varanka and Veikko Sinkkonen for their irreplaceable help in drawing the figures.

The remarkable financial support of Academy of Finland, Ministry of Education, Science and Culture, and University of Helsinki are acknowledged.

I dedicate this work

to my parents, for my life,
to my teachers, for all that I have learnt and
to Mar, for *the time we passed together*.

Helsinki, August 4, 1991.

Reino Keränen

SUMMARY

This thesis is composed of studies performed during the construction, commissioning and first year operation of the DELPHI experiment at LEP I. The individual contributions described here follow the evolution of the experiment. The authors contributions to hardware, to software development and to the final physics analysis are discussed. Within the contemporary topics in elementary particle research, the study focusses on techniques of the energy measurement in collider experiments and the search for supersymmetry in elementary particle phenomenology. From the experimental point of view, the study of both of these topics was driven by the motivation to understand to which extent complete event detection and reconstruction are realized in modern particle experiments.

Most of the author's work is documented in the appended papers in which the personal contributions can be readily seen. Due to the nature of collaborative research, the documented results include contributions of a number of physicists, but they have also been subjected to criticism and referring procedure of the collaboration.

The thesis is based on the following papers (accompanied here with the abstract and the summary of the personal contributions, and appended in the thesis)

1. *R. Keränen with DELPHI Collaboration, The Search for Scalar Quarks in Z^0 Decays, Phys. Lett. B247 (1990) 148.*

A search has been made for pairs of scalar quarks (squarks) produced in e^+e^- annihilations at LEP ($\sqrt{s} \simeq M_{Z^0}$), and decaying into a standard quark and a neutral, non-interacting, stable, massive particle (the lightest supersymmetric particle, LSP). The search has been conducted for differences in the mass of the squark and LSP of $2 \text{ GeV}/c^2$ and above. Up squarks with masses below $42 \text{ GeV}/c^2$ and down squarks below $43 \text{ GeV}/c^2$ were excluded. Six squark flavours degenerate in mass were excluded below $45 \text{ GeV}/c^2$.

The results are based on the physics analysis introduced and executed by the author. The two methods utilized in the analysis evaluate the basic characteristics of the performance of the DELPHI detector and the quality of reconstruction in multihadronic final states. The first method identifies an experimental signature of supersymmetry which constitutes a more sensitive test of mass parameters than

in any previous analyses. A robust method utilizing the special characteristics of the LEP I data is introduced in order to minimize the experimental and physical backgrounds. The analysis developed into a complementary test of supersymmetry at LEP I concerning the strongly interacting supersymmetric particles.

2. *R. Keränen with P. Eerola, K. Huitu, P. Morettini and R. Orava 'Exotica in DELPHI I; The Tools for Physics Analysis', SEFL preprint HU-SEFL-90-17 (1990).*

Signatures and backgrounds in a selected sample of new physics processes are analyzed in order to define, construct and test the hardware and software tools available for the physics analysis with DELPHI.

The simulation of the relevant characteristics of the detector response used in this early study of the physics in DELPHI is extensively based on the parametrization of the DELPHI hadron calorimetry in the fast simulation for DELPHI [58] which was constructed by the author in collaboration with the other authors of the package and the Helsinki group. The author also carried out the studies described in Section 5 ("Total Missing Energy") and 8.2 ("Squarks").

3. *R. Keränen with H. Herr et al., The Results of the Combined Beam Test of the DELPHI Hadron Calorimeter, the Forward Electromagnetic Calorimeter and the Barrel Muon Chambers (π^+ , e^+ runs), HU-SEFT-90-7 (1990).*

The responses of the DELPHI Hadron Calorimeter (HCAL) and the DELPHI Forward Electromagnetic Calorimeter (FEMC) are investigated in the beam test setup which realizes the foreseen DELPHI geometry and data acquisition system. Samples of pion and positron data in the momentum interval $10 - 60 \text{ GeV}/c$ are collected from which the responses of the HCAL, the FEMC and their combined response are analyzed. For the bare HCAL, the response to hadrons is linear in the considered momentum interval. The energy signal ratio of pions and electrons (π/e) is equal to 0.7. The hadronic energy resolution does not scale with $1/\sqrt{E}$ and the mechanisms affecting the energy resolution are studied. Calibration constants are defined for the FEMC and the HCAL separately and the combined response to hadrons is analyzed. Electron separation from pions is studied by using the FEMC and the combined information.

The individual contribution of the author was to participate in setting up of the HCAL detector hardware and the data acquisition system

for the testing. The author participated in data collection and was then responsible for the beam operations and monitoring of the HCAL detector. The author organized the early steps of the HCAL data analysis, i.e. participated in the development of the analysis software, executed the preliminary tests on the quality of data and arranged the distribution of the data between the participating institutes. The author initiated the analysis of the HCAL performance i.e. the studies on linearity, energy response, π/e signal ratio, and calibration procedures and configured the final conclusions in co-operation with the other participants.

4. *R. Keränen with P. Checchia and M. Zito, 'Evaluation of the Data Analysis Programs of the DELPHI Calorimeters' HU-SEFT-90-6 (1990).*

The role and some aspects of the development of the data analysis programs in the high energy particle experiments are discussed. A procedure related to the evaluation of the DELPHI calorimeters' data analysis algorithms is introduced and some results of the evaluation work are reported.

The author coordinated the development of the software package related to the topic, i.e. designed the structure of the package and its interface with the surrounding software. He prepared the quantities and histograms related to the shower multiplicities and to the total energy flow in the calorimetry, and contributed to the documentation of the results, particularly in the introductory part.

5. *R. Keränen and T. Jokitalo, Analysis of Cosmic Muons in the DELPHI Hadron Calorimeter during the LEP Pilot Run, HU-SEFT-1990-8.*

Cosmic muon detection in the DELPHI Hadron Calorimeter (HCAL) during the LEP pilot run, August 1989, has been analyzed utilizing supplementary information from the tracking detectors in operation at the same time. Despite the provisional running conditions, some basic performance characteristics and data quality of the barrel part of the HCAL could be checked and found to be satisfactory.

The work was coordinated by the author in the rapidly developing conditions of the being commissioned DELPHI detector. Specific software tools were applied to integrate the collected data samples of the independent detector parts and provided the collaboration with the first physically meaningful information of the HCAL performance.

The author contributed also to undocumented experimental effort which was vital in preparing the DELPHI experiment on time, and producing the first physics results. Some examples of this work are listed below:

- Installation and maintenance of the DELPHI off-line programs in the CERN CRAY XMP computer. The software consists of the Monte Carlo simulation of the DELPHI detector [54], the data analysis program [55], and the supporting packages: the data base and the application programs [56], the structural data management package [57], the data I/O package and other products, corresponding in total to about 300 000 lines of FORTRAN code written by about 60 authors. The effort was made in parallel with the development and the testing of the software on other computer systems and thus contributed to the vital stabilization of the DELPHI off-line software.
- By applying the expertise gained above, production of simulated events which well described the developing instrumental characteristics of the advent DELPHI detector and were used in the analysis of the first results on hadronic decays of the Z^0 bosons detected in DELPHI [6].
- Running the DELPHI detector during the LEP data collection, especially monitoring the HCAL operation during the detector shifts, and participating in the express line data processing.
- Collaboration in the physics working groups and later the DELPHI Physics Team 7 by organizing meetings and discussion sessions, by organizing the Physics Team 7 event viewing during the first data collection periods, and by participating in the development of Team 7 software analysis tools, especially the event tagging and DST program.
- Contributing to the development of the general DELPHI DST program.
- Participation in the installation of the HCAL hardware (assembling the front end electronics and slow control systems).

The introductory part of the thesis reviews both the experimental and theoretical motivations of the work and discusses the contents of the appended papers in a wider scope. The first Section presents the motivations of high energy physics at the most general level, discusses the current status of elementary particle theory and the deep puzzles motivating the new

generation of particle experiments. The LEP accelerator is briefly described with a discussion of its machine parameters of special interest to Section 3. The DELPHI detector is described briefly in terms of general purpose detector systems in modern collider experiments. Section 2 discusses in more detail the experimental aspects of calorimetry and energy measurement in general purpose detector systems which is the main theme of the papers 3), 4) and 5). Section 3 firstly examines some theoretical basis of supersymmetry (SUSY) and then reviews the phenomenology of the strongly interacting SUSY particles. The general instrumental and phenomenological context of the search for scalar quarks in Z^0 decays introduced in paper 1) is discussed and some clarifying aspects of the executed analysis are treated in more detail than in the original paper. In Section 4 both the direct results and the main general conclusions are presented.

1 INTRODUCTION

1.1 Theoretical basis

According to our current understanding, the elementary picture of matter consists of structureless spin one-half fermions which interact via exchange of spin one pointlike bosons.

At low energies we distinguish four types of fundamental forces. Electromagnetism is historically the best understood type of interaction and it acts as a prototype interaction for the development of field theory. Through its classical formulation in Maxwell's equations it exhibits the first example of unification of forces, and quantum electrodynamics (QED) serves as the prototype of a successful quantized gauge field theory. The electromagnetic interactions are mediated by the massless photons (γ) which carry the physical degrees of freedom of the gauge field with the symmetry $U(1)_{em}$. Weak and strong interactions are both of special interest in the current particle experiments. The universality of a multitude of weak phenomena has been subjected to systematic experimental verification. The validity of the standard model [1] as the unifying theory of electroweak interactions in the spontaneously broken group structure $SU(2)_L \times U(1)_Y$ is based on this verifying procedure. In the unified form, the electroweak force is carried by four gauge bosons, the photon and the three massive intermediate bosons (Z^0, W^+, W^-). The masses of the weak bosons explain the characteristics of the weak couplings at low energies but are also the indication of the broken gauge symmetry. The break-down of the electroweak gauge symmetry is explained by the Higgs mechanism [2] in which the fundamental scalar Higgs particle is assumed. The quantum chromodynamics (QCD) [3] based on the gauge structure $SU(3)_c$ is a nonabelian field theory similar to the electroweak model. It describes strong interaction as an exchange of massless gluons (8 eigenstates). Analogously to the electric charge, the conserved quantum number of the strong force is the colour index carried by the elementary quarks and gluons. The QCD has been verified in the perturbative region. Gravity which is the fourth fundamental force in Nature has not been considered as a gauge force in the particle experiments.

Each elementary matter particle is described in field theory by a Dirac field with four degrees of freedom. They may appear to an experimenter as stable free particles, as point-like objects in scattering experiments, as short-lived resonances, or their existence may be based on indirect evidence. They are distinguishable according to the conserved quantum

numbers carried by them, and according to their varying masses. The fundamental fermions can be divided into leptons (which do not feel the strong interaction) or quarks (which interact strongly). The character of weak force allows them to be arranged in left-handed doublets according to their isospin. Characterizing the chiral nature of fundamental fermions and explaining the maximal parity violation, the right handed components belong to the weak singlets and the relation $Q = T_3/2 + Y$, Q = electric charge, T_3 = the third component of the isospin, and Y = hypercharge, holds. Both the lepton and quark doublets appear as triplicates with gradually increasing masses (three generations). The structure is shown schematically in Figure 1.

The focus of the scientific program in contemporary high energy physics has been the systematic checking and verification of the standard model as well as the testing the quark-parton model and the QCD.

1.2 LEP physics goals

The discussion of the physics topics which can be investigated in the e^+e^- annihilations at center-of-mass energies around the mass of the Z^0 boson and at the threshold of W^+W^- pair production constituted one of the main themes of recent theoretical research in high energy physics. The conclusions of this decade long enterprise are compactly summarized in [4,5]. The physics potential at LEP is a consequence of the specific nature of e^+e^- annihilations as an initial state for various experiments and from the current theoretical status of elementary particle physics.

The physics goals have been mostly discussed in terms of the standard model of electroweak interactions and the QCD. The model of electroweak unification is well verified in present experiments but the introduced spontaneous symmetry breaking with the Higgs mechanism generates inherent theoretical puzzles with unavoidable phenomenological implications at energies at the order of $O(TeV)$. These are often summarized as the naturalness and hierarchy problems of the standard model [4].

Quarks (q) *

spin = 1/2

ELECT. CHARGE	FLAVOR		MASS GeV/c ²	FLAVOR		MASS GeV/c ²	FLAVOR		MASS GeV/c ²
$+\frac{2}{3}$	u	up	4×10^{-3}	c	charm	1.5	t	top	>45 (not yet observed)
$-\frac{1}{3}$	d	down	7×10^{-3}	s	strange	0.15	b	bottom	4.7

Leptons *

CHARGE			MASS GeV/c ²			MASS GeV/c ²			MASS GeV/c ²
0	ν_e	neutrino	$<2 \times 10^{-8}$	ν_μ	neutrino	$<2.5 \times 10^{-4}$	ν_τ	neutrino	$<3.5 \times 10^{-2}$
-1	e^-	electron	5.1×10^{-4}	μ^-	muon	0.106	τ^-	tau	1.784

*Antiparticles have the same mass and spin, but other quantum numbers are opposite the particle's.

Properties of the Interactions

Interaction Property		Gravitational	Electroweak		Strong	
			Weak	Electromagnetic	Fundamental	Residual
Acts on:		Mass-Energy	Flavor charge	Electric charge	Color charge	(See Residual Card)
Particles Experiencing it:		All	Quarks Leptons	All elect- charged	Quarks, Gluons	Hadrons
Particles Mediating:		Graviton (not yet observed)	$W^+ W^- Z^0$	γ	Gluons G	Mesons
Strength relative to e-m for:	at: 10^{-18} m	10^{-51}	0.8	1	25	Not applicable to quarks
	at: 3×10^{-17} m	10^{-41}	10^{-4}	1	50	
2 protons in nucleus		10^{-36}	10^{-7}	1	Not applicable to hadrons	20

Figure 1: Elementary structure of matter (tables of leptons and quarks in the upper part) and the gauge bosons (lower part). (Extracted from the computer program which supplements the material produced by the Fundamental Particle and Interaction Chart Committee, © 1989 F.P.I.C.C.)

As a part of the efforts in all high energy physics, the LEP physics goals are also motivated by these problems. It is widely believed that the understanding of the Higgs sector in the standard model provides fundamental answers to questions concerning the origin of the masses of elementary particles. The Higgs sector of the standard model is only the most easily identifiable core of the puzzles in elementary Nature, and the currently used picture of the elementary matter is complex and suggests that a more predictive particle theory is viable with fewer assumptions and fewer free parameters. This complexity also inspires thoughts for new experimental findings.

As far as the QCD and strong interactions are concerned, quantitative tests can be executed in a new energy interval at LEP. The analysis of hadronic final states at higher center-of-mass energies allows for the extension of the interpretation of results from previous e^+e^- experiments and to check more accurately the predicted scaling laws and universality of the fragmentation models. An example of the analysis procedures executed at LEP can be seen in the DELPHI results [6,7,8].

In the electroweak part, the LEP physics has been characterized as a new era of precision experiments. Many physical observables in final states from e^+e^- annihilations at LEP energies are directly related to the calculable parameters of the electroweak theory. They can be measured with experimental and model uncertainties which are small enough to observe effects due to the higher order quantum corrections. The precision measurements of the fundamental constants of Nature have a value in themselves. The accurate measurements of the masses and other properties of the weak intermediate bosons Z^0 and W^\pm appear similar to the $g - 2$ measurements in the case of QED.

In addition, the understanding of the higher order electroweak corrections - while challenging theorists to execute systematically related calculations - provides us with an extension of physics potential outside the directly kinematically accessible phenomena. The higher order quantum corrections are affected by the virtual presence of all physical states, in particular also by particles not yet directly observed but included in the standard model i.e. the top quark and the Higgs scalar particle. As their masses are for the moment not determined, they introduce theoretical uncertainties in all electroweak predictions. With an improved precision of the experimentally determined parameters which are sensitive to these quantities and with a better theoretical understanding of their observable effects, the theory can be further tested. In particular, it is thought to be a feasible approach for

distinguishing experimental signals of the "new physics" beyond the standard model. These aspects have a very positive impact on the design and execution of experimental analysis for precision measurements (see, as an example the DELPHI results [9,10,11]) and the systematization of the theoretical work.

Apart from the approach described above, the LEP data provides us with exceptional options for conducting direct searches for new particles. They can be again characterized in terms of the standard model and the proposed extensions beyond it. The LEP data offers the first possibility to search for the Higgs particles in theoretically sound production conditions and the LEP experiments have rapidly explored and nearly completely excluded the kinematically accessible region of the minimal neutral Higgs particle [12]. In a similar way to the lower energy e^+e^- colliders, the LEP machine has provided us with experimental conditions to search for several types of pairily produced charged particles (new generations of fermions, charged Higgs particles, supersymmetry, to name a few) resulting at search limits with very weak model assumptions.

From the point of view of new particle searches it is possibly more profitable to formulate the discovery potential in the LEP physics in an empirical context:

- The center-of-mass energy is higher than in previous comparable experiments.
- The high cross section at the peak of the Z^0 resonance (and the enhancement at the W^+W^- threshold) guarantee a satisfactory rate of events with the accessible machine luminosity¹. The expected cross sections of the potential new particles and phenomena often follow the production rate of the standard processes.
- It is known within the standard theory that the couplings in the e^+e^- annihilation at the Z^0 resonance are modified (but well understood) from the conventional photon mediated continuum region below the LEP region. This opens natural possibilities for complementary searches for particles even in the mass regions previously studied (their existence is possibly not fully excluded due to small couplings). Within the standard expectations in particular, this is realized as searches for

¹The diminishing total cross section in the continuum towards the higher energies has to be compensated with the increase in the machine luminosity which is a major challenge in their construction.

the production of electrically neutral (but coupled to the Z^0) particles in all the mass regions below the machine beam energy - this can make the experimental signatures more versatile. By considering the Z^0 particle empirically, the possibility for exotic couplings is enhanced, i.e. allowing speculation to be made on the existence of "hidden sector" of the particle spectrum as a complement to our current particle picture which is based on the studies of their production in photon and gluon mediated processes and on their detection utilizing the same forces, only.

- The kinematically constrained initial condition of the e^+e^- interactions and the general purpose detectors (see Section 2) with the nearly full solid angle coverage provide us with a lever to utilize less model dependent and versatile experimental signatures.

Thus concerning the new particle searches at LEP, experimenters explore a new discovery potential which is justified by several qualities, and can then express the results in a model independent fashion accompanied with interpretations in terms of model parametrizations of general interest.

1.3 LEP, the Large Electron Positron Storage Ring

The LEP collider (Figure 2) is a circular particle accelerator machine in which high energy electron and positron beams are accelerated in its first phase by 128 copper radio-frequency field cavities, and in which dipole and higher order magnets bend them on stable trajectories within the vacuum tube and focus them for collisions. The LEP main ring is excavated in a tunnel 26.7 km in circumference located in the Swiss and French territory at CERN. The particle beams are transmitted in four electron and four positron bunches to the main ring by the injection system which utilizes several other machines of the CERN accelerator complex. Four general purpose detectors (ALEPH, DELPHI, L3, OPAL) are installed in the interaction regions symmetrically on the main ring.

From the experimental point of view, the main parameters of the accelerator are the energy and the luminosity of the colliding beams. The beam energy determines the available center-of-mass energy of the particle interactions under study. In the case of equally energetic e^+ and e^- beams colliding head-on, the total available energy in the center-of-mass system of the interacting particles is

$$E_{C.M.S.} = 2 \times E_{\text{beam}}. \quad (1)$$

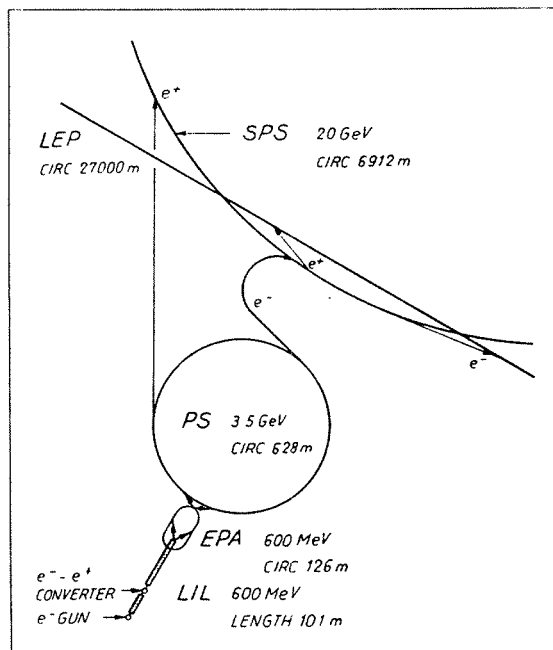
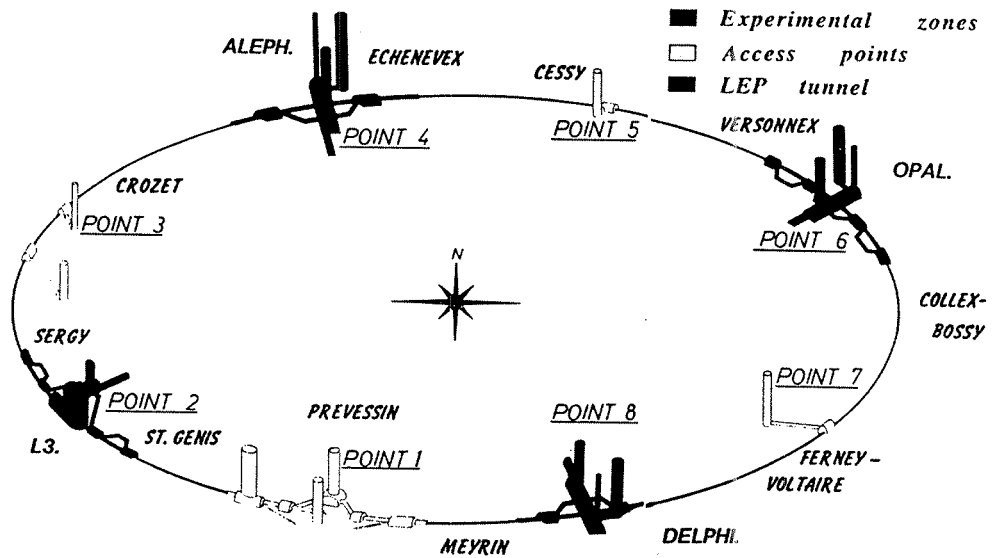


Figure 2: Schematic layout of the LEP collider, and its injection system utilizing the other machines of the CERN accelerator complex.

At LEP, a beam energy of 47 GeV was reached in the first phase in 1989, though most of the time the machine was running at center-of-mass energies around the mass of the Z^0 particle $M_{Z^0} \simeq 91$ GeV. The accelerator is designed to achieve center-of-mass energies beyond the threshold of pair production of W^+W^- pairs $E_{C.M.S.} \simeq 160$ GeV in later phases by utilizing superconducting rf-cavities.

The maximum achievable beam energy in the case of circular electron-positron colliders is limited by the energy loss of the beam particles due to synchrotron radiation. The energy loss of the circulating beam has to be balanced by continuous acceleration. At relativistic energies, the energy loss ΔE in a full cycle is proportional to $\Delta E \simeq E_{\text{beam}}^4 m_0^{-3} R^{-1}$ where E_{beam} and m_0 are the energy and the rest mass of the circulating particles and R is the radius of the accelerator ring. At LEP, the energy loss of a 50 GeV electron is about 0.22 GeV/cycle which results in about 1.6 MW synchrotron radiation power with about 16 MW of power consumed by conventional radio-frequency cavities when running the LEP at a beam energy of 50 GeV. The increase in the beam energy of light electrons becomes exhaustingly difficult at high energies and the LEP collider represents the practical upper limit of the size of circular e^+e^- accelerators.

The rate of a given type of interaction in an experiment \dot{N} is determined by the total cross-section σ of the corresponding physical process and by the luminosity \mathcal{L} of the colliding beams. The integrated luminosity $L = \int \mathcal{L} dt$ over the duration of the experiment is a good measure of the statistics of the data sample. The luminosity can be expressed in terms of the beam parameters A : effective transverse beam size at the crossing point, N_b : number of particles in bunch, f_b : frequency of the bunch cross-over in the experiment, and by using the beam current $I = eN_b f_b$

$$\dot{N} = \sigma \mathcal{L}, \quad \mathcal{L} = \frac{N_b^2 f_b}{A} = \frac{I^2}{e^2 f_b A} \quad (2)$$

The beam parameters are constrained by the machine parameters. The beam current (number of particles in the bunch) with a given number of bunches is constrained by the beam instabilities and beam losses which arise mainly during injection. The ultimate performance limit arises from beam-beam interactions of the by-passing bunches. The beam transverse size in the collision point is constrained by the beam optics (parametrized by the limiting beam-beam tune shift per beam crossing-over and the emittance factors $\beta_{x,y}$). The actual integrated luminosity over the long run depends on the overall efficiency in filling and maintaining the beams. Uninterrupted

periods of 6 – 12 hrs of stable colliding beams have been routinely produced from the beginning of LEP operation. The design luminosity of the LEP accelerator is $1.6 \times 10^{31} \text{ cm}^2\text{s}^{-1}$ and values of the order of $0.5 \times 10^{31} \text{ cm}^2\text{s}^{-1}$ were typical in the first year of operation of the machine.

Low background conditions at experiments are aimed at and often achieved in circular e^+e^- colliders. A particle background due to machine, this is, the yield of particles not originating from true physical annihilations still exists. The machine background affects general experimental conditions mainly by creating random hits and by increasing noise currents in the gaseous detectors (caused by low energy photons due to synchrotron radiation), and by increasing the charged particle trigger rates (due to high energy electrons and positrons) [13]. Because of these reasons, special attention in the machine design and operation has to be given to the sources of background, for example by shielding with collimators and by optimizing the beam optics at the interaction region [13,14]. Satisfactory conditions have been established at LEP in this respect.

Apart from the instrumental noise and fake triggers, a fraction of the machine background may generate triggers which mimic physical events (see Figure 3). Their origin is an inelastic interaction of high energy off-momentum beam particles (bremstrahlung of electrons from the bending magnets or from residual gas molecules upstream from the experiments) which hit the wall of the beam tube, or beam particles which interact with the residual gas molecules at the experimental region. The electron involved usually escapes undetected along the beam line but the fragments of the interaction may scatter as charged particles in the detector.

This source of background is of special interest for the physics topic investigated in Section 3. The rates as they were predicted in the design of the machine [15] are thus reviewed here as a check of consistency. With realistic estimates for the pressure in the beam tube varying from 2×10^{-10} to 2×10^{-9} Torr it was expected that the background of off-momentum electrons from upstream beam gas in the central detectors of an LEP experiment were to be of the order of few hundred Hz. Detailed studies [13] which take into account the other mechanisms in the production of the off-momentum particles suggest comparable or smaller rates. This is the yield of single charged particle tracks in the active detector region seen as individual tracks nearly parallel to the beam with no chance of mismatch with actual events - the rate rather indicates the difficulties in establishing reliable single track triggers even at LEP. From these studies it can be estimated that the particles encounter such inelastic interactions with the beam tube (0.03

radiation lengths) that they are triggered (by the charged particles) and reconstructed at the rate seen in the DELPHI data.

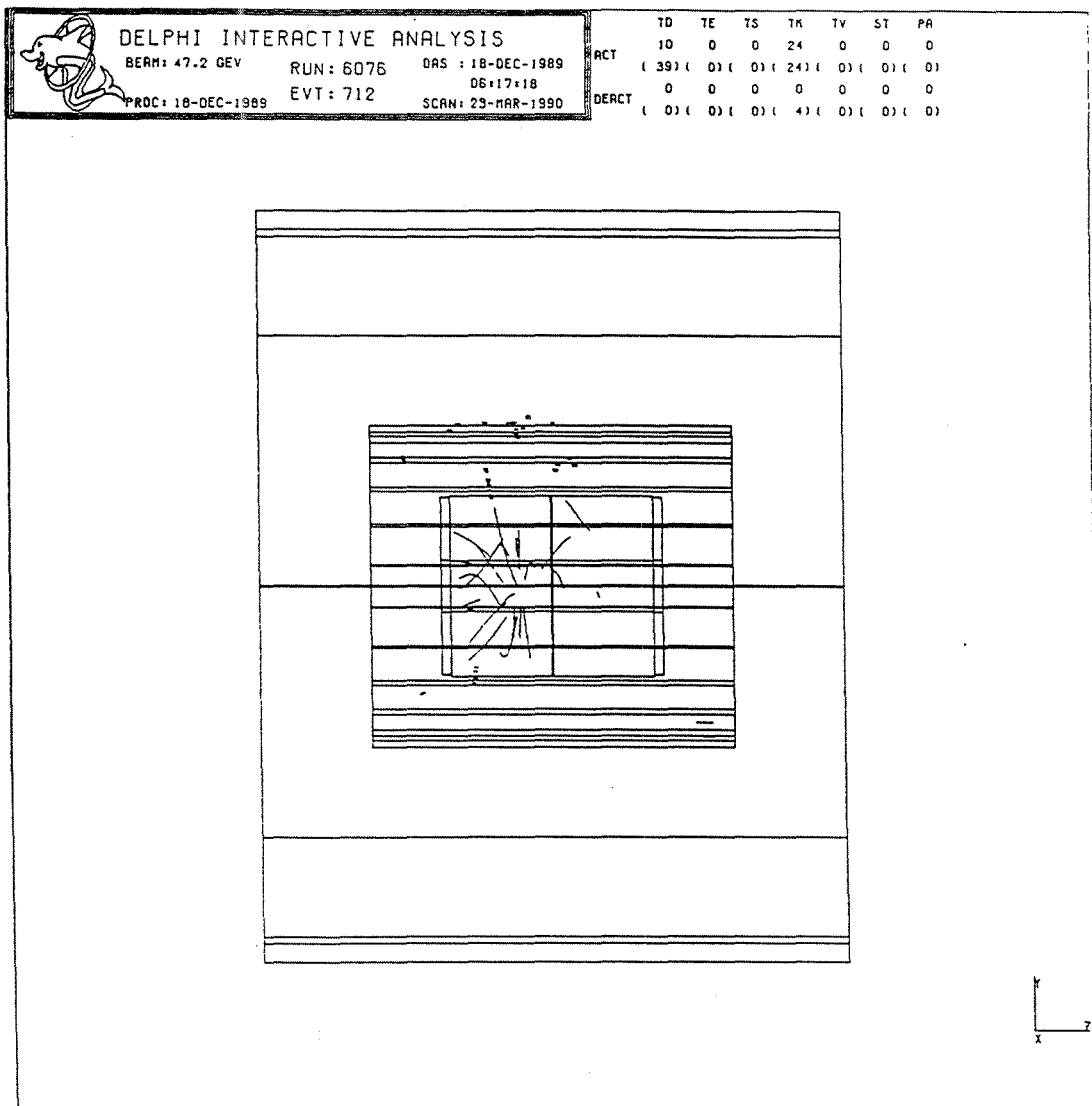


Figure 3: Example of a beam gas (or wall) interaction, recorded in the DELPHI detector. The effective vertex of interaction is significantly displaced from the center of the detector where the beams are focussed for collisions.

1.4 DELPHI, the Detector with Lepton, Photon and Hadron Identification

The DELPHI detector (Detector with Lepton, Photon and Hadron Identification) is a general purpose detector system designed to detect e^+e^- interactions at LEP energies with a special instrumental emphasis on particle identification. A large solid angle coverage and redundancy is guaranteed by the use of diversified set of subdetectors which apply many of the commonly used detection methods as well as some unique techniques at LEP. A detailed technical description and the performance of the DELPHI detector can be found in [16], [17] and [18].

1.4.1 General Purpose Detector Systems

General purpose detector systems at high energy colliders represent the state of the art of detector design in modern high energy physics. They appear as the most advanced instrumentation in experimental physics in general as far as versatility of utilized techniques, controlled extreme physical conditions, speed and volumes of data acquisition, and integrated expertise in construction and analysis are concerned.

Such a detector concept has evolved as a result of research and development of detector systems in colliding beam facilities over the past two decades. The potential resources and constraints of the design can be summarized by three major point of views:

1. There exist basic detection techniques to observe, to measure three-momenta and/or energy and to identify the majority of the various types of charged and neutral stable particles that are expected in the final states of e^+e^- annihilations with the only exception of neutrinos in the set of known particles.
2. The motivation for a large solid angle coverage favours cylindrical main geometry along the beam directions which is then completed by planar detectors in the forward and backward beam directions. A solenoidal coil provides the charged particle reconstruction (see Section 1.4.2) with a homogenous magnetic field over a large volume which has a cylindrical symmetry around the interaction region. It is geometrically and instrumentally possible to position the various subdetectors in such a way that the solid angle is maximally covered and the particle detection in any subdetector does not affect the performance of others.

This is, the techniques which are applied in each type of subdetector are operable in variable conditions of orientation of the electric and magnetic fields, temperatures and radiation levels, and so on. The electronics related to the fast signal read out and control systems can be incorporated in the configuration with necessary access for service and maintenance. An important goal is to minimize the absorbing materials in detectors through which the particles are supposed to pass by without secondary interactions, and the logic of complete absorption of the selective types of particles in subsequent detector layers. The actual configuration is a compromise of many constraints.

3. There exists technology to construct a data acquisition system which is able to collect, process and record the information of the detected particles in an integrated set of subdetectors. All the vital physical information contained in the electronic signals of the detecting devices can be recorded for later analysis procedures, though attention has to be given to handle the initially large digitized data volumes and to establish a reliable low rate trigger which selects the physical events from the high rate of beam bunch crossing overs.

The merits of a general purpose detector system meet well with the physics goals in e^+e^- experiments in which numerous studies consider the versatile features of a set of collected data. Analyses can utilize fully reconstructed final states of both low and high particle multiplicity, in inclusive or in exclusive approaches. Events reconstructed in all angular directions are of interest, often their statistical angular distributions carry physical information. The information about absolute normalization can be applied, that is, the recorded rate of events can be associated with the expected physical cross-section with small uncertainties in the trigger and detection efficiency, and data acquisition system. In this way, the nature of precision measurements and of searches for low rate new phenomena in the LEP data emphasize the desire for versatile and redundant detection capability.

In most analyses, subsets of events are selected by applying distinguishable experimental signatures to the observable final states. The large collection of applicable event signatures is a characteristic feature of LEP data. This partly arises because of the well understood initial state and the physics processes being studied. In order utilize these event signatures with sufficient efficiency, there must be an instrumental basis for their detection.

There are two reconstruction tasks which particularly employ the

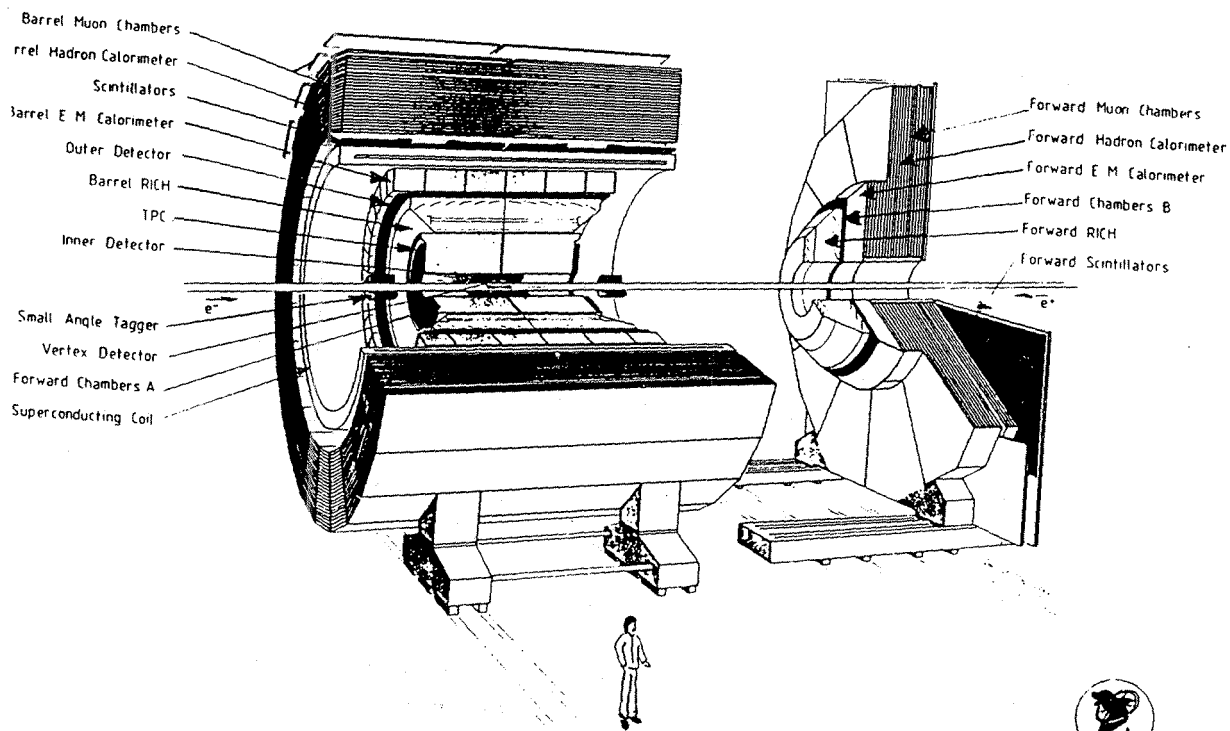
potential of the general purpose detector. They are complementary and their optimal realizations in the actual experiment affect each other. Many experimental signatures are based on inclusive particle identification. The identification procedure usually requires the combination of information from several kinds of signals in the particle trajectory. For this goal, the subsequent detection of the particle in the various types of particle detectors is a necessity, also the data analysis programs are designed to incorporate the often iterative algorithms which resolve the physical information. The identification of (isolated) muons, electrons, photons, and kaons are the most typical examples of these procedures.

As the techniques are implemented to receive signal from nearly all kind of known types of particles, it is natural to aim at the integration of their information and to reconstruct kinematically complete events, particularly for the case of multihadronic final states which represent a major part of the data. With a data sample containing such events, we avoid systematic uncertainties which may possibly enter because of kinematical corrections applied on the data (observed as induced shifts in invariant mass distributions, for example). In special cases, by applying the constraints from the fixed e^+e^- initial conditions it is possible to reconstruct one invisible particle in the event topology (this is, a particle which is not detectable with the current techniques). An example in which this technique has been put to use are the searches for heavy standard Higgs particles in the neutrino channel [19]. The kinematically correct multijet reconstruction which is the basis of a class of new particle searches relies also on the complete event reconstruction.

Finally, it is significant that the combination of several subdetectors provides some general redundancy gains in the experimentation. The local calibration of subdetectors benefits from the independent information from the other detector parts. Also some reconstruction parameters e.g. the trigger efficiencies are evaluated and improved in a controlled manner by using the redundancy due to there being several independent subsystems.

1.4.2 The DELPHI detector

In the following, the functions of the DELPHI detector (Figure 4) are described as a realization of the general purpose detector system.





 DELPHI

Figure 4: Pictorial view of the DELPHI detector.

Charged track reconstruction

The reconstruction of charged particles through their ionization tracks in gaseous detectors in a homogenous magnetic field constitutes the core of event reconstruction. This is, because nearly all physically interesting events ² contain charged particles, especially in the case of multihadronic final states they well characterize the general event topology (event orientation, jet structure, inclusive distributions).

Measurement of momentum utilizing track curvature in a magnetic field has proven to be efficient and to have a good resolution at moderate particle momenta. It suffers from the nonuniform angular performance (resolution of tracks at low polar angles is affected by the diminishing perpendicular field strength), but the three dimensional event picture provided by the modern time projection chambers (TPC) carry vital visual information and constitute a sound basis for further event reconstruction.

The DELPHI TPC consists of 6 sectors in both hemispheres 2×150 cm in z and at radii 30 – 122 cm and provides 16 track points. Additional space points (24 points from the jet chamber and 5 points from the trigger layer part [18]) are received from the Inner Detector (ID) at radii 12 – 28 cm. The Outer Detector has five layers of drift cells at radii between 198 and 206 cm at polar angles 42° to 138° and it provides useful track points outside the Barrel RICH for energetic particles and for the trigger. The track reconstruction at low polar angles is improved by the Forward Chambers A and B.

Calorimetric energy measurement

Granular and hermetic calorimeters in which deposited energy clusters originating in the energy flow of the final state particles are reconstructed provide us with complementary event information. Calorimeters are able to measure equally well both the neutral and charged incoming primary particles, their resolution improves ($\sigma/E \sim 1/\sqrt{E}$) at high energies, and it is easier to apply them homogeneously over the full solid angle than it is to apply tracking detectors - thus the complementarity. Calorimeters suffer from the lower detection efficiency of low energy hadrons and cannot compete with the momentum resolution of low energy charged particles of tracking devices. The design and operation of calorimetry in e^+e^- collider experiments is further discussed in Section 2.

The DELPHI detector consists of three major calorimeters at large polar angles. The High Density Projection Chamber (HPC) measures electromagnetic energy with high granularity over polar angles 40° to 140° .

²with the exception of detection of single photon topologies for the neutrino counting, or searches for new phenomena (rare Z^0 decays or supersymmetry).

The Forward Electromagnetic Calorimeters (FEMC) consist of 2×4500 lead glass blocks (granularity = $1^\circ \times 1^\circ$) covering polar angles from 10° to 34.5° and the complement. The Hadron Calorimeter is a sampling gaseous detector incorporated in the magnet yoke covering polar angles from 11.2° to 168.8° .

Luminosity

In e^+e^- experiments luminosity, which is required for the absolute normalization in many physics analyses, is measured most accurately by counting Bhabha scattered electron-positron pairs at low polar angles. It is calculated from the rate of Bhabha events by using the expected cross-section which can be estimated theoretically very independently³ from the physics parameters related to the annihilation events.

In DELPHI, the Small Angle Tagger consisting of a lead sheet calorimeter and a tracker in front at polar angles from 43 to 135 *mr*ad is devoted to the Bhabha counting and provides the physics analysis with the luminosity at the total systematic uncertainty of 2.0%. There is an independent device (Very Small Angle Tagger, VSAT) in the DELPHI experiment for the fast monitoring of luminosity and machine operation at a distance of 7.7 meters from the interaction point along the beam directions.

Trigger

In electronic particle experiments, the data acquisition system is triggered by the event signals themselves, in order to have the event data stored for later analysis. At the first level in DELPHI, signals from devices with rise times $O(100$ ns) are needed for the simple topological decision algorithms which determine within 3 μ s whether a passing beam bunch which occur every 22μ s (beam crossing over, BCO) produced an interesting event and whether the front end electronics of each detector should be prepared to collect the detected signals.

Signals from the scintillation layers in the inner part of the HPC, from the Time-of-Flight Counters (TOF) at a radius of 310 cm between the coil and the magnet return yoke, from the Forward Hodoscopes (HOF) located in the outer parts of the endcap yokes, from the ID and the OD, and from the FCA and FEMC are combined with rough geometrical (back-to-back or majority) selections. With this level of sophistication, a high efficiency trigger for standard multihadronic as well as leptonic Z^0 decays can be established over the maximal solid angle. For precision measurements and for new particle searches in exotic topologies, the trigger efficiency can be evaluated

³The interference with the production of the e^+e^- pairs and the higher order radiative effects, particularly in the electroweak theory, are calculated systematically to the level of applicable Monte Carlo programs.

explicitly because of the good redundancy of the DELPHI trigger system. The design trigger system also contains, within the FASTBUS standard, the HCAL first level trigger, and subsequently the second trigger level (determined $40 \mu s$ after the BCO) which applies information from the slower trigger hardware components, and which can execute more complex pattern recognition algorithms for a charged particle trigger, a muon, an electron (or photon) trigger, for example. This has been gradually implemented in DELPHI, whereas the third and the fourth trigger levels are primarily designed to cope with high luminosities and background rates.

Particle identification, time of flight measurement

Inclusive particle identification consists of algorithms which determine whether the observed particle is an electron, a photon, a muon, a pion, a kaon, a proton or other long-lived particle. The determination is based on the different signatures each type of particle produces, often in subsequent detecting devices. Some type of detectors are implemented just for these identification purposes.

Electrons and photons are identified as electromagnetic showers (see Section 2) in the calorimetry, electrons are resolved from photons as a shower with an ionizing track pointing at it, this requires a combination of information from the electromagnetic calorimeters and the tracking devices.

Muons are distinguished from other particles as penetrating minimum ionizing in the tracking detectors and calorimetry. High resolution space points detected outside of the calorimetric absorbing materials are useful in tagging the muon candidates, in particular rejecting the background due to the hadronic showers propagating deep into calorimeters. In DELPHI, the Barrel and the Endcap Muon Chambers beyond 7 to 8 nuclear absorption lengths of material cover the full solid angle except the regions in the beam directions and a gap at the polar angles around 40° .

The identification of hadrons, in the parton jets in particular is instrumentally most challenging. At low momenta ($p < 8 - 10 \text{ GeV}/c$), their ionization strengths vary according to their masses and they can be thus distinguished from the amount of ionization charge per traversed path in the TPC type of chambers (conventionally known as dE/dx measurement). Neutral long-lived hadrons (K_L^0 , n) can be reconstructed as unassociated hadronic energy deposits in the same manner as photons. In DELPHI, unique instrumental identification is expected from the Ring Imaging Cherenkov Counters, the barrel and the forward RICH. By associating the Cherenkov radiation rings in the liquid (C_6F_{14}) or the gaseous (C_5F_{12}) medium with charged particle tracks, pions are separated from kaons and

kaons from protons, over the full dynamic range of hadrons.

Measurement of the time of flight of the impinging particles from the interaction regions, optimally performed by the scintillation counters at large radius (DELPHI TOF and HOF counters) is historically another method of mass determination. In modern e^+e^- experiments time of flight measurement is applied to reject cosmic background interference.

Vertex reconstruction

Vertex reconstruction aims at resolving the observable secondary vertices in which stable particles are created as decays of short-lived particles. Most of the stable particles observed in the e^+e^- final state (with the exception of electron and muon pairs) do not originate in the primary annihilation and fermion pair production, but they result from their decays. Especially in multihadronic final states, the secondary vertices in the interaction region give us direct access to information about short-lived particles with life-times of the order of $O(10^{-10} - 10^{-11} \text{ s})$, i.e. most interesting heavy quarks and mesons.

In DELPHI, a spatial resolution ($5 \mu\text{m}$ for single tracks) is achieved in a silicon strip based Micro Vertex detector (VD) in its first design in two layers at the radii 9 and 11 cm. Redundant space points are provided from the ID.

Supporting functions and procedures

The items discussed up to now are directly related to distinct performance parameters of a modern particle experiment. There are several other functions and tasks, which are vital for the safe and controlled operation of the detector and the successful data analysis, and are thus intimately related with the detector performance.

The relative alignment of the various subdetectors in a general purpose detector should be known at an accuracy comparable to the spatial resolution of the subdetector with the better performance, in order to fully profit from the combined global reconstruction. Conventionally the alignment procedures focus on the relative positions of various tracking detectors, the DELPHI detector with numerous tracking devices is an exceptionally challenging case. The other particular challenges in DELPHI are the alignment of the vertex detector information with the rest of the track reconstruction, and the alignment of the RICH with respect to the TPC, the OD in the barrel, and with respect to the FCA and the FCB in the forward directions. The reconstruction of the neutral particles, via the association of the charged particle tracks and the energy deposits in the calorimetry (see Section 2), ends up to an alignment problem as the granularity of the

calorimeters has improved.

A specific function related closely to the alignment procedures, is the operation and control of the high magnetic field (homogenous 1.2 T in the gaseous volumes inside the coil ($O(100\ m^3)$ in DELPHI). The stable running of the DELPHI superconducting cryostat with a current of 5000 A is one of the most sensitive parts of the DELPHI operation. In addition to the successful operation of the solenoid, it is vital to know the resulting field strength inside the tracking detectors.

The input for the local pattern recognition consists of the locally calibrated raw data in which several types of calibration information is applied (drift time vs. coordinates, signal thresholds or energy assignments). These calibration constants depend on detector parameters which change in time and their controlled optimal usage sets extensive requirements on the structure of the data analysis software.

The operation of the detector instruments and the data acquisition system requires extensive monitoring and control in the experiment (the slow control system). The requirements on the centralized and extensively automatized systems are tight due to the complexity of the detector and long data taking periods during which the man power aspects become relevant. The system controls detector parameters like high voltage, gas distribution and thresholds of the front end electronics. The system measures and records continuously information about the detector conditions (temperatures, pressures and the actual values of the parameters it controls itself). All these procedures are designed and executed with one of the chief considerations being the safety in the underground experimental area, and the continuous storing of the recorded slow control data constitutes the secondary data flow for the subsequent data analysis, in addition to the actual event data recorded by the fast data acquisition system.

2 ENERGY MEASUREMENT IN COLLIDER EXPERIMENTS

In this Chapter the work related to the appended reports 3, 4 and 5 which consider the hardware and the software aspects of calorimetric energy measurement in a general purpose detector is discussed. As a starting point we recall some general aspects of the operation of calorimeters in detecting the most common event topologies of the final states in e^+e^- annihilation.

The particle detection in a calorimeter is based on the inelastic interactions which generate a cascade in which the high energy particles are absorbed in a dense material (see for example [20]). Detection of this particle shower in the calorimeter takes place in sampling layers in which a fraction of the cascade particles produce signal through ionization or scintillation or the homogenous absorber itself may generate signal that can be recorded and amplified as an electronic signal. The energy measurement is based on a linear relation between the energy of the incoming primary particle and the generated signal. The energy resolution of calorimeters follows from the statistical nature of the signal generation and ideally scales as

$$\sigma(E)/E \sim \sqrt{\frac{1 \text{ GeV}}{E}} \quad (3)$$

E = energy of the incoming particle to be reconstructed

The absorption processes are different for electromagnetically interacting light particles (photons, electrons and positrons), and for the strongly interacting hadrons. Separate instruments are usually designed for the electromagnetic and for the hadronic energy measurement. The main problem in developing calorimetric detectors has been to understand the physical mechanisms which cause the fluctuations in hadronic energy measurement [21]. Progress has been made by constructing instrumentally compensated hadron calorimeters [22]. In a compensated calorimeter the responses of the instrument to the hadronic and to the electromagnetic component of the particle cascade are equal. A compensated calorimeter can simultaneously serve as an electromagnetic calorimeter and a hadron calorimeter.

Photons and neutral hadrons are frequently produced and they carry relevant event information in e^+e^- final states. Thus calorimetric detectors are a must in general purpose detector systems. Most of the collider experiments, the DELPHI detector not being an exception, utilize the

conventional approach consisting of an electromagnetic calorimeter which is surrounded by a separate hadron calorimeter. This choice is favoured by the detector geometry: the solenoidal field with the return yoke guiding the flux of the magnetic field has to be incorporated with the calorimeter geometry. By employing the yoke as a hadronic absorber interleaved with sampling layers of detectors the cost is optimized. By installing granular electromagnetic calorimeters inside the coil, the preceding amount of passive material is minimized and a good spatial resolution can be achieved. It is the identification of particles which credits from this layout whereas the detector concept is clearly not optimal for the hadronic energy measurement due to the large amount of material in front of the hadron calorimeter. The starting point of the energy measurement of traversing hadrons is the integrated reconstruction utilizing the electromagnetic calorimeters and the hadron calorimeter, rather than the energy signal in the hadron calorimeter alone. This fact affects the data analysis structure. In this integrated hadronic energy reconstruction procedure, also particle identification aspects are to be taken into account. The identification of hadronic showers initiating in the electromagnetic calorimeters is a necessity for the unbiased energy calibration of hadronic particles because the electromagnetic calorimeters are typically undercompensated with respect to hadronic showers and because there is passive absorber material in the magnet coil. These difficulties would be overcome 1) if the calorimeters are instrumentally compensating, or 2) the pattern reconstruction of the calorimetric data analysis chain is based on the reconstruction of the averaged total jet-like energy flow in the calorimeters. For the latter approach, a Monte Carlo based predictions for the particle composition of the jets are required.

We then consider calorimetric information together with the reconstructed charged tracks. We again observe that reconstruction of the energies of various types of particles is closely related with the combined identification procedures. A complete event reconstruction of multihadronic final states is not accomplished by the most straightforward addition of charged particle information to the reconstructed neutral particles in calorimeters. The calorimeters do not distinguish the electric charge of the detected primary particle i.e. duplicate reconstruction of charged particles occurs in the track reconstruction and in the detection of calorimetric showers. Thus, photon showers have to be separated from electron/positron showers through the association of the reconstructed charged tracks with the corresponding calorimetric signals. The photons appear as the complement of remaining unassociated showers. The same procedure applies for the neutral hadrons.

These pattern recognition algorithms take place at the combinatorial phase of the data analysis i.e. at the level where the individual detectors provide their local 'best' reconstructions. This step is fragile because the conditions in each contributing detector part have to be well understood and because the mechanisms related with the combinatorics have to be controlled. The inefficiencies in either track reconstruction or in calorimeters and effects due to overlaps have to be consistently corrected for.

This difficulty has been met also in other LEP experiments apart from DELPHI [23]. It is also noticeable that the related mechanisms have been attacked at hadron colliders where jet calorimetry has played a crucial role. Nonlinearities in the jet response have been encountered and resolved, for example in studying the inclusive jet production due to QCD processes [26], or in reconstructing kinematically distinct channels of W^\pm and Z^0 decays into quark pairs [27] in the presence of the QCD continuum. These results confirm the conclusion that the data analysis chain based on the integration of the optimized single particle reconstruction algorithms is not sufficient to reconstruct kinematically complete multiparticle final states registered in general purpose detectors in collider experiments.

In applying the data to various physics topics, these effects can be overcome case by case. An analysis can merit from the optimized inclusive reconstruction by utilizing isolated particles as an experimental signature if the channel naturally allows one to do it without a major loss of efficiency. If the interesting physical information is carried by the jets, appropriate kinematic corrections can be applied. Prototypes of these analyses are the multijet analysis in search for heavy new particles [24], or the analysis that applies total energy measurement in a topology which cannot profit from the momentum imbalance (acollinearity) [23]. In the first case, the systematics related to the procedure is controlled by Monte Carlo studies on simulated data. In the latter case, the differential event reconstruction, which has been demonstrated to work for single particles [25], has to be corrected for in cases of multiparticle events by a statistical parametrization, and the systematic uncertainty that is introduced is then evaluated using physical events (radiative photons). It is generally concluded that in spite of the fact that the kinematically complete events are not fully integrated through the differential particle reconstruction, very satisfactory physics results have been extracted by utilizing these methods.

2.1 Review of the results of the combined beam test of the DELPHI Hadron Calorimeter, Forward Electromagnetic Calorimeter and Barrel Muon Chambers

The results of the appended report 3) are based on the beam test of the DELPHI Hadron Calorimeter (HCAL), Forward Electromagnetic Calorimeter (FEMC) and Barrel Muon Chambers (MUC) executed in July-August 1988 i.e. a year before the commissioning of the DELPHI experiment at LEP. The main goals met in the test procedure were related 1) with the development and test of the DELPHI data acquisition system, on-line software and monitoring tasks in real experimental conditions, 2) with the stability and calibration of the final production versions of the participated detectors, and 3) with the studies of their combined performance in a configuration corresponding the actual DELPHI geometry - in particular concerning the combined hadronic response of the FEMC and the HCAL and the muon identification. The setup realized for the first time a successful integrated operation of more than one of the DELPHI detector parts by utilizing the DELPHI FASTBUS data acquisition system.

In the following key features of the data and the results related with the contributions in this thesis and the topic of this Chapter, are reviewed. Apart from the detailed analysis of muon data [28], the collected data samples provided us with a basis to determine the energy response of the HCAL to be applied in the combined performance in DELPHI. Most naturally this took place by considering first the data samples (π^+ data in the momentum interval 10 - 60 GeV/c , positrons at the momenta 10 and 20 GeV/c and penetrating muons) in which the beam hit the HCAL without the FEMC in front of it thus allowing to determine the 'stand-alone' characteristics of the HCAL.

Recognizing the temporal status of the data acquisition chain, the first analysis studies consisted of checks on data quality. The correspondence of the off-line decoding tables with the HCAL read out geometry (tower-supertower-hypertower) was found which eliminated a class of cabling errors. Checks were routinely executed against formatting errors in the digitized FASTBUS data, the fraction of corrupted triggers was limited at the level of few per cent and rejected.

There were two main sources of systematic effects exclusively present in the beam test setup which complicated the data analysis and conclusions. The logic of the common trigger based on the random time of the arriving

beam particles did not correspond the LEP collisions which are timed by the BCO signal (beam crossing over). This affected the fast charge integration time in the HCAL front-end electronics which thus effectively varied between 1300 – 2000 ns on an event by event basis. The significance of this fact is discussed in the report. The author contributed to this subtopic with studies based on the remark that the HCAL front-end electronics provides two digitized samplings of the integrated analogue signal, namely the actual tower digitation and the analogue sum of each supertower designed for the DELPHI first level trigger. The charge collection for this trigger signal effectively varied event by event as the tower digitation but 1000 ns shorter in time i.e. 300 – 1000 ns. By comparing these two signals event by event (cf. Figure 10 in report 3)), it was firstly demonstrated that the HCAL front-end electronics provided reliable trigger signal in the FASTBUS standard as the trigger analogue sum correlates with the tower signal. The fluctuations between the two signals could then be applied in extracting possible effects due to the effectively varying integration time. Based on simple models on the signal generation dynamics determined by the characteristics of the primary read out circuit, muon data was expected to exhibit additional correlations resolving the triggers of short versus longer charge integration times. No such effects were observed at a significant level above the fluctuations caused by the inherent Landau and streamer fluctuations of the muon signal, by the pedestals and other effects (charge diffusion) of geometric dependence, which confirmed the conclusions made in the report. The second type of significant systematic effects in the collected data is of geometrical origin (the fraction of the inactive regions in the beam spot larger than a typical HCAL streamer configuration and the charge diffusion phenomena due to the low resistivity of the cathodes of the streamer tube in the test module), as discussed in details in the report.

The basic results of the 'stand-alone' energy response of the HCAL were extracted by the author as follows:

1. The HCAL response to pions is linear in the interval 10 – 60 GeV/c. It was firstly observed that the HCAL front-end electronics showed no saturation but was adequately tuned with respect to the streamer spectra which is determined by the gas mixture and high voltage. In fact, the dynamic range allowed to consider an increase in the amplification in favour of better sensitivity for the low energy signals. The linear response allows one to define a natural energy calibration procedure which has not always been reached in iron sampled hadron

calorimeters.

2. The measurements of the π/e signal ratio at two energies 10 and 20 GeV/c to be 0.7 confirmed the expectations of this type of calorimeters (sampling thickness of 5 cm iron) showing undercompensation with known effects on the achievable energy resolution.
3. The observed energy resolution $\sigma(E)/E$ does not scale as $\sim \sqrt{1 GeV/E}$ but is worse at high energies despite of several calibration procedures attempted. The nonscaling property can be associated with the compensation characteristics. The conclusions presented in the report emphasize the other reasons for the observed energy resolution.

After the 'stand-alone' HCAL energy response was understood, the combined performance of the HCAL and FEMC could be studied, where a FEMC calibration procedure was applied as described in the report. The essentials of the combined response (the Figure 12 of report 3) is commented briefly here. The fraction of pions penetrating through the FEMC without inelastic interaction can be distinguished and corresponds the expectations ($\sim 40\%$). The combined response is improved with a simple compensation formula which suggests the lead-glass of the FEMC is undercompensating by a factor of two. The HCAL response has to be further corrected for shower tails in the case of the shower starting in the FEMC, which is also understood due to the modified response along the longitudinal hadronic shower development. The improved energy resolution is an indication of the thus achieved software compensation.

2.2 A software point of view

A software point of view to the event reconstruction utilizing general purpose detector design is discussed in the report 4). The generalities and the context of the studies documented are presented in the introduction of the report.

An evaluation of a reconstruction program - as well as the design of the reconstruction program itself - most naturally starts considering few particle events. The local track and shower searches should soon demonstrate their performances in a realistic multiparticle topology. Then in combining the local reconstruction algorithms tests on the few particle events again provide useful information and are especially well motivated as such topologies also appear in the real data. The merits of independent evaluation procedures appear most clearly in consolidating general knowledge of the status of the

analysis chain, and pointing out those problems in reconstruction which require collective efforts.

The discussion of the topics in the introductory part of this Chapter is based on much of what was concluded at later stages of the software evaluation procedure beyond the results in the appended report. As the real data becomes available the analysis efforts oriented towards specific physics results naturally take over the role of driving the optimization of the data analysis chain.

2.3 A first look on the combined reconstruction of real data in a general purpose detector

The DELPHI detector was commissioned in schedule to detect Z^0 events at the start-up of the LEP collider. The integrated luminosities in the first periods of colliding beams were not sufficient for extensive studies. Some vital information of the performance of the detector can be extracted by considering triggers caused by cosmic penetrating particles recorded during runs dedicated to that purpose.

The appended study of the cosmic events is partly understood as a continuation of the efforts for combined particle reconstruction in DELPHI. With the real data several aspects in the local pattern recognition algorithms had to be rechecked that could be taken as granted in the simulated data. Particularly from this point onwards, the robustness of the complete analysis chain was faced with the time-dependent effects in the true detector operation. The essence of the report 4) is to confirm that in the fiducial regions of the HCAL defined by the sufficient statistics of cosmic triggers, the detector hardware was efficiently running, the front end electronics and the local data acquisition was running in synchronization with the central DELPHI trigger cycle, and the pattern recognition in the data analysis provided particle signals in good association with the independently reconstructed charged particle tracks.

3 THE SEARCH FOR SCALAR QUARKS IN Z^0 DECAYS

3.1 Strongly interacting supersymmetric particles

Supersymmetry (SUSY) relates particle fields of different spin (bosons and fermions) [29]. The motivations for such a symmetry in elementary particle physics are purely theoretical [30,31,32,33] and there is no direct experimental indication in particle physics of supersymmetry. The basic aspects of supersymmetry phenomenology are model independent. In supersymmetry particles are transformed in a supermultiplet in which particles have the same quantum numbers and mass (in the case of unbroken supersymmetry) but different spins. It appears that superpartners of standard matter fermions are scalar fields (sfermions) corresponding to each fermionic degree of freedom. The standard gauge vector bosons are extended to vector supermultiplets with a corresponding generalization in the gauge transformations [32]. The supersymmetric Higgs sector contains at least two chiral doublets of Higgs bosons accompanied with their fermionic superpartners.

Neither fundamental scalar particles nor gauge fermions have been observed and the masses of the superpartners must differ in the supermultiplets. In the broken supersymmetry, the particle spectrum of the standard model is duplicated by the not yet observed particle states. They are expected to exist with masses $m_{SUSY} \lesssim 1 TeV$ if supersymmetry is to solve the naturalness problem in the standard model [4]. Apart from this order of magnitude upper limit, there are no general theoretical predictions for the masses of the supersymmetric particles. Attempts to construct a SUSY phenomenology with fewer new particle states tend to lead to the violation of lepton and baryon numbers [32]. Interesting particle models have been developed and they reduce the number of free parameters in the supersymmetry breakdown, relate observable quantities so making them experimentally testable.

It is convenient to introduce a global (or discrete) R -symmetry or R -parity $R_p = (-1)^{3B+L+2S}$, (B baryon number, L lepton number, S spin) which is conserved even if supersymmetry is broken and which labels the new particles. The R -symmetry constrains the supersymmetric Lagrangian to avoid problems with violation of the observed lepton and baryon number conservation and proton stability [32]. Models have been proposed also in which R parity is broken [34]. It should be emphasized that the R -parity does not follow from the supersymmetry principle itself. It is not

an explicit consequence of the specific models of supersymmetry breaking mechanisms or the theory inspiring the SUSY breakdown. It is rather a supersymmetric extension of lepton and baryon numbers which appear as conserved quantities in Nature. The conserved R -parity has important phenomenological implications: supersymmetric partners are produced in pairs and the lightest supersymmetric particle (LSP) is stable. The LSP is cosmologically interesting because it is most probably a very weakly interacting (massive) particle (WIMP) and it is a candidate for solving "the dark matter" problem [35]. The R -parity conservation and the concept of LSP alone defines much of the strategy in the direct search for the supersymmetric particles: the elusive LSPs carry a significant fraction of the energy in the final states of decayed supersymmetric particles. Such event topologies are often distinguishable from the standard events.

The expected spectrum of strongly interacting supersymmetric particles contains 72 components of scalar fields corresponding to the quarks and 24 physical gluino components in the $SU(3)$ gauge supermultiplet. The search strategies for these SUSY partners of the nuclear matter differ in two ways from the case of particles purely in the electroweak sector. At low energies, the confinement due to the strong interaction has made it nontrivial in some cases to exclude the existence of these particles in the mass region ($\lesssim 2 - 5 \text{ GeV}$). Instead, at high energies, the large couplings of these particles with the hadronic constituents turn out to be an advantage and the hadron colliders are allowed to probe higher mass regions of these hypothetical particles than for the other particles of the SUSY spectrum.

The physics processes, their experimental signatures and the searches in the confining mass region are reviewed in [33] and references therein. A summary of the expectations concerning the production and the decays, i.e. the signature of SUSY particles at collider experiments at higher energies can be found in [33,36]. It is characteristic of collider searches that each analysis is optimized for the mass parameter space next to the previously excluded regions and the improved limits appear as slices on top of the previous results. As a starting point of the discussion one can thus cite the latest results [37,38,39] of the independent experiments and the highest limits as shown in Figure 5.

It can be then considered under which conditions the last limits of this additive procedure can be viewed as a summary of the all the work so far. One can ask whether the order of magnitude improvements in the search limits themselves, the other SUSY search limits and a better understanding of the standard processes in general could bring any new insight in the search

strategies, in particular in the experimental signature in direct searches. And finally one can study whether the LEP data could provide some new information about the topic.

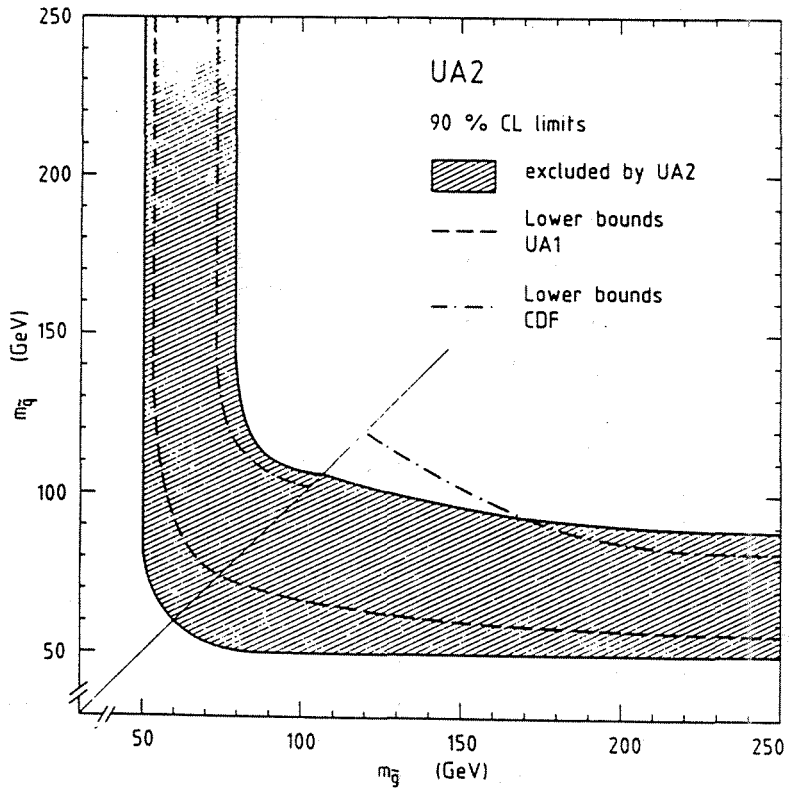


Figure 5: Squark and gluino mass limits deduced from the search for events with a large missing transverse momentum, by the UA2 experiment [39].

The collider limits have been deduced with the common assumptions on the supersymmetry and the SUSY particles, as follows.

1. R -parity is conserved i.e. the lightest supersymmetric particle (LSP) is a stable noninteracting particle.

2. It is assumed that the LSP is photino-like and the squark (the gluino) decays into the LSP and the quark (the gluon) directly i.e. they are the "next-to-LSP" particles. The relative masses of the squarks and the gluinos are not fixed. The analysis then results in correlated search limits of these two types of particles.
3. It is assumed that the LSP is much lighter than the squarks and gluinos.
4. A mass degeneracy is assumed in the squark sector, i.e. the masses of the scalar fields corresponding to the left and right handed quark fields (degenerate in mass themselves) as well as the masses of the various squark flavors are degenerate.

The first three assumptions are vital in validating missing energy (missing momentum) as an experimental signature of supersymmetry. The fourth assumption is used to enhance the expected rate of signal events. Originally, the assumptions have been somehow natural and even suggested by indirect experimental data. A good example is the expected mass degeneracy of squark fields which follows from the indirect bounds, i.e. studies of the virtual effects of possible SUSY particles in well understood and constrained physics phenomena.

The observed nonexistence of significant flavor changing neutral currents constrains the possible spectrum of supersymmetric particles (as many other proposed new physics beyond the standard model). The most stringent limits on the mass degeneracy within the two lightest generations of squarks arise from the measured parameters of the $K^0 - \bar{K}^0$ mass matrix [40]. Parity conservation in strong nucleon-nucleon interactions constrains the mass differences in the first generation left and right handed squark fields [41]. Also other processes and phenomena have been studied from which indirect bounds can be deduced [33]. It is speculated that the masses of squarks could be even within the width of the beam energy in e^+e^- colliders thus showing a sudden jump of the total hadronic cross-section in the continuum energy regions.

Concerning the hadron collider analyses, the mass degeneracy of squark fields is apparently necessary only to the extent that the quoted squark degrees of freedom have masses in the mass slice of squarks being probed in the analysis which ranges typically over several tens of GeV . Nevertheless, the assumption of having six squark flavors [38] in a short mass interval can be criticized. The special role of the superpartners of the third generation of quarks has been a subject of subsidiary theoretical discussions from their

first beginning. Due to the higher masses of the standard bottom and the expected top quark there are no such severe constraints on the mass degeneracy of the corresponding squarks - the top squark is especially subject to model speculations, because there is a mixing mechanism which generates an explicit mass splitting between the left and right handed components [42]. Even for the two lightest generations the argument of the mass degeneracy, constrained for example by the graphs in the $K^0 - \bar{K}^0$ mixing, is weakening if the gauginos are heavy. The direct experimental limits show that this seems to be the case. Similar discussions could be executed on the other indirect bounds on mass degeneracies.

Concerning the other three assumptions, the speculations on the R -parity have been mentioned above and those scenarios would modify the expected experimental signatures also in e^+e^- experiments at LEP I energies. As gradually higher mass regions of squarks and gluinos have been probed, the interesting possibility increases that there are several gaugino particles at masses below the squark or gluinos, invalidating the assumption of them being "next-to-LSP" particles. The effects of this possibility have been studied quantitatively [43,44]. The significance of suggested cascade decays spoiling the missing p_T signature turns out to be more severe at higher masses than being probed at LEP energies - essentially because there is no mass parameter space available for the additional gauginos below squark masses due to the existing limits.

In the early SUSY models the LSP was assumed to be massless and the photino was the most natural LSP candidate. As the models and their predictions have been analyzed in more details, particularly the neutralino sector has been studied in the hypothesis of common mass terms due to SUSY breaking, the nature of the LSP has become more complicated. The physical state could be a general mixture of neutral gaugino eigenstates. More importantly, it appears in the mass matrix containing other eigenstates which are apparently massive - thus the LSP itself naturally can be thought to have a mass. The argument for a possible massive LSP kinematically invalidating the experimental signature is trivial compared to the phenomenology of cascade decays (the argument is reviewed for clarity in Section 3.3) and its relevance to the hadron collider results has been analyzed [44,45]. The results can be summarized as the "50 % rule" of energy transfer in two-body decays of squarks: if the mass of the LSP is more than half of the squark mass the energy sharing of the decay is rapidly modified.

The actual effects of releasing the assumptions 1)-4) partially depend on the imposed experimental selections and have to be studied case by case, as

done for example in [39]. In conclusion, the searches for strongly interacting SUSY particles (the scalar quarks which are produced in pairs) in the e^+e^- annihilations can provide new information on the topic in spite of the limited mass region accessible. The high cross-section and the characteristic electroweak couplings achieved on the Z^0 pole enhance the potential at LEP I for realizing the arguments given in Section 1.2.

One of the interesting features of the LEP I data is the pair of complementary methods that can be used to search for scalar quarks. They can be searched directly from the data i.e. as individual events which exhibit a distinctive signature (missing energy carried by the noninteracting stable LSPs in the final state) and are separated from the background by using selection criteria (acollinearity or analogous variables, see Section 3.3). This procedure has been well tested in the several e^+e^- experiments at lower center-of-mass energies and the reapplication at LEP has been quite straightforward. At LEP, the more hermetic tracking and calorimetry in the new detector systems make the searches even easier than before. The modified couplings at the Z^0 resonance allow also for limits to be set for the single down type of squarks (electric charge $-1/3$) which have not been probed with the same sensitivity in photon mediated annihilations due to their lower production cross section.

The second approach is to compare the measured Z^0 widths with the predictions of the standard model. This possibility arises as the line shape parameters of the Z^0 resonance i.e. the physical mass and the lifetime of the Z^0 particle and the hadronic partial width (the peak cross-section) are precisely measured. Apart from the relations of these experimental quantities with several basic parameters of the standard model - the number of light neutrino species, for example [9,10], the parameters can be interpreted in terms of potential new particles. Any new particle degree of freedom coupled to the Z^0 particle would typically increase the total width and enhance also the experimentally measured partial width(s) - which the observed (or invisible) final state of this channel would imitate. In the case of an absence of distinguishable deviations one can set a conservative limit for the existence of such a particle with the hypothesis that the potential additional width would arise due to this specific particle type alone. The logic resembles many previous phenomenological studies in which the virtual effects of exotic particles have been searched for in well understood physical processes. The merit of the LEP I bounds compared with the other indirect constraints is the very transparent model independence of the results.

3.2 Introduction to the squark search in Z^0 decays

The first physics runs of the recently commissioned LEP collider provided the four experiments with data samples containing unforeseen high statistics of Z^0 decays. Each order of new data reduced the statistical and experimental systematic uncertainties, as the understanding of the detector and the data increased. Because the hadronic branching ratio of the Z^0 decays is large, the analysis proceeded most rapidly in terms of the hadronic events resulting from the data collection at various center-of-mass energies around the Z^0 resonance (scanning of the Z^0). This program of LEP runs was devoted to the collecting of data for measurements of the Z^0 resonance parameters but the data was also well suited for the other analysis purposes, for example fragmentation studies, QCD tests and the direct searches for new particles.

The experimental analysis utilizing the data proceeds in two complementary lines:

Approach 1): Analyze the data in terms of expected event topologies, this is, select the data sample to contain standard events ($e^+e^- \rightarrow$ hadrons, for example). Determine (measure) (a) parameter(s) characterizing the sample and conclude the physics result.

Approach 2): Focus on the significantly nonstandard events which exhibit a signature which could be associated with a new physics channel, determine the significance of the rate of the signal events with respect to the known sources of background events. Conclude a discovery, or explain the signals as background and deduce a search limit by using the expectations for the new physics in a given model.

In the analysis of both type, possible significant systematic uncertainties have to be explored and eliminated. The approach aiming at a measurement must avoid bias in the result due to faulty data selection or because the correctly analyzed data (i.e. the experimental effects properly eliminated) is misinterpreted due to unexpected physical features in the data. In data samples tagged in direct searches for new phenomena, one must consider the relevant systematic effects which are most naturally determined in analysis of the bulk of standard events. In practice both of the approaches converge to the same problem, namely the understanding of the detector and the experimental conditions.

The search for scalar quarks in the data sample consisting of hadronic events with very low visible energy is an extreme example of a direct search. Such a large sample in the recorded DELPHI data has drastically

different characteristic compared to the expected hadronic Z^0 decays. A significant fraction of them were naturally rejected as uninteresting in the event selections of many other physics topics of Z^0 decays.

The hadronic events with very low visible energy (see characterisation in the selection criteria of the appended paper 1) are usually interpreted either as triggers due to the beam particle interactions with the remaining gas molecules in the beam pipe or with the beam pipe itself (off-momentum beam particles). These events imitate true events when they occur at the interaction point. The standard Z^0 decays could exhibit similar characteristics if reconstructed only fractionally due to the instrument or the data analysis. The physical background consists of the second order QED process of t -channel interaction of the electrons and positrons (two photon interactions with hadronic final states).

These events could also result from nonstandard Z^0 decays in which a very large fraction of the center-of-mass energy is carried away by invisible particles, for example by the heavy LSPs in the squark decays or other similar topologies. Such a possibility has been pointed out in the searches for heavy sequential charged leptons in e^+e^- experiments [46].

At LEP energies around the mass of the Z^0 particle, the visible energy spectrum of these signal events and the standard events is distinctly different, compared to the situation at lower center-of-mass energies. The small overlap, however, constitutes a systematic uncertainty in the measurement of the hadronic cross section. The study of the low visible energy events is connected to the analysis of the systematic uncertainties in the measurement of the Z^0 resonance parameters through its hadronic decays and the fit of the number of light neutrino species. Understanding the low visible energy tail of the multihadronic events is thus a necessary precaution for this measurement.

The method which compared the low visible energy tail at each center-of-mass energy separately (differentiation) has an additional merit of testing explicitly the possibility of having physical (Z^0 coupled) background. In this way the uncertainty due to potential new physics in the measurement of the resonance parameters was further reduced.

The procedure then points out systematic uncertainties that are related with the indirect limits of new particles extracted from the width measurements of the Z^0 particle, for example in [47]. If partial widths of the Z^0 particle are used in an analysis it is usually assumed that the contribution of the new component is fully contained in the measured partial width which actually involves the experimental selection criteria optimized to the standard expectations. In the hadronic scan at the Z^0 resonance a very high efficiency

for the standard events was achieved but their efficiency is reduced for events exhibiting significantly different experimental signature. For scalar quarks, for example, this arises as the events at low end of the spectrum of the visible energy are cut out by the selection criteria for standard hadronic events and the visible contribution in the hadronic partial width is reduced even in case of the massless LSP.

The discussions of the three last Sections can be summarized as follows:

- Supersymmetry is theoretically well motivated. At LEP, the gaugino sector has been extensively and systematically examined and a significant part of the parameter space of the most favourite models has been excluded. The experimental searches have concentrated on the the leptonic channels. The searches for strongly interacting supersymmetric particles appear as a complementary analysis.
- The advances in the search for supersymmetry (both experimental and theoretical) have generated critical considerations of the experimental signatures assumed. Apart from the true modifications in the expected phenomenology (R -parity, cascade decays) varying masses of the produced new particles cause different event signatures due to kinematics.
- The study of low visible energy events has also purely instrumental motivations, i.e. the understanding and evaluation of detector performance in the most common final states.
- The study of low visible energy events as a potential signature of new physics affecting the determination of the number of light neutrino species (a systematic bias in the optimization and the determination of the selection efficiency used in the hadronic scan).
- The analysis procedure discusses systematic uncertainties present in the determinations of indirect bounds for new particles by utilizing LEP results on the partial widths of the Z^0 particle.

3.3 The massive LSP as a kinematical effect on the missing energy signature

The following is a discussion of the effects of the massive LSP on the missing energy signature utilized for example in SUSY searches. As an example, the case of two-body decays of squarks (decaying into a standard quark and a

LSP) produced in the final state of e^+e^- annihilations are considered. Since the discussion is based on kinematics, the remarks apply to other similar topologies as well.

3.3.1 Acollinearity and missing transverse momentum

The missing energy signature arises in high energy particle interactions when short lived particles are produced which decay into standard particles and stable and noninteracting (electrically neutral and not strongly interacting) particles which thus do not generate a signal in the detector (the LSP in the supersymmetry case). The reconstructed events appear kinematically incomplete, the total reconstructed energy does not sum up to the center-of-mass energy and the three momenta in the laboratory frame do not cancel - except for the random case in which the invisible particles escape in opposite directions ("back-to-back").

At hadron and e^+e^- colliders, the three momentum imbalance is experimentally more applicable than the scalar total energy. In hadron collider data samples of the wide band parton center-of-mass energies, event variables which are sensitive to large missing transverse momentum with respect to the colliding beams ($/p_T$) are utilized (typically the energy flow seen in the calorimetry). In e^+e^- experiments, the center-of-mass of the events is at rest in the laboratory frame and a good measure of the momentum imbalance is the acollinearity defined for example in [48]

$$\alpha_{\text{acoll}} = 180^\circ - \theta(\vec{p}_1, \vec{p}_2) \quad (4)$$

$\theta(\vec{p}_1, \vec{p}_2)$: the angle between the resultant vectors $\vec{p}_{1,2}$ which are summed up of the three momenta of particles in each event hemisphere defined by the thrust axis; if there are no particles in either of the hemispheres (monojet) $\alpha_{\text{acoll}} = 180^\circ$

Sometimes transverse components of the three momenta (with respect to the beam axis) have been preferred in order to reduce the sensitivity against physical background due to the second order QED processes (two-photon interactions boosted usually in the beam directions) and against the worse momentum resolution in forward-backward directions.

The purpose of utilizing acollinearity is to separate the signal events from the background of standard multihadronic events. A high selection efficiency

($O(50\%)$) is typically achieved with a negligible background by requiring the candidates to show acollinearity $\alpha_{\text{acoll}} > 45^\circ$. The merit of the conducted searches is that the separation is based on the pure kinematical effect, i.e. the model dependence is trivially minimal (apart from the assumption of conserved R -parity). Standard events can contaminate the signal only in cases of instrumental failures in event reconstruction (for example by not detecting hard radiative photons) and these are controllable in general purpose detectors.

In order to eliminate all the background originating in other sources than the annihilations one has to apply selections which effectively reject events of very low visible energy (or low multiplicities or invariant mass). They unavoidably enter in the e^+e^- data as multihadronic events from the second order QED processes (two photon interactions) and from the unphysical triggers due to the machine background (see Section 1.3). Their rates are implicitly affected by the reduced trigger efficiency. The trigger systems are designed to the expected event topologies in the first place. The manageable total event rate often prevents to increase the sensitivity of the trigger to significantly nonstandard events, which were often thought to be unphysical, particularly in the early experiments. The significance of the efforts to observe efficiently this class of events with diminishing total energy (or invariant mass) and to resolve them arise from the fact that at mass parameters $M_{\text{LSP}} \rightarrow M_{X^\pm}$, (X^\pm is the decaying massive particle), the experimental signature approaches this limit.

In the search published in [49], a variant definition of acollinearity utilizing a jet cluster finding algorithm is applied with a condition of observing two jets (the acollinearity is defined as the complement angle between them). As a relatively high invariant mass (effectively $m_{\text{inv}} \simeq 12 \text{ GeV}$) of the jet system is required, many events with a low visible energy (or monojet type of events) drop out of the candidate sample and the low energy limit is effectively left intact (noted also in the analysis). Additional rejection may result from preselection of the charged multiplicity. In the recent analysis [50] events with visible energies down to $E_{\text{vis}} > 0.1 \times E_{\text{C.M.S.}}$ have been included. In general, the effects of massive invisible particles modifying the applied signature have not been explicitly discussed in the results referred to. The trigger efficiencies are quoted only in the default topology. The significant variations in the selection efficiencies are not acknowledged. As some of the searches have been executed in knowing the results from hadron colliders, the physics value of the searches utilizing e^+e^- data would particularly have been explicitly exploring this region of the

mass parameter space which is physically inaccessible in hadron colliders.

3.3.2 Visible energy and acollinearity in decays of pairly produced heavy particles into massive invisible particles

The pair production of heavy scalar particles subsequently decaying into two particles and the relevant kinematical quantities are described in Figure 6. The energy carried by the visible part of the final state particles in the two-body decay of a heavy particle is

$$E_{\text{vis}} = \frac{E_{\text{C.M.S.}}}{2} \left[1 - \frac{M_0^2}{M_{\pm}^2} \right] \{1 + 1/2\beta^* (\cos \theta'_1 + \cos \theta'_2)\} \quad (5)$$

$$\beta^* = P_{\pm}^*/E_{\pm}^* = \sqrt{1 - \frac{4M_{\pm}^2}{E_{\text{C.M.S.}}^2}} \quad (6)$$

$\cos \theta'_{1,2}$: distributed uniformly for scalar decays

in which the mass of the visible particle is assumed to be negligible.

The distribution is shown in Figure 7. The quadratic dependence on the mass of the missing particle guarantees that the selection efficiency is maintained when the mass of the invisible particle is less than half of the decaying particle. Above this level the selection efficiencies (and possibly trigger efficiencies) should be apparently evaluated as free parameters. In case of spinless decays, the average visible energy does not depend on the boost (mass) of the decaying particle. The tail of the wide spread distribution at low decaying masses reduces the selection efficiency only to a minor extent.

For the acollinearity distribution, the decay angles $\theta'_{1,2}$ between the visible three-momenta and the production axis in the over all center-of-mass frame after a straightforward Lorentz transformation [51] are expressed as

$$\begin{aligned} \cos \theta'_{1,2} &= \frac{\gamma^* (\cos \theta'_{1,2} + g^*)}{\sqrt{\gamma^{*2} (\cos \theta'_{1,2} + g^*)^2 + \sin^2 \theta'_{1,2}}} \quad (7) \\ \gamma^* &= E_{\pm}^*/M_{\pm} = E_{\text{C.M.S.}}/2M_{\pm} \\ g^* &= \beta^*/\beta' = \frac{P_{\pm}^*/E_{\pm}^*}{P'_{1,2}/E'_{1,2}} < 1 \\ &= \beta^* = P_{\pm}^*/E_{\pm}^*, \quad \text{when } m = 0 \end{aligned}$$

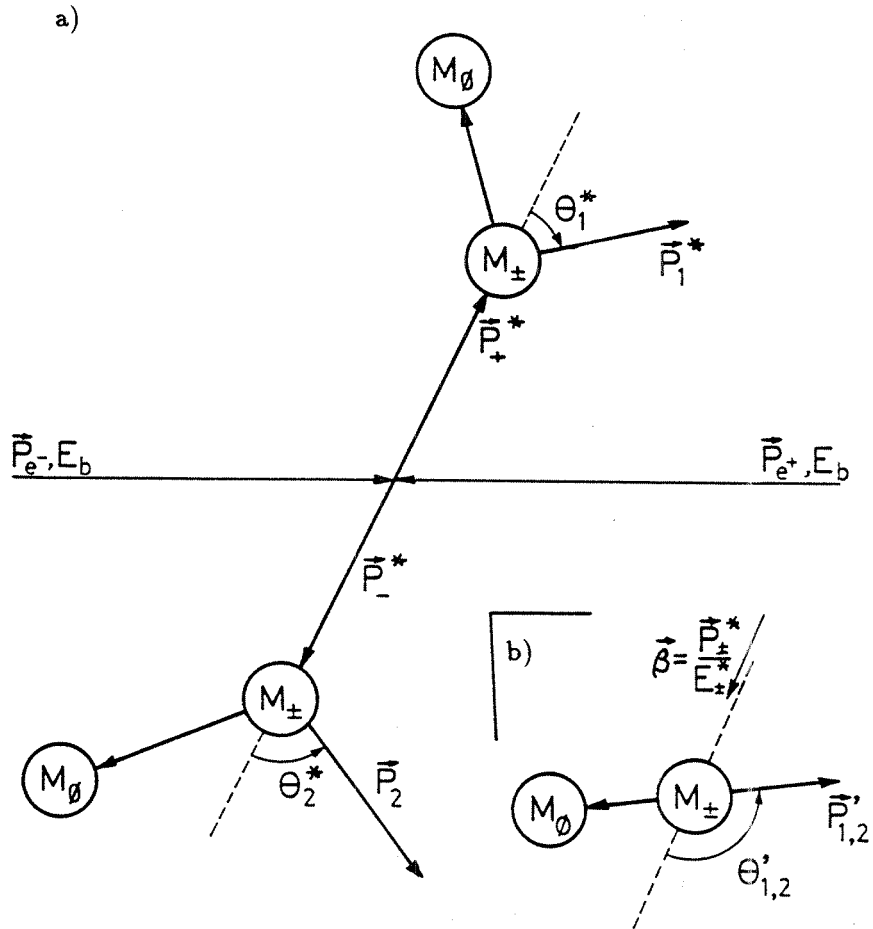


Figure 6: Kinematics of the two body decays of massive particles produced in pairs in e^+e^- annihilation. The kinematical quantities in the production center-of-mass frame are shown in a), and the quantities in the rest frame of the other decaying particle are shown in b).

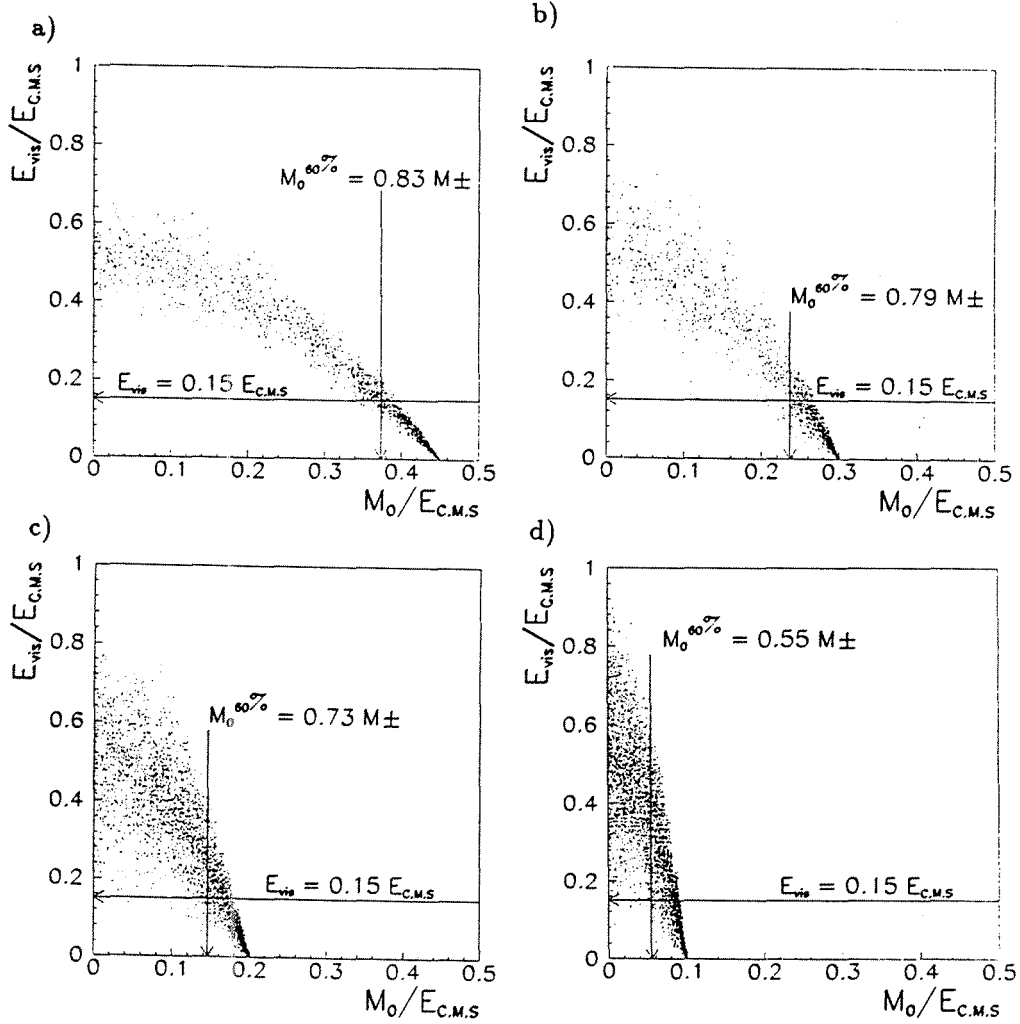


Figure 7: Distributions of the visible energy in two body decays of scalar quarks (see Figure 6) as a function of the mass of the invisible LSP. Several cases corresponding to the masses of the decaying particles a) $M_{\pm} = 0.45 E_{C.M.S.}$ b) $M_{\pm} = 0.30 E_{C.M.S.}$ c) $M_{\pm} = 0.20 E_{C.M.S.}$ d) $M_{\pm} = 0.10 E_{C.M.S.}$ are plotted. The vertical arrows show the value of invisible mass at which the selection efficiency utilizing a lower energy cut $E_{\text{vis}} > 0.15 \times E_{C.M.S.}$ is reduced to 60 % of the nominal case in which all events showing acollinearity more than 45° are selected.

The acollinearity angle $\cos \alpha_{\text{acoll}} = -\cos \theta_1^* \cos \theta_2^* + \sin \theta_1^* \sin \theta_2^* \cos(\phi_+^* - \phi_-^*)$ is thus distributed as (decays assumed to be independent of each other)

$$\cos \alpha_{\text{acoll}} = \left[\gamma^{*2} - (\cos \theta_1' + g^*)(\cos \theta_2' + g^*) + \sin \theta_1' \sin \theta_2' \cos(\phi_1' - \phi_2') \right] \times \left[\gamma^{*2} (\cos \theta_1' + g^*)^2 + \sin^2 \theta_1' \right]^{-1/2} \left[\gamma^{*2} (\cos \theta_2' + g^*)^2 + \sin^2 \theta_2' \right]^{-1/2} \quad (8)$$

$\cos \theta_{1,2}', \phi_{1,2}'$ uniformly distributed for spinless decays

The distributions of the average acollinearity as a function of the mass of the decaying particle are shown in Figure 8 in the case of a visible particle with negligible mass. The acollinearity distribution does not depend on the mass of the invisible particle. Instead, it depends on the boost of the decaying particle (approaching tau like decays if objects which are light in comparison to the beam energy are being examined).

3.3.3 Discussion

Formulae 5 and 8 show that the dependence of the selection efficiency at various mass parameters on the cuts on acollinearity and lowest visible energy are apparently factorizable. This fact simplifies the determination of the search limits which are subsequently deduced from the selection efficiencies at various masses and from the expected production cross-section. In particular, the systematization reduces the potential uncertainties entering in this phase, for example due to the coarse grid of the mass configurations applied in the Monte Carlo studies or due to their being wrongly interpreted.

The mass limit along the diagonal $M_{LSP} \simeq M_{X_{\pm}}$ utilizing the method of acollinear jets is determined by the diminishing efficiency, in particular when the mass of the decaying particle X_{\pm} is significantly smaller than the beam energy. In this case the selection efficiency is affected already when the mass of the LSP is about half of the decaying mass (see Figure 6).

The case of searching for light pairly produced and unstable particles is an interesting kinematic limit itself. It becomes particularly relevant at LEP because the exceptional couplings allow us to search for new types of particles in the full kinematical accessible range, i.e. for particles not looked for in other colliders due to their small or vanishing couplings. The d type of squark is the closest example here, but more generally the kinematical effects in searches for pairly produced neutral SUSY or other exotic particles at LEP have not been identical to the analogous searches for charged particles in which the low mass region is checked by earlier results.

The low mass of the decaying particle constrains the distribution of the acollinearity and at the limit the signature approaches the one of $\tau\bar{\tau}$ events. Because of the domination of multijet events at LEP, due to fragmentation effects and due to the presence of heavy quarks (c and b) it is not apparent that a hypothetical heavy parton state inside the hadronic jets would be resolved with such a simple criterium as acollinearity, particularly if produced at rates not exceeding the indirect constraints on the hadronic width of the Z^0 particle. The leptonic channels allow the searches closer to the kinematic limits [52], but there attention has to be given to the reconstruction of the final state photon radiation.

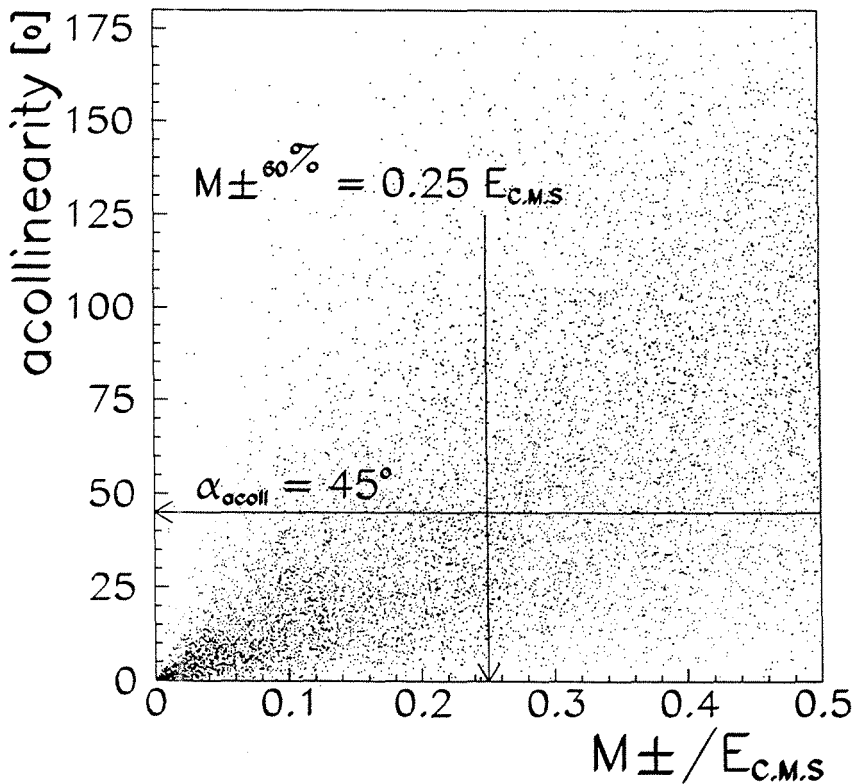


Figure 8: Distributions of the acollinearity angle in the two-body decays of scalar quarks (see Figure 6). The arrow labelled as 60% M_{\pm} shows the value at which the selection efficiency given by the cut $\alpha_{\text{acoll}} > 45^\circ$ is reduced to 60 % of the nominal value.

3.4 Comments on the executed search

Some aspects of the conducted analysis are reviewed here in more detail than in the original letter, especially because the first method utilized in the search for scalar quarks in Z^0 decays has not been conventionally applied in the SUSY searches. The aspects are chosen here as the topics which were extensively discussed in the preparatory phase of the analysis or commented by the collaborators during the evaluation of the analysis and circulation of the manuscript of the original letter.

3.4.1 Expected signature, model dependencies and the correspondence to the selected candidates

The characteristics of the signal events was studied by a squark pair production Monte Carlo generator [53] interfaced with the detailed DELPHI detector simulation program [54]. Apart from the unambiguously predetermined distributions of the production angles and the decay kinematics of scalar quarks, the fragmentation and hadronization of the intermediate state was described by choosing the JETSET package version 7.2 [59]. The (anti)squark was first allowed to decay into the LSP and a standard (anti)quark and the remaining quark-antiquark system was subsequently fragmented in its rest frame and finally boosted to the laboratory frame. The choice is one of the safest in practice, because quark systems with center-of-mass energies down to few GeV can be consistently fragmented within JETSET package. The selection criteria of the analysis are essentially sensitive to particle multiplicities and their momentum spectra only, thanks to the simplicity of the criteria. The charged particle multiplicities and their momentum distributions in the model are fitted to the real data and known to agree even at the very low center-of-mass energies [60]. The trigger efficiency and the selection criteria profit from the fact that the expected final state is a multiprong topology (several charged particles) to the limit of the investigated mass difference. The produced Monte Carlo samples and the extracted results are summarized in Table 1. The chain of the detector simulation and the analysis program which was the same as used in the reconstruction of the real data has been shown to reproduce well the characteristics of the charged tracks in hadronic final states of the data sample [6].

$(M_{\tilde{q}}, M_{LSP})$ (GeV)	# events	tr. eff.		sel. eff.	tot. eff.
		(data)	(DELTRIG)		
<i>(10,06)</i>	2000	0.90 ± 0.10	-	0.12 ± 0.01	0.11 ± 0.02
(20,18)	500	0.70 ± 0.3	0.67 ± 0.03	0.57 ± 0.03	0.38 ± 0.06
<i>(20,01)</i>	2000	0.95 ± 0.05	-	0.10 ± 0.01	0.10 ± 0.02
(30,28)	958	0.62 ± 0.3	0.51 ± 0.04	0.44 ± 0.02	0.22 ± 0.05
(30,26)	699	0.80 ± 0.3	0.74 ± 0.03	0.49 ± 0.03	0.36 ± 0.07
(30,24)	500	0.78 ± 0.3	0.83 ± 0.02	0.47 ± 0.03	0.39 ± 0.08
<i>(30,20)</i>	2000	0.88 ± 0.2	-	0.26 ± 0.01	0.23 ± 0.05
<i>(30,15)</i>	2000	0.92 ± 0.1	-	0.12 ± 0.01	0.11 ± 0.01
<i>(30,10)</i>	2000	0.95 ± 0.05	-	0.07 ± 0.01	0.06 ± 0.01
(40,38)	1000	0.48 ± 0.3	0.37 ± 0.01	0.34 ± 0.02	0.13 ± 0.03
(40,36)	200	0.70 ± 0.3	0.70 ± 0.05	0.56 ± 0.05	0.39 ± 0.08

Table 1: Combination of the trigger and selection efficiencies in the search for squarks and massive LSPs. Values for the selection efficiencies (of the method applied for the heavy LSP) are based on the full simulation (bold face, errors statistical) or generation simulation (italics). For the trigger efficiencies measured trigger efficiency is taken as the average total charge energy of the signal (errors are estimates of the systematic uncertainty). The DELTRIG efficiency is calculated for a subsample of each simulated sample which satisfies criteria equivalent to the selection criteria of the analysis. In addition the selection efficiencies were calculated for the second selection based on acollinearity utilizing the same data and an extra sample of 2000 events at masses (30,02).

The expected production cross section is most conventionally expressed proportionally to the standard neutrino production cross section (significant radiative effects are thus accounted for)

$$\sigma(e^+e^- \rightarrow \tilde{q}_{i,f}\bar{\tilde{q}}_{i,f}) = 1/2 \times \sigma_{\nu\bar{\nu}} \times \beta^3 \times N_c \times C_{i,f} \quad (9)$$

$\sigma_{\nu\bar{\nu}}$ is the physical cross section of a neutrino generation at Z^0 peak, N_c is a colour factor 3, $\beta = \sqrt{1 - \frac{4M_{\tilde{q}}^2}{E^2_{\text{C.M.S.}}}}$. The coupling coefficients $C_{i,f}$ and the resulting peak cross sections are summarized in Table 2.

Because the method aimed at maintaining a high efficiency to the potential signal and the differentiation as a function of the beam energy was applied instead, in order to understand and eliminate the existing backgrounds, sizable candidate samples (284 events in the final selection,

flavour and chirality	coupling $C_{i,f}$	peak cross section [nb]
u_L	$4 \left(1/2 - 2/3 \sin^2 \theta_W\right)^2$	$2.09 \beta^3$
u_R	$4 \left(2/3 \sin^2 \theta_W\right)^2$	$0.388 \beta^3$
d_L	$4 \left(-1/2 + 1/3 \sin^2 \theta_W\right)^2$	$3.09 \beta^3$
d_R	$4/18 \left(\sin^2 \theta_W\right)^2$	$0.0969 \beta^3$

Table 2: Coupling constants for the up (u,c,t) and down (d,s,b) type squark pair production and expected rates at the Z^0 peak. $\sin^2 \theta_W = 0.226$ for the weak mixing angle and $\sigma_{\nu\bar{\nu}}^{peak} = 2.854 \text{ nb}$ are used.

one of them visualized in Figure 9) were considered. The basis of the search strategy was being probed by the question whether the selected events roughly resembled the expected signal events, allowing some uncertainty because the sample was known to contain a fraction of events of other understood origin. In this analysis, this question conceptually replaces the discussion of the systematic uncertainties in other direct searches due to the selection steps which eliminate the candidates completely (as background). The correspondence between the selected candidates and the expectations is relevant because of the extensive studies of nonuniform selection and trigger efficiencies in which the real candidate events were differentiated in the same way as the simulated data, namely as functions of various event variables (total charged visible energy, for example). Satisfactory results were reached in this respect, for example by comparing the distributions of various event variables of the generated Monte Carlo samples and the real data, and by event viewing. The selected real candidates resemble mostly the events with the mass of the LSP very close to the squark (events of small visible energy dominate the sample). An example of the comparisons of event variables is shown in Figure 10 in which the thrust distribution and the inclusive momentum distribution of charged particles of the a Monte Carlo sample and real data are plotted (see also the discussion of the trigger efficiencies later).

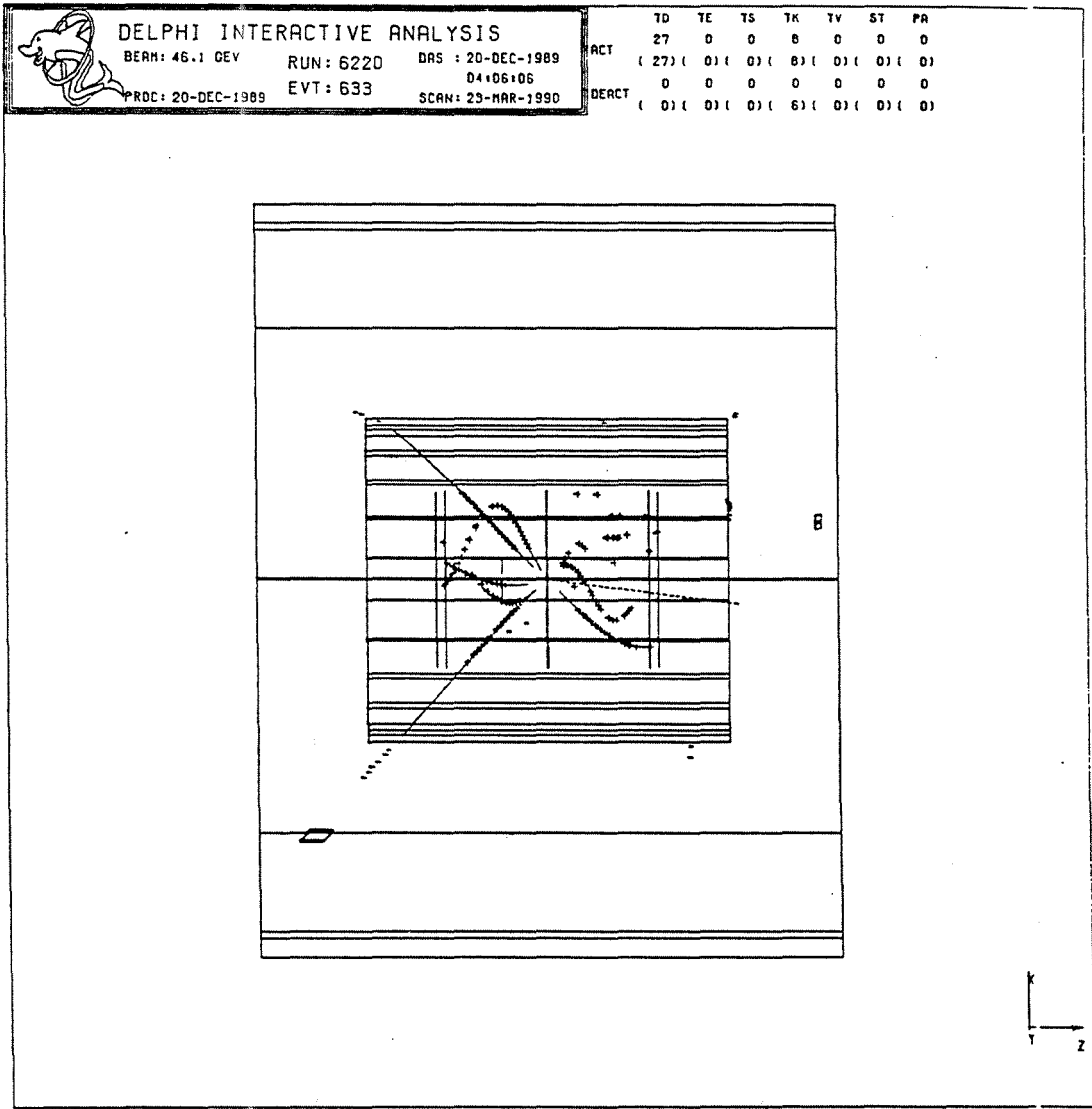


Figure 9: Example event in the selected squark candidate sample.

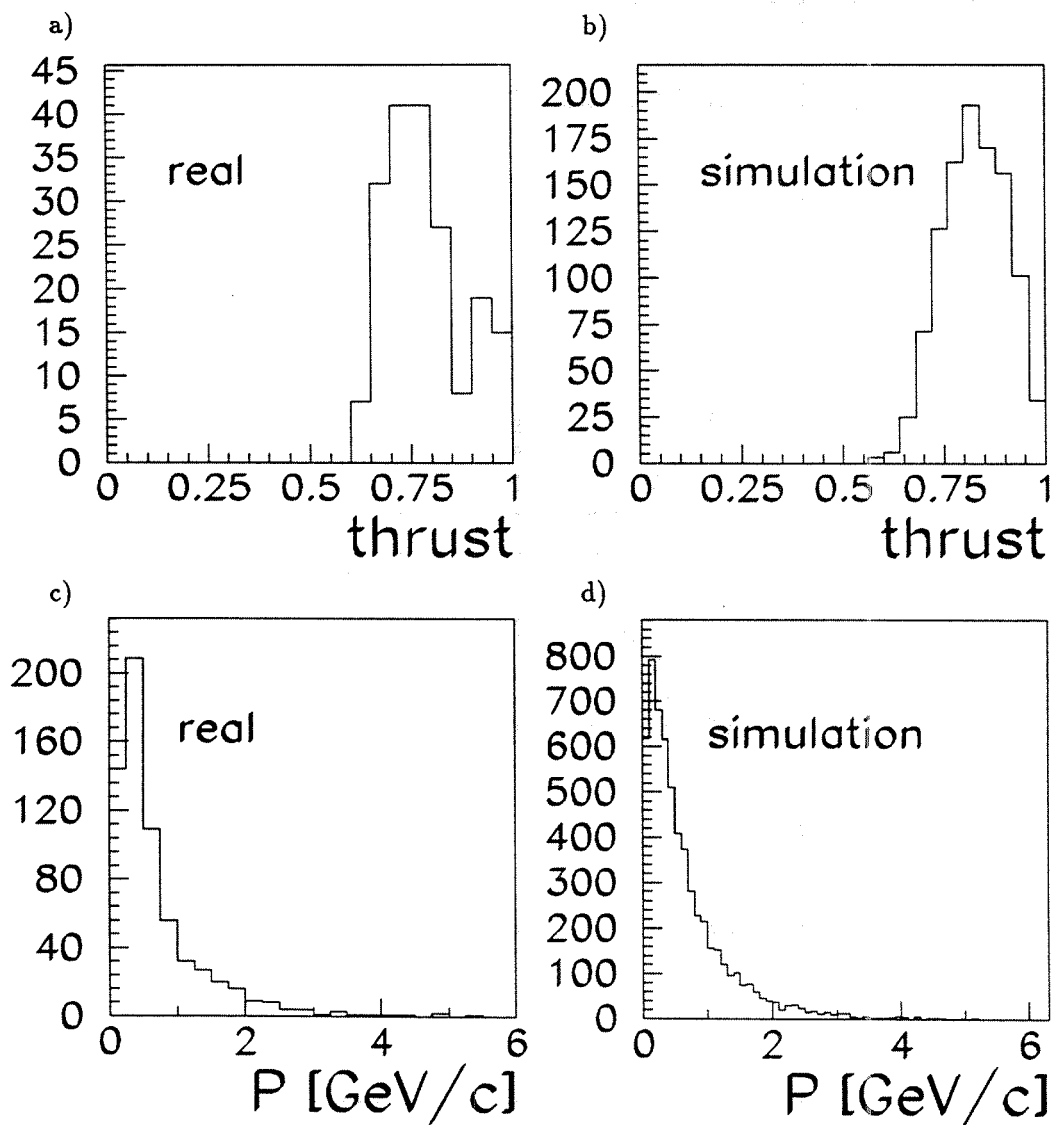


Figure 10: Distributions of the thrust and the momentum of charged particles of the real candidate events selected (a) and c), respectively) and from the expected signal events in the Monte Carlo simulation (b) and d), respectively).

In the executed search, a configuration was discussed in which the gluino is heavier than the produced squark (i.e. the decay $\tilde{q} \rightarrow q LSP$ dominates). The consideration of the opposite case was omitted because of simplicity in the first place (to emphasize the role of e^+e^- data providing us with the complementary information about the massive LSP). Also, qualitatively we can argue that the possibility of having the gluino lighter than the squarks as such is well excluded by the hadron collider results, and even if existed (for example as a single flavour of light squark) it would have been observed with a high efficiency in the parallel searches which utilized event variables like sphericity and thrust which look for hadronic final states with high mass intermediate decays at LEP (b' and top quarks [61]).

It is interesting to notice that as the mass of the LSP approaches to the one of the squark, the life time of the squark increases [33]⁴. At the zero mass of the LSP the hypothesis of squark decaying faster than fragmentation of the parton system is acceptable. At the limit $M_{LSP} \rightarrow M_{\tilde{q}}$ fragmentation may occur faster than the supersymmetric decay and supersymmetric hadrons (R -hadrons) should emerge with their characteristic decays. However, this possibility does not modify the distributions of the total visible energy (determined by kinematics). The spectrum of charged particles would be harder as it takes place in the decays of heavy mesons.

3.4.2 Evaluation of the trigger efficiency

The variation of the trigger efficiency on the visible energy, especially in the limit of low visible energy must be taken into account when the total detection efficiency is determined for search limits. The DELPHI trigger system is described in [18] and [10]. There is a good redundancy which allowed to study the efficiencies utilizing the real data. In addition, the DELPHI trigger simulation were used to examine the sensitivity to topological effects of expected signal events.

The barrel track trigger in the DELPHI detector was constrained by the back-to-back condition in the data samples under study. As the expected events apparently do not show the collinear jet structure because of the escaping LSPs and because of fragmentation effects, their trigger efficiency could be affected, or the evaluation of the efficiency could be biased when using real candidates with possibly different topological properties. This was

⁴ $\Gamma(\tilde{q} \rightarrow q LSP) = \alpha e_q^2 (M_{\tilde{q}}^2 - M_{LSP}^2 - m_q^2) p_q / M_{\tilde{q}}^2$, $M_{\tilde{q}, LSP, q}$: masses of the squark, LSP and quark, respectively, p momentum of the quark in the rest system of the squark.

demonstrated not be dominant by differentiating the trigger efficiency of the real candidate sample as a function of acollinearity, seen in Figure 11. For comparison, the efficiency is also plotted for events containing two charged particles. It is concluded that the trigger efficiency is largely maintained even for the acollinear events and the sensitivity to this topological feature is thus reduced. For lepton like two prong events the effect of the back-to-back constrained trigger has to be accounted for.

3.4.3 Time dependent effects and the run selection

The data samples utilized in this analysis correspond to the data referred in [10] in which the run selection sums up to the integrated luminosity of 573 nb^{-1} . The run selection applied there optimizes the measurement of the standard hadronic cross section at various center-of-mass energies around the Z^0 resonance. It is based on systematic cross-checks on the time dependent effects in the quality of the data. Thus it is of value to all other analyses of the same data, and was also applied in this analysis. The integrated luminosity of 330 nb^{-1} introduced in this analysis results from the specific run selection applied in order to control the systematic uncertainties due to trigger.

The characteristics of the events studied in this analysis (very low visible energy) deviates drastically from the standard hadronic Z^0 decays, especially the rate of selected events depends on the specific components of the trigger configuration. This is why a parallel systematic check was executed resulting in a more severe run selection in which the time dependent effects of the track trigger were eliminated.

The check was executed utilizing the possibility to trace back the active trigger bits in each event. The efficiencies of various trigger components were calculated for each run and those runs showing significant reduction ($\sim 30\%$) of the averaged efficiency for events of the type used in the final analysis (enhanced by the hadronic Z^0 decay candidates) were rejected.

It appeared that in this way many runs in the beginning and at the end of the machine fills were rejected. This reduced also the uncertainties due to the varying machine background rates, because they are often high and rapidly changing when the beams are being stabilized. The rejection of these samples is more significant in this analysis than in case of standard Z^0 decays because the standard selection criteria eliminate the machine background efficiently.

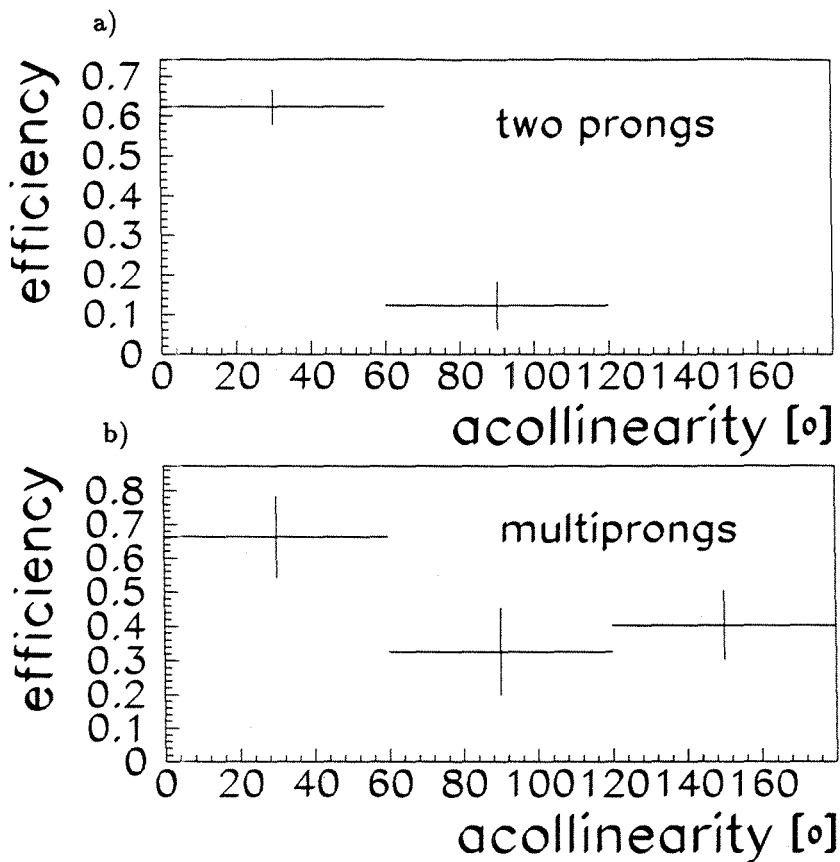


Figure 11: The efficiency of the DELPHI barrel track trigger for the selected candidate events at low visible energies as a function of the acollinearity, a). For comparison, the efficiency is also plotted for events containing two charged particles b), in which the effect of the back-to-back condition in the track trigger is apparent.

4 CONCLUSIONS

The functions of calorimetry in general purpose detectors are versatile. In complementing the event information of the tracking detectors, subsequent layers of electromagnetic and hadronic calorimeters particularly suit the identification aims of the DELPHI detector.

The performance of the DELPHI Hadron Calorimeter is typical of an iron sampled gaseous calorimeter. It responds linearly to hadronic showers in the energy interval $10 - 60 \text{ GeV}$. It is undercompensated with the signal ratio $\pi/e = 0.7$, and this affects the energy resolution. The passive material seen by hadrons traversing the inner parts of DELPHI and the electromagnetic calorimeters before the Hadron Calorimeter worsen the effective energy resolution. As far as electron and muon identification are concerned, the DELPHI calorimeter system with adequate thickness in radiation and interaction lengths, with high granularity and multilayer signal read out, with low signal pedestals and with hierarchical pattern recognition algorithms optimized for the inclusive particle reconstruction provide us with efficient information over the maximal coverage of the solid angle.

In agreement with the experiences gained in other LEP experiments, it has been observed that this kind of geometry of a general purpose detector accompanied with the reconstruction chain which has been optimized for single particles, does not directly reconstruct kinematically complete multihadronic final states in e^+e^- annihilations.

The strongly interacting sector of the supersymmetric particles has been explored in the search for scalar quarks in Z^0 decays as events with a missing energy signature. In order to maximally cover the parameter space of the free masses of the squarks and the lightest supersymmetric particle (LSP), two methods were utilized. The conventional selection distinguishes the signal events from the background of standard multihadronic events as acollinear jet structures with a significant imbalance in momentum. This method proves to be inefficient in the case of massive LSPs for which the experimental signature evolves to events with vanishing visible energy. A complementary method was introduced here in order to resolve the existing backgrounds which are well recorded due to the redundant trigger arrangement of DELPHI. This approach profits from the exceptional characteristics of the LEP data collected at center-of-mass energies around the mass pole of the Z^0 boson. As a result of these direct searches, new lower limits near the kinematic limit of the LEP I data i.e. $42 \text{ GeV}/c^2$ for the single up type of squarks and $43 \text{ GeV}/c^2$ for the single down type of squarks, were set

allowing for arbitrary masses of the invisible LSP up to $M_{\tilde{q}} - 2 \text{ GeV}/c^2$ over the majority of the squark mass interval with an explicit discussion of the nonuniform efficiencies.

In addition to gaining understanding for physical interpretations of the events of very low visible energy, the studies helped in mapping the detector performance and the quality of the data. By investigating data samples which are larger than those usually selected for other physics topics, the understanding of the data which is a prerequisite to the control of systematic uncertainties is increased. The measurement of the rate of low visible energy events at various center-of-mass energies could be used for cross-checking the systematic uncertainties in the measurement of the Z^0 resonance parameters utilizing hadronic final states, and thus the uncertainties in the fit of the number of light standard neutrino species. Finally, the explanatory case of evaluating the experimental signature of strongly interacting supersymmetric particles demonstrates the systematic uncertainties present in the indirect limits which have been deduced for new particles from the measured partial widths of the Z^0 boson.

The results from the high statistics LEP data have drastically improved the precision of the basic free parameters of the Standard Model, and they have significantly constrained the most popular scenarios of the new physics beyond it. The model is being verified at the level of quantum corrections thus conceptually approaching the status of quantum electrodynamics. The current picture of elementary matter, the $SU(3)_c \times SU(2)_L \times U(1)_Y$ structure of fundamental interactions appear as a nearly complete system - mixtures or couplings of the Z^0 particle to hypothetical new elementary structures are apparently small. Still, the origin of masses is still to be explained (the question of existence of the Higgs particle(s) or a corresponding mechanism) and the matter and the gauge structures appear complex. This justifies the searches for new symmetries, and the arguments for the unceasing hunt for smaller substructures of matter still exist.

References

- [1] S. Glashow, Nucl.Phys.**B22** (1961) 597. S. Weinberg, Phys.Rev.Lett. (1967) 1264. A. Salam, Proc. of the 8th Nobel Symposium, ed. N. Svartholm, (Almqvist and Wiksell, Stockholm, 1968).
- [2] P.W. Higgs, Phys. Lett. **12** (1964) 132;
Phys. Rev. Lett. **13** (1964) 508;
Phys. Rev. **145** (1966) 1156;
F. Englert and R. Brout, Phys. Rev. Lett. **13** (1964) 321.
- [3] D.J. Gross and F. Wilczek, Phys. Rev. Lett. **30** (1973) 1343;
H.D. Politzer, *ibid.* 1346;
D.J. Gross and F. Wilczek, Phys. Rev. **D8** (1973) 3633;
S. Weinberg, Phys. Rev. Lett. **31** (1973) 494.
- [4] Physics at LEP, ed. J. Ellis and R. Peccei, CERN 86-01, 02 (1986).
- [5] Z Physics at LEP 1, ed. G. Altarelli et al., CERN 89-08 (1989).
- [6] DELPHI Coll., P. Aarnio et al., Phys. Lett. **240B** (1990) 271.
- [7] DELPHI Coll., P. Abreu et al., Phys. Lett. **247B** (1990) 167.
- [8] DELPHI Coll., P. Abreu et al., Z. Phys. **C50** (1991) 185;
DELPHI Coll., P. Abreu et al., Phys. Lett. **255B** (1991) 466.
- [9] DELPHI Coll., P. Aarnio et al., Phys. Lett. **231B** (1989) 539.
- [10] DELPHI Coll., P. Abreu et al., Phys. Lett. **241B** (1990) 435.
- [11] DELPHI Coll., P. Aarnio et al., Phys. Lett. **241B** (1990) 425;
DELPHI Coll., P. Abreu et al., A measurement of the Partial Width of the Z^0 Boson into b Quark Pairs, *contr.* to the 24th Int. Conf. in High Energy Phys., Singapore 1990;
DELPHI Coll., P. Abreu et al., DELPHI Results on the Z^0 Resonance Parameters Through its Hadronic and Leptonic Decay Modes, *contr.* to the 24th Int. Conf. in High Energy Phys., Singapore 1990;
DELPHI Coll., P. Abreu et al., Phys. Lett. **260B** (1991) 240.
- [12] DELPHI Coll., P. Abreu et al., Nucl. Phys. **342** (1990) 1;
DELPHI Coll., P. Abreu et al., Search for Higgs Bosons Using the DELPHI Detector, *contr.* to the 24th Int. Conf. in High Energy Phys.,

- Singapore 1990;
ALEPH Coll., D. Decamp et al., Phys. Lett. **236B** (1990) 233;
ALEPH Coll., D. Decamp et al., Phys. Lett. **241B** (1990) 141;
ALEPH Coll., D. Decamp et al., Phys. Lett. **245B** (1990) 289;
ALEPH Coll., D. Decamp et al., Phys. Lett. **246B** (1990) 306;
L3 Coll., B. Adeva et al., Phys. Lett. **248B** (1990) 203;
OPAL Coll., M.Z. Akrawy et al., Phys. Lett. **236B** (1990) 224;
OPAL Coll., M.Z. Akrawy et al., Phys. Lett. **251B** (1990) 211.
- [13] G. von Holtey, Estimates of Particle Backgrounds at the LEP Detectors, CERN/LEP-BI/88-52, (1988).
- [14] LEP Design Report, CERN-LEP/84-01 June 1984.
- [15] G. von Holtey, Dependence of Electron Background on Initial Vacuum Pressure at LEP, LEP/BI, memorandum to B. Burkhardt et al. 8th February, 1989, unpublished.
- [16] DELPHI Technical Proposal, DELPHI 83-66/1, CERN/LEPC/83-3, May 1983.
- [17] DELPHI Progress Report, DELPHI 4-86 GEN-11/1 (1984).
- [18] DELPHI Coll., P. Aarnio et al., Nucl.Inst.Meth. **A303** (1991) 233.
- [19] ALEPH Coll., D. Decamp et al., Phys. Lett. **246B** (1990) 306.
- [20] U. Amaldi, Physica Scripta **23** (1981) 409-424.
- [21] R. Wigmans, Nucl. Inst. Meth. **A259** (1987) 389.
- [22] ZEUS Collaboration, Technical Proposal for the ZEUS Detector, DESY, Hamburg, March 1986;
H. Brückmann et al., On the Theoretical Understanding and Calculation of Sampling Calorimeters, DESY 87-064, (1987).
- [23] ALEPH Coll., D. Decamp et al., Phys. Lett. **246B** (1990) 306.
- [24] DELPHI Coll., P. Abreu et al., Phys. Lett. **241B** (1990) 449;
ALEPH Coll., D. Decamp et al., Phys. Lett. **241B** (1990) 623.
- [25] ALEPH Coll., D. Decamp et al., Nucl. Inst. Meth **A294** (1990) 121.
- [26] CDF Coll., F. Abe et al., Phys. Rev. Lett. **62** (1988) 613.

- [27] UA2 Coll., J. Alitti et al., Zeitschrift für Physik C **49** (1991) 17.
- [28] R. Keränen with E. Veitch et al, Muon Identification Efficiencies from the HFM Experiment, DELPHI 89-57, PHYS-48, (1989).
- [29] D.V. Volkov and V.P. Akulov, Phys. Lett. **46B** (1973) 109;
J. Wess and B. Zumino, Nucl. Phys. **B70** (1974) 39;
A. Salam and J. Strahdee, Nucl. Phys. **B76** (1974) 477.
- [30] J. Wess and B. Zumino, Phys. Lett. **49B** (1974) 52.
- [31] S. Ferrara, Phys. Rep. **105** (1984) 5;
P. Fayet, Phys. Rep. **105** (1984) 5.
- [32] H.P. Nilles, Phys. Rep. **110** (1984) 1.
- [33] H.E. Haber and G.L. Kane, Phys. Rep. **117** (1984) 75.
- [34] C.S. Aulakh and R.N. Mohapatra, Phys.Lett. **121B** (1983) 147;
L.J. Hall and M. Suzuki, Nucl. Phys. **B231** (1984) 419.
- [35] J. Primack et al., Ann. Rev. Nucl. Part. Sci. **38** (1988) 751.
- [36] S. Dawson, E. Eichten, and C. Quigg, Fermilab-PUB-83/82-THY.
- [37] UA1 Coll., Albajar C. et al., Phys. Lett. **B198** (1987) 261.
- [38] CDF Coll., F.Abe et al., Phys. Rev. Lett. **62** (1989) 1825.
- [39] UA2 Coll., Alitti J. et al., Phys. Lett. **B235** (1990) 363.
- [40] J. Ellis and D. Nanopoulos, Phys. Lett. **B110** (1982) 44;
B.A. Campbell, Phys. Rev. **D28** (1983) 209;
J.F. Donoghue et al. Phys. Lett. **B128** (1983) 55.
- [41] M. Suzuki, Phys. Lett. **B115** (1982) 40;
M.J. Duncan, Nucl. Phys. **B214** (1983) 21.
- [42] J. Ellis and S. Rudaz, Phys. Lett. **B128** (1983) 248;
Ken-ichi Hikasa and M. Kobayashi, Phys. Rev. **D36** (1987) 724.
- [43] H.Baer et al. Phys. Lett. **B161** (1985) 175.
- [44] H.Baer, et al. Phys. Rev. Lett. **63** (1989) 352.

- [45] H. Baer et al. Phys. Lett. **B183** (1987) 220.
- [46] M. Perl, in Proc. of the 23rd Int. Conf. on High Energy Physics, ed. S. Loken, Berkley, California, 1986;
Mark II Coll., K. Riles et al., Phys. Rev. **D42** (1990) 1.
- [47] H. Baer et al. Constraints on Supersymmetric Particles from the LEP Data on Z^0 Decay Properties, CERN-TH 5582/89, (1989);
S. Nussinov, Phys. Lett. **B254** (1991), 279.
- [48] T. Barklow, in Proceedings of the Second Mark II Workshop on SLC Physics, SLAC-306.
- [49] TOPAZ Coll., I. Adachi et al. Phys. Lett. **B218** (1989) 105.
- [50] Mark II Coll., T. Barklow et al., Phys. Rev. Lett. **64** (1990) 2986.
- [51] E. Byckling, K. Kajantie, Particle Kinematics, (John Wiley & Sons Ltd., London, New York, Sydney, Toronto) 1973.
- [52] ALEPH Coll., D. Decamp et al., Phys. Lett. **237B** (1990) 291.
- [53] F. Bianchi et al., SUSY at LEP, DELPHI 85-67 PHYS-7 (1985).
- [54] DELPHI Collaboration, DELSIM, DELPHI Event Generation and Detector simulation, User's Guide, DELPHI 89-67 PROG-142, (July 1989);
DELPHI Collaboration, DELSIM, DELPHI Event Generation and Detector simulation, Reference Manual, DELPHI 89-68 PROG-143, (September 1989).
- [55] DELPHI Collaboration, DELPHI Data Analysis Program (DELANA) User's Guide, DELPHI 89-44 PROG-137, (May 1989).
- [56] Yu. Belokopytov, et al. Detector Description Application Package, User Manual for Version 3.00, DELPHI 88-87, PROG-121, (1988).
- [57] D. Bertrand, L. Pape, TANAGRA Track Analysis and Graphics Package, DELPHI 87-95 PROG-98, (June 1988).
- [58] J. Cuevas, et al. Fast Simulation for DELPHI, Version 2.0 DELPHI 87-26, PROG-71, (1987);
R. Keränen, Hadron Calorimetry in the Fast Simulation for DELPHI, DELPHI 88-10, PROG-105, (1988).

- [59] T.B.Sjöstrand, *Comp. Phys. Comm* **27** (1983) 243; *ibid.* **28** (1983) 229;
T.B.Sjöstrand and M. Bengtsson *Comp. Phys. Comm* **43** (1987) 271.
- [60] T.B.Sjöstrand, private communication, 1989.
- [61] DELPHI Coll., P. Abreu et al., *Phys. Lett.* **242B** (1990) 536.

Search for scalar quarks in Z^0 decays

DELPHI Collaboration

P. Abreu ^a, W. Adam ^b, F. Adami ^c, T. Adye ^d, G.D. Alexeev ^e, J.V. Allaby ^f, P. Allen ^g, S. Almehed ^h, F. Altied ^g, S.J. Alvsvaag ⁱ, U. Amaldi ^f, E. Anassontzis ^j, W.-D. Apel ^k, B. Asman ^l, C. Astor Ferreres ^m, J.-E. Augustin ⁿ, A. Augustinus ^f, P. Baillon ^f, P. Bambade ⁿ, F. Barao ^a, G. Barbiellini ^o, D.Y. Bardin ^c, A. Baroncelli ^p, O. Barring ^h, W. Bartl ^b, M.J. Bates ^q, M. Baubillier ^r, K.-H. Becks ^s, C.J. Beeston ^q, P. Beilliere ^t, I. Belokopytov ^u, P. Beltran ^v, D. Benedic ^w, J.M. Benlloch ^g, M. Berggren ^l, D. Bertrand ^x, S. Biagi ^y, F. Bianchi ^z, J.H. Bibby ^q, M.S. Bilenky ^c, P. Billoir ^r, J. Bjarne ^h, D. Bloch ^w, P.N. Bogolubov ^e, D. Bollini ^a, T. Bolognese ^c, M. Bonapart ^l, P.S.L. Booth ^y, M. Boratav ^r, P. Borgeaud ^c, H. Borner ^q, C. Bosio ^p, O. Botner ^y, B. Bouquet ⁿ, M. Bozzo ^o, S. Braibant ^f, P. Branchini ^p, K.D. Brand ^s, R.A. Brenner ^e, C. Bricman ^x, R.C.A. Brown ^f, N. Brummer ^l, J.-M. Brunet ^t, L. Bugge ^z, T. Buran ^z, H. Burmeister ^f, C. Buttar ^q, J.A.M.A. Buytaert ^x, M. Caccia ⁿ, M. Calvi ⁿ, A.J. Camacho Rozas ^m, J.-E. Campagne ^r, A. Champion ^y, T. Camporesi ^f, V. Canale ^p, F. Cao ^x, L. Carroll ^y, C. Caso ^o, E. Castelli ^o, M.V. Castillo Gimenez ^g, A. Cattai ^f, F.R. Cavallo ^a, L. Cerrito ^p, P. Charpentier ^f, P. Checchia ^o, G.A. Chelkov ^c, L. Chevalier ^c, P. Chliapnikov ^u, V. Chorowicz ^r, R. Cirio ^z, M.P. Clara ^z, J.L. Contreras ^g, R. Contri ^o, G. Cosme ⁿ, F. Couchot ⁿ, H.B. Crawley ^k, D. Crennell ^d, M. Cresti ^o, G. Crosetti ^o, N. Crosland ^q, M. Crozon ^t, J. Cuevas Maestro ^m, S. Czellar ^e, S. Dagoret ⁿ, E. Dahl-Jensen ^l, B. Dalmagne ⁿ, M. Dam ^f, G. Damgaard ^l, G. Darbo ^o, E. Daubie ^x, M. Davenport ^f, P. David ^r, A. De Angelis ^o, M. De Beer ^c, H. De Boeck ^x, W. De Boer ^k, C. De Clercq ^x, M.D.M. De Fez Laso ^g, N. De Groot ^l, C. De La Vaissiere ^r, B. De Lotto ^o, A. De Min ⁿ, C. Defoix ^t, D. Delikaris ^f, P. Delpierre ^t, N. Demaria ^z, L.Di Ciaccio ^p, A.N. Diddens ^l, H. Dijkstra ^f, F. Djama ^w, J. Dolbeau ^u, K. Doroba ^u, M. Dracos ^w, J. Drees ^s, M. Dris ^z, W. Dulinski ^w, R. Dzhelyadin ^u, D.N. Edwards ^y, L.-O. Eek ^y, P.A.-M. Eerola ^c, T. Ekelof ^y, G. Ekspog ^g, J.-P. Engel ^w, V. Falaleev ^u, A. Fenyuk ^u, M. Fernandez Alonso ^m, A. Ferrer ^g, S. Ferroni ^o, T.A. Filippas ^z, A. Firestone ^k, H. Foeth ^f, E. Fokitis ^z, F. Fontanelli ^o, H. Forsbach ^s, B. Franek ^d, K.E. Fransson ^y, P. Frenkiel ^t, D.C. Fries ^k, R. Fruhwirth ^b, F. Fulda-Quenzer ⁿ, H. Furstenau ^k, J. Fuster ^f, J.M. Gago ^a, G. Galeazzi ^o, D. Gamba ^z, U. Gasparini ^o, P. Gavillet ^f, S. Gawne ^y, E.N. Gazis ^z, P. Giacomelli ^a, K.-W. Glitza ^s, R. Gokieli ^r, V.M. Golovatyuk ^e, A. Goobar ^l, G. Gopal ^d, M. Gorski ^u, V. Gracco ^o, A. Grant ^f, F. Grard ^x, E. Graziani ^p, M.-H. Gros ⁿ, G. Grosdidier ⁿ, B. Grosssetete ^r, S. Gumenyuk ^u, J. Guy ^d, F. Hahn ^s, M. Hahn ^k, S. Haider ^f, Z. Hajduk ^l, A. Hakansson ^h, A. Hallgren ^y, K. Hamacher ^s, G. Hamel De Monchenault ^c, F.J. Harris ^q, B. Heck ^f, I. Herbst ^s, J.J. Hernandez ^g, P. Herquet ^x, H. Herr ^f, E. Higon ^g, H.J. Hilke ^f, T. Hofmohl ^u, R. Holmes ^k, S.-O. Holmgren ^l, J.E. Hooper ^l, M. Houlden ^y, J. Hrubec ^b, P.O. Hulth ^l, K. Hultqvist ^l, D. Husson ^w, B.D. Hyams ^f, P. Ioannou ^j, P.-S. Iversen ⁱ, J.N. Jackson ^y, P. Jalocho ^z, G. Jarlskog ^h, P. Jarry ^c, B. Jean-Marie ⁿ, E.K. Johansson ^l, M. Jonker ^f, L. Jonsson ^h, P. Juillot ^w, R.B. Kadyrov ^e, G. Kalkanis ^j, G. Kalmus ^d, G. Kantardjian ^f, F. Kapusta ^r, P. Kapusta ^z, S. Katsanevas ^j, E.C. Katsoufis ^z, R. Keranen ^e, J. Kesteman ^x, B.A. Khomenko ^c, B. King ^y, N.J. Kjaer ^l, H. Klein ^f, W. Klempt ^f, A. Klovning ⁱ, P. Kluit ^x, J.H. Koehne ^k, B. Koene ^l, P. Kokkinias ^y, M. Kopf ^k, M. Koratzinos ^f, K. Korcyl ^z, A.V. Korytov ^c, B. Korzen ^f, C. Kourkoumelis ^j, T. Kreuzberger ^b, J. Krolikowski ^u,

U. Kruener-Marquis ^s, W. Krupinski ^π, W. Kucewicz ^η, K. Kurvinen ^ε, M.I. Laakso ^ε,
 C. Lambropoulos ^ν, J.W. Lamsa ^κ, L. Lanceri ^ο, V. Lapin ^υ, J.-P. Laugier ^c, R. Lauhakangas ^ε,
 P. Laurikainen ^ε, G. Leder ^b, F. Ledroit [†], J. Lemonne ^x, G. Lenzen ^s, V. Lepeltier ⁿ,
 A. Letessier-Selvon ^r, E. Lieb ^s, E. Lillestol ^f, E. Lillethun ⁱ, J. Lindgren ^ε, I. Lippi ^θ, R. Llosa ^ε,
 B. Loerstad ^h, M. Lokajicek ^c, J.G. Loken ^q, M.A.Lopez Aguera ^m, A. Lopez-Fernandez ⁿ,
 D. Loukas ^ν, J.J. Lozano ^ε, R. Lucock ^d, B. Lund-Jensen ^γ, P. Lutz [†], L. Lyons ^q, G. Maehlum ^f,
 J. Maillard [†], A. Maltezos ^ν, F. Mandl ^b, J. Marco ^m, J.-C. Marin ^f, A. Markou ^ν, L. Mathis [†],
 C. Matteuzzi ⁿ, G. Matthiae ^p, M. Mazzucato ^θ, M. McCubbin ^ν, R. McKay ^κ, E. Menichetti ^z,
 C. Meroni ⁿ, W.T. Meyer ^κ, W.A. Mitaroff ^b, G.V. Mitselmakher ^e, U. Mjoernmark ^h, T. Moa ^ε,
 R. Moeller ^λ, K. Moenig ^s, M.R. Monge ^δ, P. Morettini ^δ, H. Mueller ^k, H. Muller ^f, G. Myatt ^q,
 F. Naraghi ^r, U. Nau-Korzen ^s, F.L. Navarria ^α, P. Negri ⁿ, B.S. Nielsen ^λ, V. Nikolaenko ^υ,
 V. Obraztsov ^υ, R. Orava ^ε, A. Ouraou ^c, R. Pain ^r, H. Palka ^π, T. Papadopoulou ^ξ, L. Pape ^f,
 P. Pasini ^α, A. Passeri ^p, M. Pegoraro ^θ, V. Perevozchikov ^υ, M. Pernicka ^β, M. Pimenta ^a,
 O. Pingot ^x, C. Pinori ^θ, A. Pinsent ^q, M.E. Pol ^a, B. Poliakov ^υ, G. Polok ^π, P. Poropat ^ο,
 P. Privitera ^α, A. Pullia ⁿ, J. Pyyhtia ^ε, A.A. Rademakers ^β, D. Radojicic ^q, S. Ragazzi ⁿ,
 W.H. Range ^ν, P.N. Ratoff ^q, A.L. Read ^ξ, N.G. Redaelli ⁿ, M. Regler ^b, D. Reid ^ν,
 P.B. Renton ^q, L.K. Resvanis ^j, F. Richard ⁿ, J. Ridky ^c, G. Rinaudo ^z, I. Roditi ^f, A. Romero ^z,
 P. Ronchese ^θ, E.I. Rosenberg ^κ, U. Rossi ^α, E. Rosso ^f, P. Roudeau ⁿ, T. Rovelli ^α,
 V. Ruhlmann ^c, A. Ruiz ^m, H. Saarikko ^ε, Y. Sacquin ^c, E. Sanchez ^ε, J. Sanchez ^ε, E. Sanchis ^ε,
 M. Sannino ^δ, M. Schaeffer ^w, H. Schneider ^k, F. Scuri ^ο, A. Sebastia ^ε, A.M. Segar ^q,
 R. Sekulin ^d, M. Sessa ^ο, G. Sette ^δ, R. Seufert ^k, R.C. Shellard ^f, P. Siegrist ^c, S. Simonetti ^δ,
 F. Simonetto ^ο, A.N. Sissakian ^c, T.B. Skaali ^ξ, J. Skeens ^κ, G. Skjevling ^ξ, G. Smadja ^c,
 N.E. Smirnov ^υ, G.R. Smith ^d, R. Sosnowski ^μ, K. Spang ^λ, T. Spasoff ^c, E. Spiriti ^p,
 S. Squarcia ^δ, H. Staeck ^s, C. Stanescu ^p, G. Stavropoulos ^ν, F. Stichelbaut ^x, A. Stocchi ⁿ,
 J. Strauss ^b, R. Strub ^w, C.J. Stubenrauch ^f, M. Szczekowski ^μ, M. Szeptycka ^μ, P. Szymanski ^μ,
 S. Tavernier ^x, G. Theodosiou ^ν, A. Tilquin [†], J. Timmermans ^β, V.G. Timofeev ^c,
 L.G. Tkatchev ^c, D.Z. Toet ^β, A.K. Topphol ⁱ, L. Tortora ^p, D. Treille ^f, U. Trevisan ^δ,
 G. Tristram [†], C. Troncon ⁿ, E.N. Tsyganov ^c, M. Turala ^π, R. Turchetta ^w, M.-L. Turluer ^c,
 T. Tuuva ^ε, I.A. Tyapkin ^c, M. Tyndel ^d, S. Tzamarias ^f, F. Udo ^β, S. Ueberschaer ^s,
 V.A. Uvarov ^υ, G. Valenti ^α, E. Vallazza ^z, J.A. Valls Ferrer ^ε, G.W. Van Apeldoorn ^β,
 P. Van Dam ^β, W.K. Van Doninck ^x, N. Van Eijndhoven ^f, C. Vander Velde ^x, J. Varela ^a,
 P. Vaz ^a, G. Vegni ⁿ, M.E. Veitch ^q, J. Velasco ^ε, L. Ventura ^θ, W. Venus ^d, F. Verbeure ^x,
 L.S. Vertogradov ^c, L. Vibert ^r, D. Vilanova ^c, N.K. Vishnevskiy ^υ, E.V. Vlasov ^υ,
 A.S. Vodopyanov ^c, M. Vollmer ^s, G. Voulgaris ^j, M. Voutilainen ^ε, V. Vrba ^c, H. Wahlen ^s,
 C. Walck ^ε, F. Waldner ^ο, M. Wayne ^κ, P. Weilhammer ^f, J. Werner ^s, A.M. Wetherell ^f,
 J.H. Wickens ^x, J. Wikne ^ξ, W.S.C. Williams ^q, M. Winter ^w, D. Wormald ^ξ, G. Wormser ⁿ,
 K. Woschnagg ^γ, N. Yamdagni ^ε, P. Yepes ^β, A. Zaitsev ^υ, A. Zalewska ^π, P. Zalewski ^μ,
 P.I. Zarubin ^c, E. Zevgolatakos ^ν, G. Zhang ^s, N.I. Zimin ^c, R. Zitoun ^r,
 R. Zukanovich Funchal [†], G. Zumerle ^θ and J. Zuniga ^ε

^a LIP, Av. Elias Garcia 14 - 1e, P-1000 Lisbon Codex, Portugal

^b Institut für Hochenergiephysik, Österreichische Akademie der Wissenschaften, Nikolsdorfergasse 18, A-1050 Vienna, Austria

^c DPhPE, CEN-Saclay, F-91191 Gif-Sur-Yvette Cedex, France

^d Rutherford Appleton Laboratory, Chilton, Didcot OX11 0QX, UK

^e Joint Institute for Nuclear Research, Dubna, Head Post Office, P.O. Box 79, SU-101 000 Moscow, USSR

^f CERN, CH-1211 Geneva 23, Switzerland

^g Instituto de Fisica Corpuscular (IFIC), Centro Mixto Universidad de Valencia-CSIC, Avda. Dr. Moliner 50, E-46100 Burjassot (Valencia), Spain

^h Department of Physics, University of Lund, Sölvegatan 14, S-223 63 Lund, Sweden

ⁱ Department of Physics, University of Bergen, Allégaten 55, N-5007 Bergen, Norway

- ^j *Physics Laboratory, University of Athens, Solonos Street 104, GR-10680 Athens, Greece*
- ^k *Institut für Experimentelle Kernphysik, Universität Karlsruhe, Postfach 6980, D-7500 Karlsruhe 1, FRG*
- ^l *Institute of Physics, University of Stockholm, Vanadisvägen 9, S-113 46 Stockholm, Sweden*
- ^m *Facultad de Ciencias, Universidad de Santander, av. de los Castros, E-39005 Santander, Spain*
- ⁿ *Laboratoire de l'Accélérateur Linéaire, Université de Paris-Sud, Bâtiment 200, F-91405 Orsay, France*
- ^o *Dipartimento di Fisica, Università di Trieste and INFN, Via A. Valerio 2, I-34127 Trieste, Italy and Istituto di Fisica, Università di Udine, I-33100 Udine, Italy*
- ^p *Istituto Superiore di Sanità, Istituto Nazionale di Fisica Nucleare (INFN), Viale Regina Elena 299, I-00161 Rome, Italy and Dipartimento di Fisica, Università di Roma II and INFN, Tor Vergata, I-00173 Rome, Italy*
- ^q *Nuclear Physics Laboratory, University of Oxford, Keble Road, Oxford OX1 3RH, UK*
- ^r *LPNHE, Universités Paris VI et VII, Tour 33 (RdC), 4 place Jussieu, F-75230 Paris Cedex 05, France*
- ^s *Fachbereich Physik, University of Wuppertal, Postfach 100 127, D-5600 Wuppertal 1, FRG*
- ^t *Laboratoire de Physique Corpusculaire, Collège de France, 11 place M. Berthelot, F-75231 Paris Cedex 5, France*
- ^u *Institute for High Energy Physics, Serpukhov, P.O. Box 35, SU-142 284 Protvino (Moscow Region), USSR*
- ^v *Greek Atomic Energy Commission, Nuclear Research Centre Demokritos, P.O. Box 60228, GR-15310 Aghia Paraskevi, Greece*
- ^w *Division des Hautes Energies, CRN-Groupe DELPHI, B.P. 20 CRO, F-67037 Strasbourg Cedex, France*
- ^x *Physics Department, Universitaire Instelling Antwerpen, Universiteitsplein 1, B-2610 Wilrijk, Belgium and IIHE, ULB-VUB, Pleinlaan 2, B-1050 Brussels, Belgium and Service de Physique des Particules Élémentaires, Faculté des Sciences, Université de l'Etat Mons, Av. Maistriau 19, B-7000 Mons, Belgium*
- ^y *Department of Physics, University of Liverpool, P.O. Box 147, Liverpool L69 3BX, UK*
- ^z *Dipartimento di Fisica Sperimentale, Università di Torino and INFN, Via P. Giuria 1, I-10125 Turin, Italy*
- ^{aa} *Dipartimento di Fisica, Università di Bologna and INFN, Via Irnerio 46, I-40126 Bologna, Italy*
- ^{ab} *NIKHEF-H, Postbus 41882, NL-1009 DB Amsterdam, The Netherlands*
- ^{ac} *Department of Radiation Sciences, University of Uppsala, P.O. Box 535, S-751 21 Uppsala, Sweden*
- ^{ad} *Dipartimento di Fisica, Università di Genova and INFN, Via Dodecaneso 33, I-16146 Genoa, Italy*
- ^{ae} *Department of High Energy Physics, University of Helsinki, Siltavuorenpenger 20 C, SF-00170 Helsinki 17, Finland*
- ^{af} *Physics Department, University of Oslo, Blindern, N-1000 Oslo 3, Norway*
- ^{ag} *Dipartimento di Fisica, Università di Milano and INFN, Via Celoria 16, I-20133 Milan, Italy*
- ^{ah} *Dipartimento di Fisica, Università di Padova and INFN, Via Marzolo 8, I-35131 Padua, Italy*
- ^{ai} *Ames Laboratory and Department of Physics, Iowa State University, Ames IA 50011, USA*
- ^{aj} *Niels Bohr Institute, Blegdamsvej 17, DK-2100 Copenhagen Ø, Denmark*
- ^{ak} *Institute for Nuclear Studies, and University of Warsaw, Ul. Hoza 69, PL-00681 Warsaw, Poland*
- ^{al} *Physics Department, National Technical University, Zografou Campus, GR-15773 Athens, Greece*
- ^{am} *High Energy Physics Laboratory, Institute of Nuclear Physics, Ul. Kawory 26 a, PL-30055 Cracow 30, Poland*

Received 8 June 1990

A search has been made for pairs of scalar quarks (squarks) produced in e^+e^- annihilations at LEP ($\sqrt{s} \approx M_{Z^0}$), and decaying into a standard quark and a neutral, non-interacting, stable, massive particle (the lightest supersymmetric particle, LSP). The search has been conducted for differences in the mass of the squark and LSP of $2 \text{ GeV}/c^2$ and above. Up squarks with masses below $42 \text{ GeV}/c^2$ and down squarks below $43 \text{ GeV}/c^2$ were excluded. Six squark flavours degenerate in mass were excluded below $45 \text{ GeV}/c^2$.

1. Introduction

A large number of high energy e^+e^- annihilations have been recorded during the 1989 running period of LEP, the CERN electron-positron collider. Novel strategies that use the large statistics around the Z^0 resonance and rely on the clean machine conditions can be applied in searching for new phenomena.

This paper reports a search, using the DELPHI detector, for new heavy unstable charged particles which are pair produced in Z^0 decays, and decay immediately producing a neutral and non-interacting stable particle together with a standard quark. Decays of this type are to be expected in some theories beyond the standard model. In particular, supersymmetric models predict reactions of the type

$$e^+e^- \rightarrow Z^0 \rightarrow q\bar{q} \rightarrow \tilde{\chi}^0 q \tilde{\chi}^0 \bar{q}, \quad (1)$$

where the scalar supersymmetric partners \tilde{q} and $\tilde{\bar{q}}$ of the quark and antiquark decay into the undetected lightest supersymmetric particle (LSP) $\tilde{\chi}^0$ and a quark q . Previous searches for these types of processes were based on the signature of a momentum imbalance appearing either as acollinear jets or as events with large missing transverse momentum [1-5]. Such approaches require a large difference between the mass of the charged decaying particle and the mass of the neutral invisible particle. In the case of a *heavy* invisible object, close in mass to the decaying particle, the experimental signature changes from a clearly distinguishable acollinear jet topology to events of small visible energy. At hadron colliders these events have low trigger efficiencies and high backgrounds due to soft processes. At e^+e^- colliders they are contaminated by two-photon interactions and machine backgrounds.

The present search was based on two different analyses. The *first* one applies to heavy invisible objects and is new. It utilises e^+e^- annihilations at center-of-mass energies around the Z^0 boson mass. The cross section of the new process is expected to follow the standard line shape of the Z^0 boson and, thus, to exceed on the peak the cross section due to s -channel photon exchange by several orders of magnitude. Data points at center-of-mass energies around the Z^0 pole are a direct experimental check of the estimates for the backgrounds which are decoupled from the Z^0 . Hence the rates of these background events may be reliably determined. The *second* analysis which follows previous works [1,2], is based on searching for acollinear jets and puts limits for LSP masses less than about half of the squark mass. Most of the paper is devoted to an explanation of the new approach applied in the first analysis.

The squarks \tilde{q} and $\tilde{\bar{q}}$ of eq. (1) couple to the Z^0 analogously to the corresponding fermionic quark fields and the expected cross sections are calculable for each flavour and helicity [6]. In case of low squark masses, the cross sections are the level of 3 nb for single flavours and they can contribute to the hadronic or to the invisible width of the Z^0 (depending on the mass of the LSP). The phase space factor $\beta^3 = (1 - 4M_{\tilde{\chi}^0}^2/s)^{3/2}$ affects the rates over a wide portion of the kinematically accessible region.

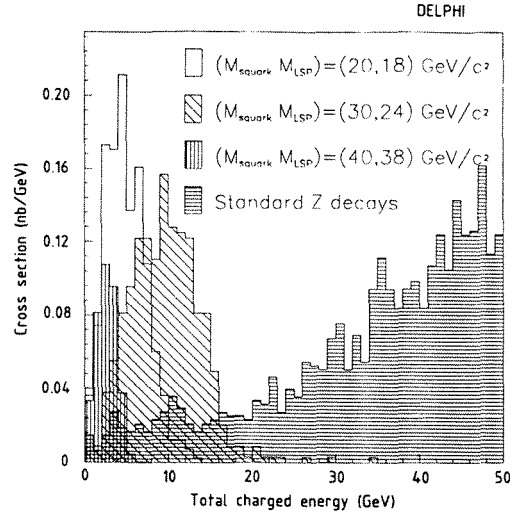


Fig. 1. The distributions of total charged visible energy in the final state of squark pair production for various squark and LSP masses.

In both analyses presented here, each squark was assumed to decay immediately with a 100% branching ratio into a LSP (heavy gluino assumed) and a quark. Only mass differences between the squark and the LSP above 2 GeV were investigated, since closer masses lead to theoretical uncertainties in the multiplicities of the fragmentation of low energy quark-antiquark systems. Some characteristics of the expected signal are shown in fig. 1 in which the distributions of the total charged energy are plotted for three combinations of the masses of the scalar quarks and the heavy LSP. In the first analysis the search was concentrated on events having a total charged energy smaller than 20 GeV whereas in case of LSP masses less than half of the squark mass, the total charged energy is well within the distribution from the standard quarks and events with visible energy larger than 15 GeV were considered.

2. The detector and trigger arrangement

The components of DELPHI [7] relevant for this work are the Time Projection Chamber (TPC), the Inner and the Outer Detectors (ID, OD), and the Small Angle Tagger (SAT).

The ID is a cylindrical drift chamber covering the polar angle range 30° – 150° . It contains five trigger layers giving information about the cylindrical $r\phi$ and longitudinal z coordinates at the radius of 22 cm around the beam axis. The jet chamber section providing the $r\phi$ coordinates of 24 points. The TPC is a cylinder with an inner radius of 30 cm, outer radius of 122 cm and with anode wires at a distance of 134 cm from the central high plane at $a=0$. The TPC records 16 space points (for polar angles of 40° – 140°), z -coordinates derived from the drift time onto the wires and $r\phi$ coordinates from the circular pad rows behind the anode wires. At least six space points are registered down to polar angles of 24° . The OD is a cylindrical tracking device consisting of 24 aluminium drift tube assemblies in five layers at a radius of 198–208 cm. It provides five accurate $r\phi$ space points and three fast z coordinates per track at polar angles between 50° and 130° and contributed also to the track trigger. The SAT calorimeters cover polar angles of 43 – 135 mrad in the beam directions. They consist of scintillating fibres embedded in a lead absorber and they measure the integrated luminosity by monitoring the rate of small angle Bhabha scattering. Details of the luminosity measurement are given in ref. [8].

The component of the DELPHI trigger that is most

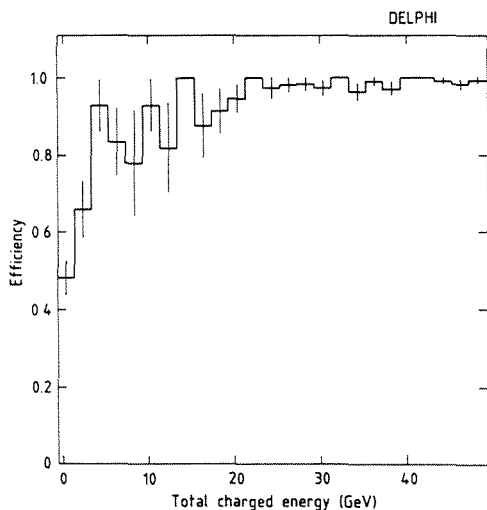


Fig. 2. Efficiency of the DELPHI barrel track trigger used for this analysis as a function of the total visible charged energy.

important for this analysis is the barrel track trigger consisting of the coincidence of back to back OD quadrants with any signal from the ID trigger layers. The information about all the trigger components was included in the data on an event-to-event basis, and the efficiency of this particular trigger could be measured by using the redundancy of the independent barrel trigger information from the scintillator layer behind the first 5 radiation lengths of the barrel electromagnetic calorimeter combined with the 172 time of flight counters outside the solenoid. Fig. 2 shows the trigger efficiency as a function of the visible charged energy calculated from the data.

3. Event selection for heavy LSPs

Events used in this analysis contain at least one reconstructed charged track with a momentum larger than 0.5 GeV/ c , a radial impact parameter less than 15 cm and a longitudinal distance z from the interaction point less than 30 cm. These selection criteria were chosen to include events to measure the machine backgrounds, as discussed later. The detector conditions were checked for the detector parts which were necessary for the reconstruction and the trigger. After this run selection 13 500 events remained, corresponding to an integrated luminosity of 330 nb $^{-1}$ divided into ten samples at center-of-mass energies between 88.28 and 95.04 GeV.

In each event, the average impact distance in the z -direction, \hat{z} , and its variance, $\sigma(z)$, were calculated for the selected charged particle tracks.

The candidates were selected by requiring

- (1) a total visible charged energy less than 20 GeV,
- (2) more than two charged particles (this criterion rejected cosmic triggers, beam-halo tracks, and leptonic Z^0 decays, including a large fraction of the tau pairs, but had a high efficiency for signal events, because the average charged multiplicity in them is always larger than five,)
- (3) $|\hat{z}| < 4$ cm (to reject events that are not at the expected interaction point),
- (4) $\sigma(z) < 6$ cm (to reject events with an ill defined vertex),
- (5) $|\cos \theta_{\text{thrust}}| < 0.8$, where θ_{thrust} is the polar angle of the thrust axis with respect to the beam (to reject most two-photon interactions),

(6) all tracks to have at angles greater than 25° to the beam axis (to veto events oriented very close to the beam direction),

(7) energy in the SAT smaller than 4 GeV (to veto two photon candidates and machine backgrounds).

After the selections the sample contained 284 events. It was checked by scanning that the general features of the events were those expected from a combination of two-photon events, Z^0 decays with low reconstructed charged energy and events due to machine backgrounds. Most of the off momentum tracks and the beam-gas or beam-wall interactions were rejected by the vertex criteria described above. The reference interval $5 < |\hat{z}| < 30$ cm was used to estimate the remaining beam associated background and its uncertainty. The 390 events in this interval were found to be uniformly distributed in the variable \hat{z} within statistics. By extrapolating the event density to the vertex interval $|\hat{z}| < 4$ cm, a background of 62 ± 3 (stat.) events was estimated. The background rate turned out to be stable from machine fill to machine fill within the relatively poor statistics (often less than ten events per fill); to take into account possible variations, a 30% systematic

error was added in quadrature with the statistical error. This background was subtracted from the 284 selected events in the subsequent analysis. The number of selected events at each energy was normalized to the SAT measured luminosity to give the measured cross sections which are presented as a function of the center-of-mass energy in fig. 3.

The data of fig. 3 are taken to be the sum of a resonance-shaped contribution due to remaining Z^0 decays and a slowly energy dependent contribution due to the two photon events, that satisfy the selection criteria.

4. Expected signal and search limits in the case of a heavy LSP

A high statistics sample of Monte Carlo events was generated with first-order radiative corrections, quark fragmentation according to the Lund 6.3 parton shower model [9] and with the detailed simulation of the detector (ref. [10] shows the general properties of the hadronic Z^0 decays). This was used to estimate the contribution from standard hadronic Z^0 decays (reconstructed only partially due to either a very forward-backward event axis or high neutral content), and from decays into $\tau\bar{\tau}$ pairs. The result

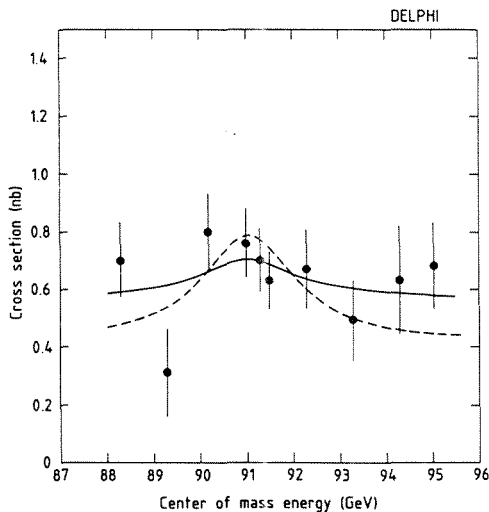


Fig. 3. Measured cross sections (corrected for the machine background) of events satisfying the selection criteria as a function of the center-of-mass-energy. The solid curve is the result of a two-parameter fit to a Z^0 line shape plus a constant term both with a free normalization. The dashed curve corresponds to the 95% CL upper limit.

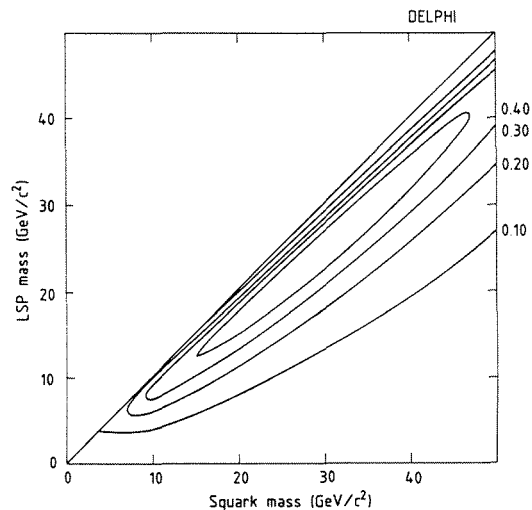


Fig. 4. Combined trigger and the selection efficiencies as a function of the squark mass and the LSP mass.

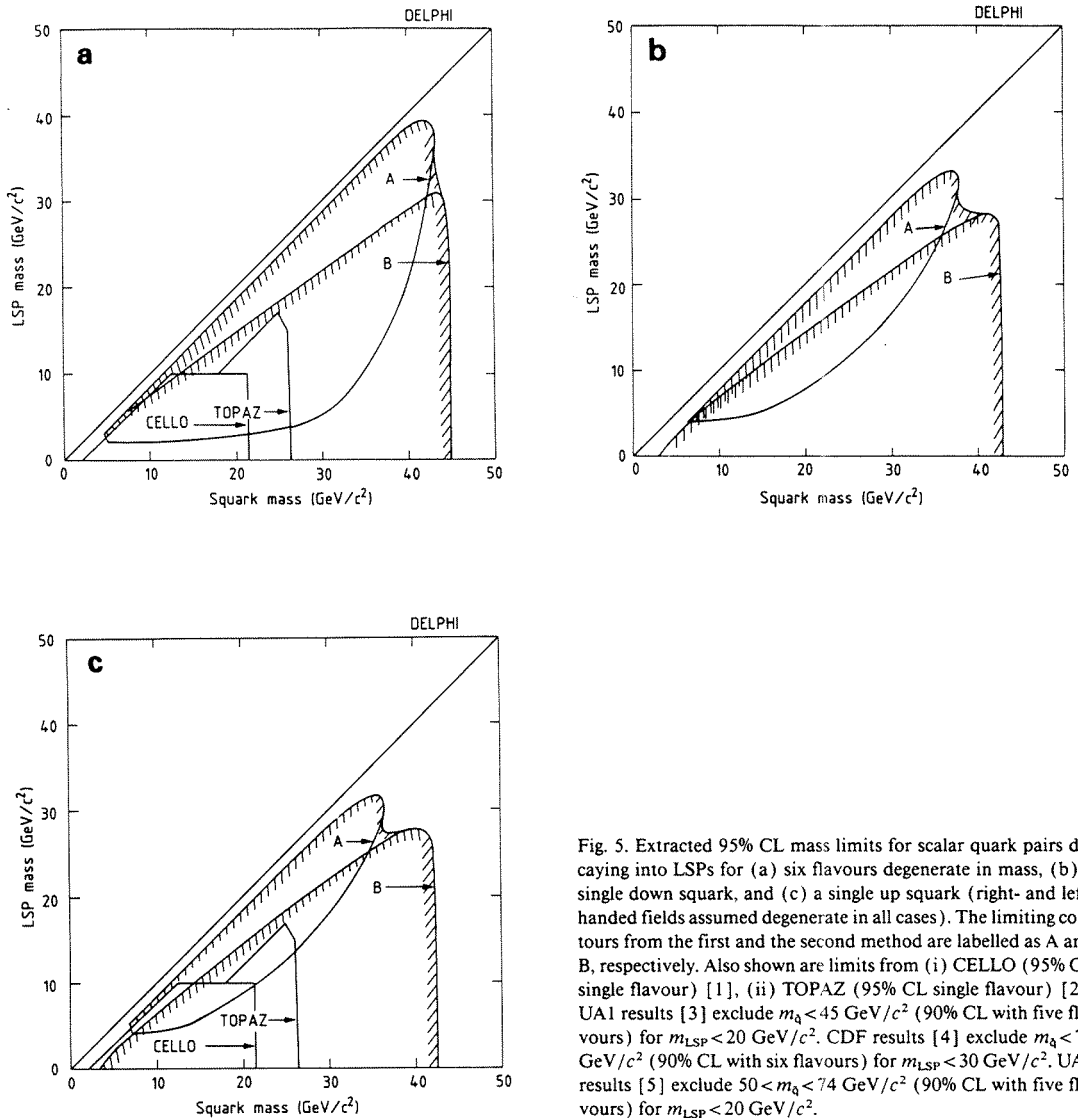


Fig. 5. Extracted 95% CL mass limits for scalar quark pairs decaying into LSPs for (a) six flavours degenerate in mass, (b) a single down squark, and (c) a single up squark (right- and left-handed fields assumed degenerate in all cases). The limiting contours from the first and the second method are labelled as A and B, respectively. Also shown are limits from (i) CELLO (95% CL single flavour) [1], (ii) TOPAZ (95% CL single flavour) [2]. UA1 results [3] exclude $m_q < 45 \text{ GeV}/c^2$ (90% CL with five flavours) for $m_{\text{LSP}} < 20 \text{ GeV}/c^2$. CDF results [4] exclude $m_q < 74 \text{ GeV}/c^2$ (90% CL with six flavours) for $m_{\text{LSP}} < 30 \text{ GeV}/c^2$. UA2 results [5] exclude $50 < m_q < 74 \text{ GeV}/c^2$ (90% CL with five flavours) for $m_{\text{LSP}} < 20 \text{ GeV}/c^2$.

was that $(0.75 \pm 0.25)\%$ of the standard Z^0 decays satisfy the selection criteria. The 0.25% systematic error was mainly due to uncertainties in the angular dependence of the trigger efficiency. The dependence of the tails of the charged energy distribution on the fragmentation model was investigated by comparing the α_s^2 matrix element Monte Carlo model with string fragmentation in Lund 6.3 and found to be negli-

ble. These remaining Z^0 's were assumed to be distributed according to the line shape and were normalised to the peak cross section measured in ref. [8]. Their contribution at the peak is equal to $0.23 \pm 0.07 \text{ nb}$.

The measured cross section for all Z^0 associated processes was estimated by fitting to fig. 3 a Z^0 line shape [8] with a free normalization (representing the

remaining standard Z^0 plus possible nonstandard Z^0 decays) plus a constant term (representing the two-photon contribution). The fit had $\chi^2/\text{DOF}=7.9/8$ (fig. 3). The expected background due to the standard Z^0 decays as estimated above was then subtracted from the result. The remaining nonstandard signal associated with the Z^0 , for example due to process (1) was (-0.09 ± 0.14) nb on the peak. This corresponds to -20 ± 32 events integrated over the whole energy interval. The remaining constant background was 0.56 ± 0.09 nb. The upper limit for a physical, i.e. positive cross section, associated to nonstandard Z^0 decays was determined by excluding 95% of the probability density (gaussian) in the region of positive cross sections (ref. [11]). The limit was 0.23 nb, corresponding to 52 events. This number of events was used for deriving the search limits reported below.

The expected rate of the signal events depends on their production cross section, trigger efficiency and selection efficiency. The trigger and selection efficiencies were studied at various mass values by passing Monte Carlo samples through the same analysis chain as the real data. The trigger part of the simulation was cross checked against real data by comparing the simulation results with the trigger efficiency extracted from real events of a similar topology. The selection efficiency was found to vary from 34% to 56% as the mass difference between the squark and the LSP varied from 2 GeV to 6 GeV. For larger mass differences the efficiency decreases again since those events have more than 20 GeV of visible charged energy. The combined efficiency was parametrized as shown in fig. 4 and is known with an uncertainty of about 5%.

The 95% confidence level search limits for six degenerate flavours, for a single flavour dntype and for a single flavour uptype from this method are shown labelled as A in figs. 5a, 5b and 5c, respectively.

5. Analysis and limits for light LSP

In the second analysis, which used a sample corresponding to 9300 hadronic Z^0 decays, two-jet events were selected using the jet clusterization algorithm LUCCLUS [9]. The acoplanarity angle α_{xy} was calculated as the angle between the two jets projected on

the plane perpendicular to the beam axis. The candidates were selected with the following criteria:

- (1) total visible charged energy larger than 15 GeV,
- (2) more than five charged particles,
- (3) $|\hat{z}| < 4$ cm,
- (4) $\sigma(z) < 6$ cm,
- (5) $|\cos \theta_{\text{thrust}}| < 0.7$,
- (6) $\alpha_{xy} \leq 135^\circ$.

The first criterium was chosen in order to complement with some coverage the selection of section 3.

After the selection the sample contained 31 candidates. For estimating the expected background from standard Z^0 decays, the Monte Carlo events described in section 4 were used. It was found that 0.37% of the simulated standard hadronic Z^0 decays satisfied the selection criteria, which corresponds to 34 ± 4 (stat.) events in the selected sample. The systematic error was estimated to be 10% by comparing the distributions of the Monte Carlo events (with the parton shower fragmentation as well as with the string fragmentation) and the data in the variable α_{xy} . The background was subtracted from the number of candidate events, and a 5% systematic error in the normalization was added in quadrature with the other errors. The result was -3 ± 7.5 events. The upper limit of 13 for the number of signal events satisfying the selection criteria was determined by excluding 95% of the positive gaussian probability density.

The detection efficiency for the squark signal was parametrized analogously to fig. 4, being typically 25% for masses of the LSP up to half of the squark mass and for the squark masses larger than about 20 GeV/c^2 . It was assumed to be known with about 5% uncertainty.

The 95% confidence level search limits based on this search are shown in fig. 5 labelled as B.

In conclusion, it is seen from fig. 5 that the combination of the two analyses exclude in the case of a LSP lighter than 20 GeV/c^2 three generations of squarks below 45 GeV/c^2 , as single flavour dntype squark below 43 GeV/c^2 and a single flavour uptype squark below 42 GeV/c^2 . For heavier LSPs (up to $m_{\tilde{q}} - 2 \text{ GeV}/c^2$) the limits extend to 44 GeV/c^2 , 38 GeV/c^2 and 36 GeV/c^2 , respectively. These results greatly improve the limits deduced from previous experiments, and are entirely new for the case of down type squarks.

After the completion of the present work a paper

by the Mark II Collaboration was received [12] where similar conclusions are reached.

Acknowledgement

We are greatly indebted to our technical staffs, collaborators and funding agencies for the support in building the DELPHI detector and to the members of LEP Division for the speedy commissioning and superb performance of the LEP collider.

References

- [1] CELLO Collab., H.-J. Behrend et al., *Z. Phys. C* 35 (1987) 181.
- [2] TOPAZ Collab., I. Adachi et al., *Phys. Lett. B* 218 (1989) 105.
- [3] UA1 Collab., C. Albajar et al., *Phys. Lett. B* 198 (1987) 261.
- [4] CDF Collab., F. Abe et al., *Phys. Rev. Lett.* 62 (1989) 1825.
- [5] UA2 Collab., J. Alitti et al., *Phys. Lett. B* 235 (1990) 363.
- [6] H. Haber and G. Kane, *Phys. Rep. C* 117 (1985) 75.
- [7] DELPHI detector, to be submitted to *Nucl. Instrum. Methods*.
- [8] DELPHI Collab., A precise measurement of the Z^0 resonance parameters through its hadronic decays, CERN preprint CERN-EP/90-32, submitted to *Phys. Lett. B*.
- [9] T. Sjöstrand, *Comput. Phys. Commun.* 27 (1983) 243; 28 (1983) 229; T. Sjöstrand and M. Bengtsson, *Comput. Phys. Commun.* 43 (1987) 367.
- [10] DELPHI Collab., P. Aarnio et al., *Phys. Lett. B* 240 (1990) 271.
- [11] Particle Data Group, G.P. Yost et al., Review of particle properties, *Phys. Lett. B* 204 (1988) 80-81.
- [12] Mark II Collab., T. Barklow et al., SLAC preprint SLAC-PUB 5196 (March 1990).

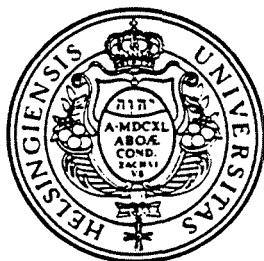
**DEPARTMENT OF HIGH ENERGY PHYSICS
UNIVERSITY OF HELSINKI**

REPORT SERIES

HU-SEFL-90-17

**EXOTICA IN DELPHI I;
THE TOOLS FOR PHYSICS ANALYSIS**

P. Eerola, K. Huitu, R. Keränen, P. Morettini and R. Orava



ISSN 0783-5760

**UNIVERSITY OF HELSINKI
DEPARTMENT OF HIGH ENERGY PHYSICS
SILTAVUORENPENGER 20 C · SF-00170 HELSINKI · FINLAND**

Abstract

Signatures and backgrounds in a selected sample of new physics processes are analyzed in order to define, construct and test the hardware and software tools available for the physics analysis with DELPHI.

Contents

1	General - Goals and Strategy	3
2	Signatures of the New Physics	5
2.1	Theoretical Expectations	5
2.2	Experimental Surprises	6
3	Backgrounds	7
3.1	Standard Physics Processes	7
3.2	Experimental Bias	7
4	Global Event Observables	9
4.1	Event Shape Parameters	10
4.2	Isolation Criteria	12
4.3	Cluster Algorithm	12
5	Total Missing Energy	13
5.1	Instrumental Effects	14
5.2	Vetoing Possibilities	15
5.3	Additional Tagger in the 40° Region	19
5.4	Conclusions of the Geometrical Study	19
6	Cluster Analysis	22
6.1	Combined Calorimetry Information in FASTSIM	22
6.2	Jet Reconstruction	24
7	The Muon	30
8	Example: Supersymmetric Processes	33
8.1	Selectrons	33

8.1.1 Analysis	34
8.2 Squarks	38
9 Conclusions	44
10 Acknowledgements	45

Chapter 1

General - Goals and Strategy

When dealing with the detector complex as sophisticated as DELPHI a thorough analysis of the tools available for the physics analysis – both instruments and software – is required. For the physics feasibility studies a package of programs with the detector description in a parametrized form is available as the DELPHI FASTSIM code ([1]). For the serious detector simulation and final physics analysis the DELANA – DELSIM package of simulation routines is to be used.

We report here on our efforts to develop and test the tools required for evaluating the response of DELPHI to physics beyond the standard model. To accomplish this we have first selected a set of representative observables characterizing the topology and the general structure of the events exhibiting the presence of a new particle or process at the Z^0 pole. We first started by constructing these observables within FASTSIM and then continued by analyzing the efficiency with which DELPHI reproduces these quantities when the simulated response (FASTSIM) is introduced.

Our work described in this report is rather general and includes analysis on the muon, photon/electron, hadron and missing energy signals in DELPHI. Our report also contains an analysis of the jet reconstruction systematics and a description of the event shape parameters now available in FASTSIM. The missing energy analysis provides us with one of the most sensitive tools when evaluating the capabilities of a detector – and a thorough investigation of DELPHI's ability to measure missing energies is reported here, as well. As examples of the new physics processes two supersymmetric reactions are chosen: selectron and squark pair production.

We shall continue our work by utilizing the tools described in this report in order to perform feasibility studies on a set of processes representing physics beyond the standard model.

Chapter 2

Signatures of the New Physics

2.1 Theoretical Expectations

Despite of the experimental success of the standard model serious shortcomings force us to consider extensions and modifications of the $SU(3)_C \times SU(2)_L \times U(1)_Y$ theory. The Higgs sector seems to be the main culprit: there is no mechanism to prevent the Higgs boson from attaining a mass of the order of the Planck mass due to the loop corrections to the bare mass. The proposal of fine tuning the bare mass on ad hoc basis with a cancellation arranged with the loop contributions such that the desired Higgs mass (< 1 TeV) sounds unsatisfactory. To solve the problem two possibilities are proposed: 1) supersymmetry and 2) various composite models where the Higgs is constrained to be composite so that the integrals in the loop calculations have to be cut off at the composite scale, normally of the order of 1 TeV. Questions like particle masses or number of generations should be enlightened in these models, as well. To include gravity superstring theories have been introduced. These theories are formulated in a 10-dimensional supersymmetric GUT. All of the extensions and modifications of the standard model lead to the phenomenology similar to the standard model at the low energy limit, and their predictive power lies only at higher energies. New physics expected may be divided in the following categories:

1. variations of the standard model: top quark, 4th generation, heavy leptons, non-minimal Higgs, axial gluons, new stable hadrons,....,
2. supersymmetry: partners of the matter fermions, gauginos,....,

3. compositeness: excited leptons, coloured leptons, preon mass scale (contact interaction).

2.2 Experimental Surprises

From the present theoretical extensions of the standard model we expect a wide variety of new particles and interactions. New discoveries may not be uniquely connected with a definite theoretical prediction and they will be limited by the basic uncertainty on the particle masses, for example. An experimentalist at LEP may be, therefore, confronted by a surprise observation which cannot be, with certainty, predicted by any theoretical dogma. For this a thorough analysis on the variables describing the event topologies, shapes and missing four-momenta is required.

The experimental surprises at LEP may include:

- combinations of missing energy with a number of leptons
- acoplanar lepton/cluster pairs
- large energy imbalances E_{had}/E_{em}
- small visible energy events with a close mass lepton pairs
- multilepton events with multiple clusters
- strange event topologies with asymmetric cluster configurations – monojets
- spherical events
- enhanced heavy flavour production in connection with the above and/or
- with an identified hadron tag
- multilepton events
- single isolated photons or leptons
- heavily ionizing tracks through the detector, strange identification hypothesis with RICH
- jumps in R, decay vertices of new long lived particles

Chapter 3

Backgrounds

3.1 Standard Physics Processes

The physics processes producing signals similar to the non-standard physics predictions and to the unusual experimental observations listed above are

1. radiative processes in which a photon or a lepton escapes detection,
2. tau-pair production with an acoplanar lepton configuration in the final state due to the unobserved neutrinos,
3. heavy quark production with a weak decay of one of the quarks in the final state,
4. higher order QCD corrections producing highly spherical events, and
5. unusual decay modes of the known particles like D^0 decaying into a muon, K_L^0 and a neutrino may simulate single isolated lepton events.

3.2 Experimental Bias

The hardware tools of DELPHI consist of the

1. energy calibration: VSAT, SAT, MIG,
2. vertex detection: microvertex detector, outer detector, inner detector, SAT, VSAT,

3. tracking detectors: TPC, inner detector, outer detector, forward detectors A&B, SAT,
4. hadron identification: RICH, TPC, TOF, HPC, HCAL,
5. calorimetry: HPC, FEMC, HCAL, SAT, VSAT,
6. muons: muon chambers, forward hodoscope detector, tracking detectors, calorimeters.

In order to simulate the bias by the varying detector dependent factors in the observables sensitive to the new physics processes we 1) utilize the existing DELPHI FASTSIM package of simulation routines, 2) develop FASTSIM compatible descriptions for the muon, clusters of combined calorimetry and 3) calculate efficiencies of the photon, muon and neutral hadron reconstruction.

In the following, we do not consider the background processes inherent to the LEP-machine.

Chapter 4

Global Event Observables

Several variables have been constructed to describe how the particles in the event are distributed in space.

The sphericity and the aplanarity describe the 'cigar shapeness' of the event. These are widely used, but they are quadratic in momentum and, from a theoretical point of view, parameters which are linear in momentum are preferred [2]. This kind of shape parameters are thrust and oblateness.

There is also a large amount of variables, which are sensitive to certain event types. In calculating many of these sphericity or thrust information is used, e.g. for the acollinearity the sphericity axis is used. The acollinearity is sensitive to processes where large amounts of energy is missing, e.g. supersymmetric events.

We have included the above mentioned shape parameters and also some other event parameters (the number of clusters, the isolated lepton parameter and the variable $P_{T,visible}/E_{visible}$) to the DELPHI fast simulation package FASTSIM.

4.1 Event Shape Parameters

Sphericity and aplanarity

The momentum tensor is defined as [3]

$$M_{\alpha\beta} = \frac{\sum_i p_{i\alpha} p_{i\beta}}{\sum_i p_i^2},$$

which is a symmetrical real matrix and has eigenvalues $\lambda_1 \geq \lambda_2 \geq \lambda_3 \geq 0$.

The eigenvector \mathbf{n}_1 corresponding to the eigenvalue λ_1 is the event axis and the plane $(\mathbf{n}_1, \mathbf{n}_2)$ is the event plane. The sphericity is defined as

$$S = \frac{3}{2}(\lambda_2 + \lambda_3),$$

so that for totally isotropic events $S = 1$ and for collinear events $S = 0$.

The aplanarity is $A = \frac{3}{2}\lambda_3$. For coplanar events $A = 0$ and generally $0 \leq A \leq 1/2$.

Thrust and oblateness

Thrust is defined as [4][2]

$$T = \max_{|\mathbf{n}|=1} \frac{\sum_i |\mathbf{n} \cdot \mathbf{p}_i|}{\sum_i p_i},$$

where $1/2 \leq T \leq 1$ and the thrust axis is given by \mathbf{n} for which the maximum is attained.

The maximum value of the above mentioned variable in the plane perpendicular to the thrust axis is called the major value and the corresponding axis the major axis. The value of the variable along the axis perpendicular to the thrust and the major axis is the minor value. The difference between the major and the minor values is called the oblateness (O_B). Thus the oblateness describes, how the event is distributed around the thrust axis.

Acollinearity

The event acollinearity $ACOL$ is defined as follows [6]

- (a) The event is divided into two hemispheres by sphericity axis, which is calculated by LUSPHE.
- (b) The momenta of all the tracks are summed vectorially (\mathbf{P}_1 and \mathbf{P}_2).
- (c) $ACOL = 180 - \phi$, where ϕ is the angle between \mathbf{P}_1 and \mathbf{P}_2 . If all the tracks are in one hemisphere $ACOL = 180$.

Variable $P_{T,visible}/E_{visible}$

The variable $P_{T,visible}/E_{visible}$ is defined as [6]

$$P_{T,visible}/E_{visible} = \frac{|\sum_i \mathbf{P}_{T,i}|}{\sum_i E_i},$$

where $P_{T,i}$ is the transverse momentum and E_i is the energy of track i . This variable can be used with the acollinearity to distinguish between the background and the signal in supersymmetric events.

4.2 Isolation Criteria

The isolated lepton parameter ρ is defined as follows [6]

- (a) Remove the candidate lepton from the track list.
- (b) Perform LUND cluster algorithm ($d_{join}=0.5$) on the remaining tracks.
- (c) For each jet form the quantity
$$\eta = \sqrt{2E_{lepton} \times (1 - \cos(\text{angle between lepton and jet}))},$$
$$\rho = \min_{jets} \{\eta\}.$$

The lepton is considered isolated if the parameter ρ is greater than 1.8.

4.3 Cluster Algorithm

The distance measure between two particles is chosen to be [5]

$$d_{ij}^2 = \frac{4p_i^2 p_j^2 \sin^2(\theta_{ij}/2)}{(p_i + p_j)^2}.$$

The distance scale above which two clusters may not join is the only parameter on which the jet reconstruction depends.

Chapter 5

Total Missing Energy

A mismatch between the measured total energy and the known initial state energy provides us with a possible signature of new physics at Z_0 at LEP. The **total missing energy resolution** constitutes one of the basic characteristics of the detector performance. In the pure calorimetric energy measurement the complexity of the reconstruction of the combined track and calorimetric information is avoided.

The basic parameters of a calorimetric measurement are the **energy resolution** ($\sim 1/\sqrt{E}$) and the **efficiency**, which are affected by the restricted geometry and the energy thresholds - for evaluating them a detailed knowledge of the geometry and of the dynamic range of the arriving particles is required.

The DELPHI calorimeters (HPC, EMF, and HCAL) cover 98% of the solid angle - the "holes" in the **beam direction** are partly covered by the SAT detectors, which deliver the E.M. energy information and allow us to tag the charged particles. The effective energy resolution and efficiency decreases in the $\theta \simeq 40^\circ$ **supply region**, in which there exists a significant amount of passive materials and a gap between the electromagnetic calorimeters (6% of 4π). One should remember that the Hadron Calorimeter coverage is **not** much impaired in this region, but due to the passive materials and ineffective regions (cryogenics sectors and the barrel-end cap connection) the effective resolution of HCAL is reduced somewhat. It should be noticed that this problematic HCAL acceptance interval

does not coincide with the hole between the E.M. calorimeters but is shifted towards the barrel region - in total the "40° problem" represents 15% of 4π .

The consequences of the limited acceptance and inefficiencies in the calorimetric total energy measurement are studied here by utilizing the parametrized detector simulations of FASTSIM. It is not the aim of this study to find out the ultimate setup of the selection algorithms to be used in the missing energy analysis, but the simulated sample and applied cuts are chosen in order to **study the importance of the lacking geometrical acceptance** and the capability to recover from them. The sample under study consists of the standard hadronic events ($q\bar{q}$'s produced by JETSET6.3 $O(\alpha_s^2)$ with the flavours u,d,c,s,b) and it can be considered as a set of ideally triggered hadronic events in DELPHI (no charged multiplicity cuts or total energy trigger conditions are applied here). The rough scale for the desired missing energy resolution is set in terms of a signal expected for the supersymmetric quark pairs with $m_{\tilde{q}} = 40$ GeV decaying into invisible photinos ($m_{\tilde{\gamma}} = 20$ GeV) carrying large energies ($O(60\text{GeV})$). Ordinary $q\bar{q}$ events act as the background with the signal-to-background ratio of $R = \sigma_{\tilde{q}\tilde{\gamma}}/\sigma_{q\bar{q}} \simeq 5.5\%$.

5.1 Instrumental Effects

The starting point of our analysis is the missing energy distribution of the $q\bar{q}$ final state seen by the DELPHI calorimeters without any selections. As a reference we use the distribution produced by a naive parametrization in which no inefficiencies in addition to the the beam holes are simulated and the we assume energy resolutions of σ/\sqrt{E} (electromagnetic) = 20%, σ/\sqrt{E} (hadronic) = 100%. The energy carried by the neutrinos and muons is included in the missing energies plotted in Fig. 5.1.

As a result of our parametrization it is seen that in a typical $q\bar{q}$ event an average total energy of 75 ± 15 GeV is reconstructed in the calorimeters when a proper calibration procedure is assumed. The shift from zero and the width of the distribution are due to the instrumental inefficiencies and fluctuations in the calorimetric

energy measurement - in the hadronic sector the complex structure of DELPHI calorimetry, with the coil, contributes to the reduced efficiency of low energy hadrons seen over the whole acceptance interval. The events with a large missing energy in the distribution shown in Figure 5.1 are the culprit to be studied. The tail originates in the following contributions:

- the neutrinos accompanied by the energetic muons from the weak decays of the heavy quarks carry away an amount of energy which is not fully detected in the calorimeters. These final states may be identified e.g. by the isolated lepton criterium and/or by the vertex analysis with the μ -vertex and inner detectors;
- the beam hole is not covered by the EMF+HPC+HCAL complex. SAT covers part of the acceptance interval and it has a finite electromagnetic energy resolution, with strip layers it can register charged tracks.
- the special characteristics of the 40° region.

In Figure 5.1 (solid line) one can observe that, without any selections, 8.4% of all the $q\bar{q}$ events exhibit missing energy ($E_{\text{miss}} \geq 40$ GeV) characteristic to the SUSY events used as a reference.

The importance of the geometric contribution is displayed in Figure 5.1 in which the missing energy is plotted as a function of $\cos(\theta)$ (the calorimetric missing energy vector normalized to the scalar missing energy). The contributions of the beam hole and also the 40°-region are clearly seen.

5.2 Vetoing Possibilities

In the elimination of the background one may apply geometrical selection criteria. In the beam region SAT is described with the following characteristics ¹:

¹The SAT performance was parametrized in terms of estimated SAT characteristics by L. Bugge (Oslo) and P. S. Iversen (Bergen).

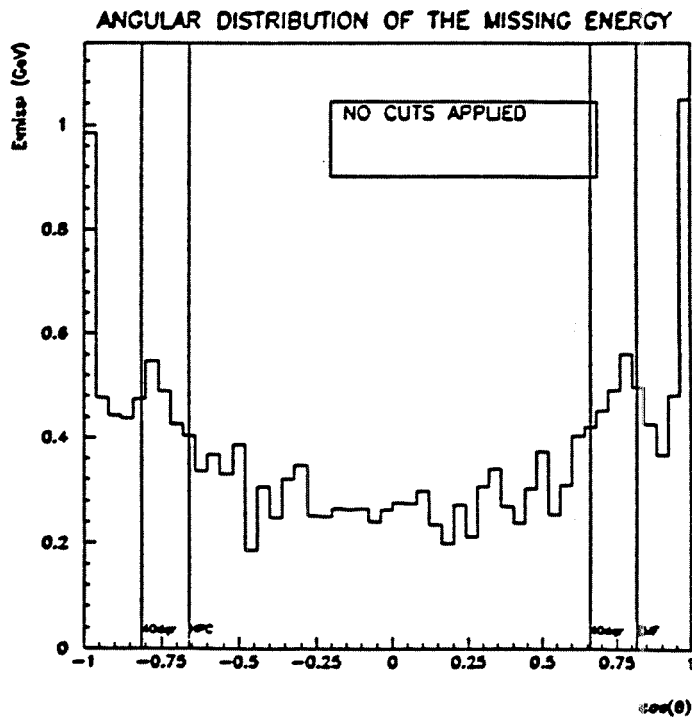
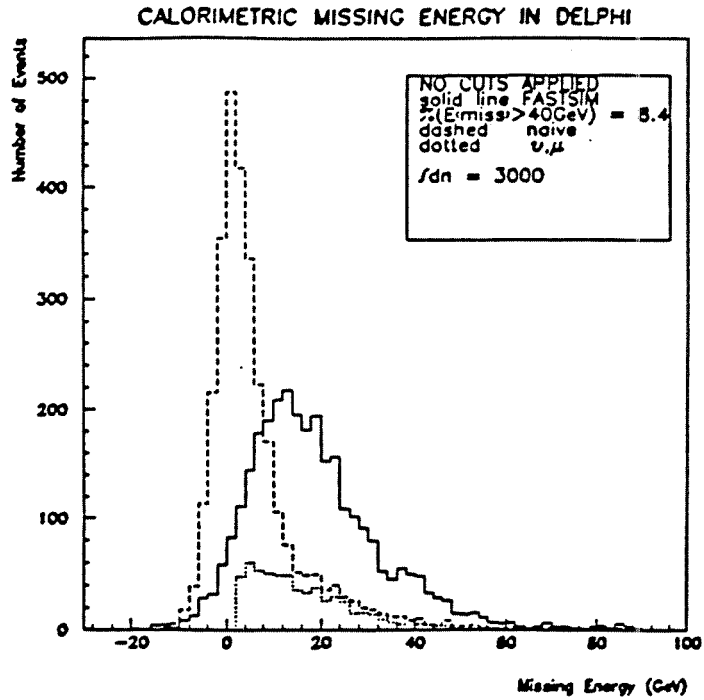


Figure 5.1: a) Calorimetric missing energy without any geometrical selections. b) Angular distribution of the missing energy.

- acceptance interval $\theta, 180^\circ - \theta \in [1.91^\circ, 6.89^\circ]$ covered for $\phi \in 2\pi$ (actually the coverage of the SAT strips is less than the calorimeter coverage),
- veto signal generated for all the photons and charged particles above 2 GeV.

With the veto from SAT the sample is reduced to 92 % of the original. The resulting missing E and angular distribution compared to the original distribution are shown in Figure 5.2. One can note here that the missing energy tail is reduced down to 5.5% of the reduced sample. The effect of the radiative corrections was not studied here.

In the second step, the events with any observed activity in the 40° region were tagged. Here we use any signal from HCAL in the "hole" $[35.5^\circ, 41.5^\circ]$ as a veto (JVVT40D). Since the decreased efficiency of HCAL in the interval $[41.5^\circ, 48.5^\circ]$ contributes to the missing energy we check the MIP signals in HPC in this angular region. If these signals are not associated with the observed hits in HCAL the veto is on (JVTHPC). The particle multiplicity in a typical $q\bar{q}$ final state with all the secondary particles generated in the inner parts of DELPHI are large enough to produce some of these signals in a large fraction of the events. Here one can use a multiplicity selection.

The (SAT veto .OR. 40° veto) cuts the statistics of the original sample down to 57 %, but, as a result, the missing energy tail is significantly reduced. The peaks are eliminated in the angular distribution (some "over compensation" in the endcaps is unavoidable) which indicates that any reduction has to be achieved by dynamical cuts rather than by geometrical vetos (Figure 5.2). As a quick reference to the SUSY channel, the remaining background rate is still considerable: the standard $q\bar{q}$ events contain a fraction of 3.6% of events with the missing energy ≥ 40 GeV, which originates mainly from the ν 's and energetic μ 's together with the typical average loss of the order of 13 GeV due to the low energy inefficiencies. This straightforward interpretation of the SUSY background implicitly assumes that the rate of the SUSY states is reduced proportionally to the sample under study.

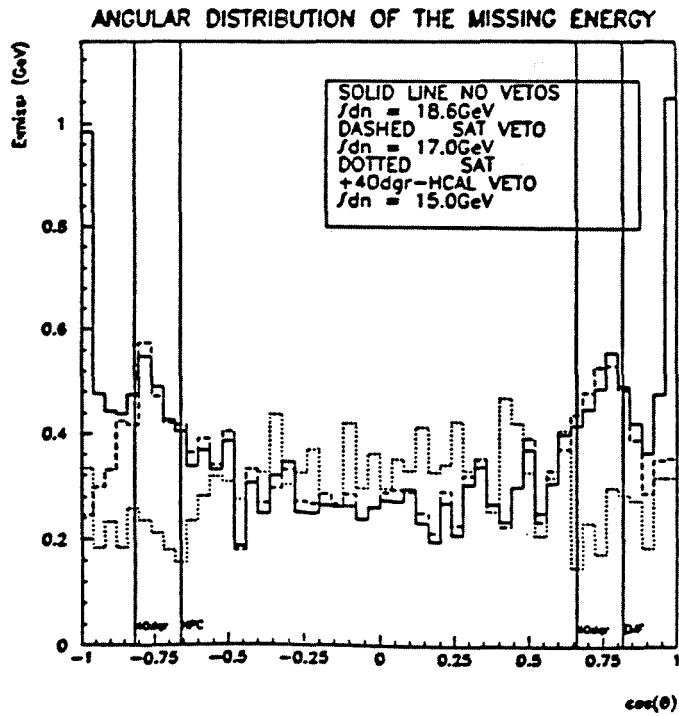
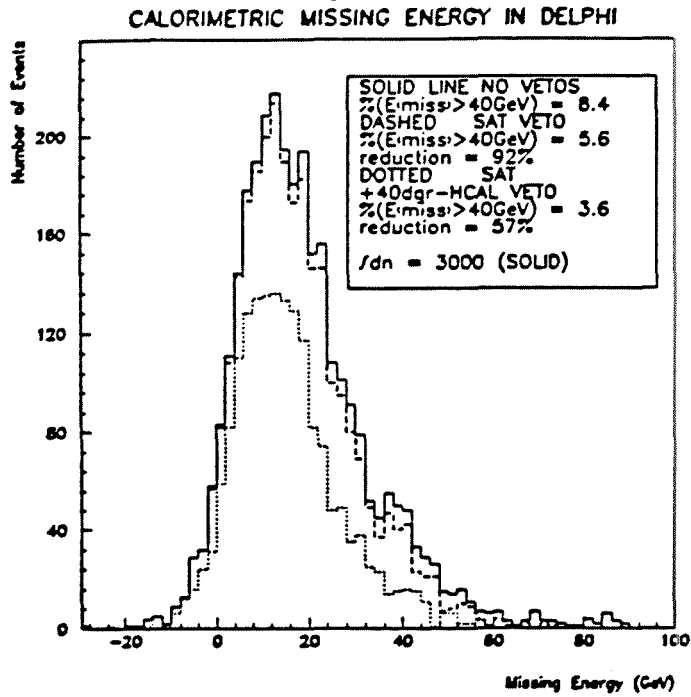


Figure 5.2: a) Calorimetric missing energy after different geometrical selections. b) Angular distribution of the missing energy.

5.3 Additional Tagger in the 40° Region

The lower efficiency in the 40° region weakens its vetoing power. Additional information about the multiplicity in this location could help in finding more selective methods of vetoing. The scintillators in the support structures of RICH improve the photon detection efficiency. We studied the effect of additional taggers in FASTSIM by inserting an extra module which covers the acceptance interval $[35.5^\circ, 41.5^\circ]$ (+ complement). We parametrized its efficiency for electrons, photons, and hadrons separately according to the CASCADE simulations. The 60% coverage in ϕ is assumed averaged over 2π . It is assumed that the taggers are capable to give multiplicity information with a 15° granularity (module-by-module).

With the help of the proposed extra tagging device one can release the strict condition of **any** seen signal in the 40° hole to a more selective criterion based on the seen **multiplicities**. As a result, we are able to tag more efficiently the direction of the jets and of the very energetic nonreconstructed hits (see Figure 5.3). With an appropriate choice one achieves the same confidence level in the missing energy identification ≥ 40 GeV as with the pure HCAL selection, but with a smaller reduction of 69% in the sample of events.

5.4 Conclusions of the Geometrical Study

By using appropriate selection criteria the geometric contribution in the missing energy tail (8-9% $E_{\text{miss}} \geq 40$ GeV) of the hadronic events can be eliminated down to the level of dynamical neutrino missing energy contribution (2-3%). Although the effective resolution is not isotropic over the solid angle, the complete 4π coverage of the proposed tagging tools enables us to apply veto with a moderate reduction ($\sim 30 - 50\%$) in the statistics.

Also in the hadronic final states an additional tagging device in the 40° region improves the sample purity. It does not completely eliminate the rest of the missing energy tail, which has to be attacked finally with a set of dynamical cuts. It should be noted that for

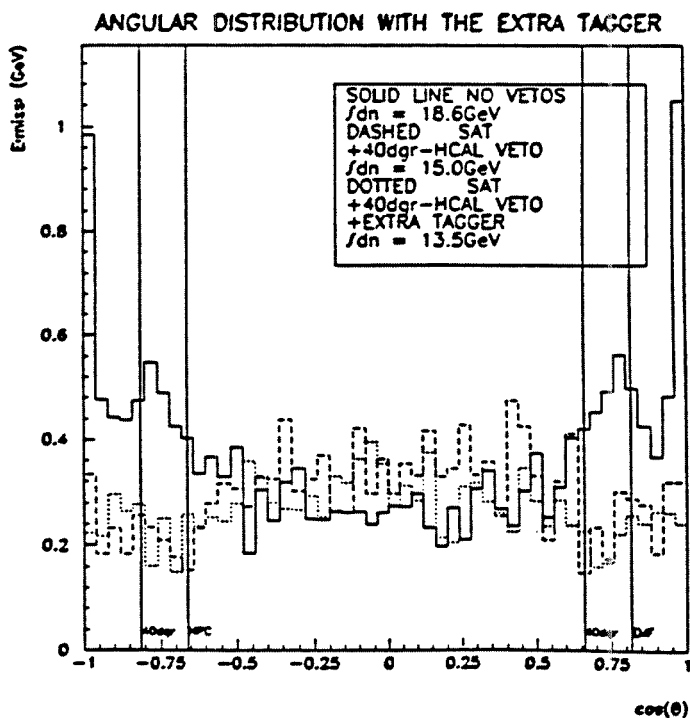
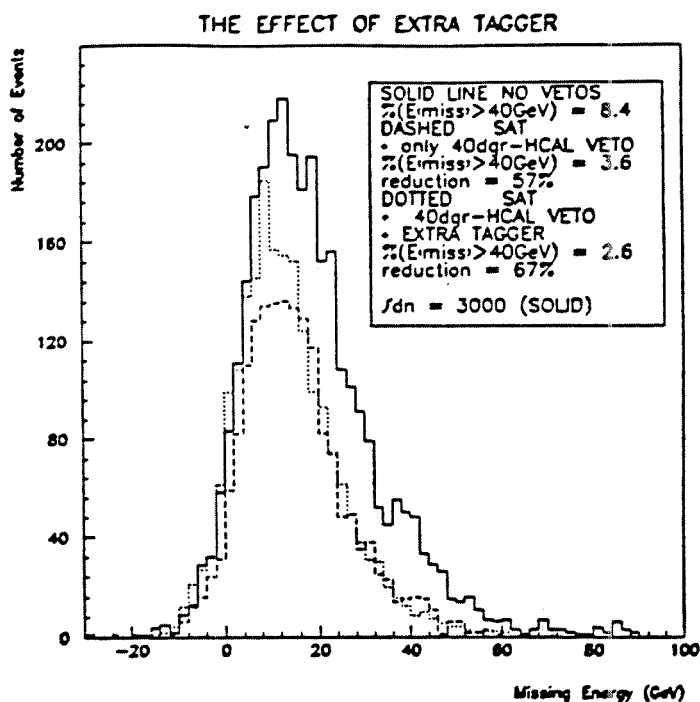


Figure 5.3: The effect of an additional tagger in the 40° region on the a) calorimetric missing energy and b) angular distribution of the missing energy.

the soft photons and electrons/positrons the importance of the extra device in the 40° gap between HPC and EMF may be more pronounced.

Chapter 6

Cluster Analysis

6.1 Combined Calorimetry Information in FASTSIM

In the parametrization of the calorimetric information the following quantities characterize the measurement capability of a calorimeter:

- 1) **efficiency** (which consists of the geometrical acceptance and dynamical energy dependence),
- 2) **energy resolution**,
- 3) **granularity**, and
- 4) **particle identification**.

The first two aspects are purely **single-particle** parameters, the third one defines the observable **multiparticle topology** in the detector - a nonnegligible fraction of the overlapping particles depends on the instrumental granularity and the density of the arriving particles (degree of collimation). The fourth quantity can be considered as a special capability of the instrument (e.g. HPC e/π separation) but it also depends on the first three aspects (e.g. the muon identification, which has contributions from several parts of DELPHI). In the DELPHI calorimetry these parameters have to be **defined locally in each calorimeter** due to the differences in the basic detection techniques of the devices. However, for the event reconstruction (energy, multiplicity, and particle identification) **combinatory information** from several calorimeters is desired. This is due to

the simple **geometrical reasons** (e.g. EMF vs. HPC, and the gap between them covered by HCAL) and absorption properties of the various calorimeters (e.g. EMCAL's represent several radiation lengths but also a significant thickness in absorption lengths - thus a fraction of the **hadronic energy** is deposited in the EMCALs contributing to the signal topology there).

Motivated by these arguments, the parametrization of the calorimetry in FASTSIM is based on a **two-step principle** in which the detector response to an event is simulated first locally in each calorimeter module, and the combined calorimetry topology is then created by considering this simulated information in the second stage. This resembles the logic of the off-line analysis procedure in DELANA. Thus the aspects of the **combined pattern recognition** process are taken into account in the FASTSIM parametrization. This approach allows us also to include and study the **compensation problematics** in the DELPHI calorimetry.

As the **input** the parametrization of the calorimetry in FASTSIM we utilize the simulated **particle flow including the secondary processes up to the calorimeters** (/SPXHIS/), as described in the discrete geometry of FASTSIM. The **output of the combined calorimetry is a set of observed (reconstructed) energy clusters** (/SPXCLU/) with their energy contents. The output of each calorimeter module can be found in the commons (/SPxCLU/ x for H:HPC, E:EMF, C:HCAL). The energy information is accompanied with the resolution estimate according to which it is smeared as well as with the spatial information, which is smeared according to the effective granularity. The combined clusters contain the topological information (i.e. of which local energy depositions the combined cluster consists of). The estimate of the combined energy resolution can be chosen either as a quadratic sum of the local resolutions or as a global resolution estimate.

The algorithm of building up the combined clusters is as follows. For each cluster seen in HCAL, the seen clusters in EMCALs are scanned through and the matching criterium is checked. The matching criterium consists of a geometrical check and, in the case of HPC, of the identification information as parametrized in the local HPC simulation applied (if HPC identifies the cluster as e/γ it is not asso-

ciated with a HCAL cluster). A **tunable parameter** in the linking procedure is the distance between the c.f.g. of the local clusters considered. In the barrel it is defined as a pair $(\Delta\theta\Delta\phi)$ and in the end cap as $\Delta R = \sqrt{\Delta X^2 + \Delta Y^2}$ with the default values of $(0.1, 0.2)$ and 25 cm corresponding roughly to the HCAL granularity and the width of a hadronic shower.

It should be noted that in this clustering process only the information from the **simulated detector response** of HPC, EMF, and HCAL is applied and no "short cut" information from the inherent part of FASTSIM. In a typical $q\bar{q}$ event (JETSET6.2 $O(\alpha_s^2)$) the 47 ± 13 local clusters (a part of them being truly pieces of a single hadronic shower) are combined in 23 ± 8 combined clusters, which gives an idea of the effective granularity of the DELPHI calorimetry.

6.2 Jet Reconstruction

We have studied the parton reconstruction efficiency in DELPHI by utilizing the FASTSIM package of simulation routines. Our study is motivated by the topological signatures expected for the events produced in the processes predicted within the standard model. For the event topology to be useful as an observable, jet reconstruction algorithms should be analyzed.

Two, three and four jet events are produced by the JETSET 6.3 package and the clusters are formed by utilizing the LUCLUS algorithm with the optimized value of the *djoin* parameter.

We have used two independent sources of data as the input: the track information taken from the SPXANA common of FASTSIM and the energy deposition information as parametrized in the FASTSIM description of DELPHI.

Jet reconstruction efficiency

In Figure 6.1 we plot the reconstruction efficiencies for different event topologies, containing 2 – 4 jets. The dynamic jet reconstruction efficiency is of the order of 90 – 95% and there are relatively few

misidentified topologies. When the track or energy deposition information is used for the jet reconstruction these efficiencies fall to 70 – 80% and a significant number of multijet events (20% of the three or four jet events are misidentified as having one missing jet.

Jet energy distribution

To study the efficiency of the jet energy reconstruction we plot the observed cluster energy normalized to the initial parton energy as a function of the parton energy in Figure 6.2 for the track and energy LUCLUS clusters. For the soft partons both the track and energy clusters contain more than 80% of the initial parton energy. For the energetic cluster, however, there is a significantly higher energy reconstruction efficiency with the method based on the use of the calorimetric energy depositions: while the track reconstruction of the 45 GeV partons contains only about one half of the initial energy, the energy deposition information alone allows one to recover about 80% of the original parton energy.

One should note here that, in any case, part of the jet energy is lost to neutrinos and non-reconstructed neutral hadrons.

Jet axis determination

For the event topologies to be useful in the physics analysis one has to be able to check the four momentum conservation event-by-event. The jet axis can be determined either by using the track information or by utilizing the energy depositions independently. In Figure 6.3 we plot the angular difference between the LUCLUS cluster axis and the original parton direction. The soft parton direction is reconstructed with roughly the same efficiency in both methods. At higher parton energies the track information seems to give somewhat better indication of the original parton direction. The track jet reconstruction efficiency is, however, very low at large parton energies (see Figure 6.2).

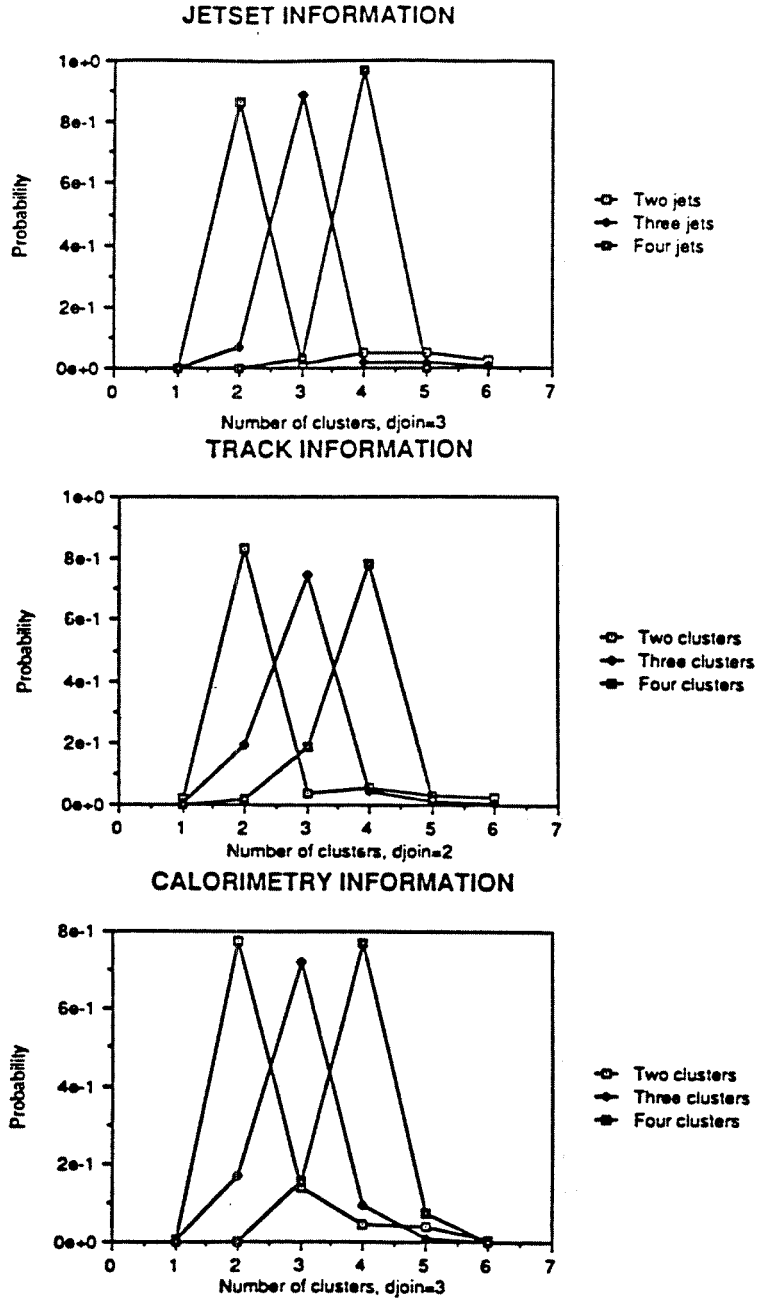


Figure 6.1: Reconstruction efficiencies for two, three and four jet events.

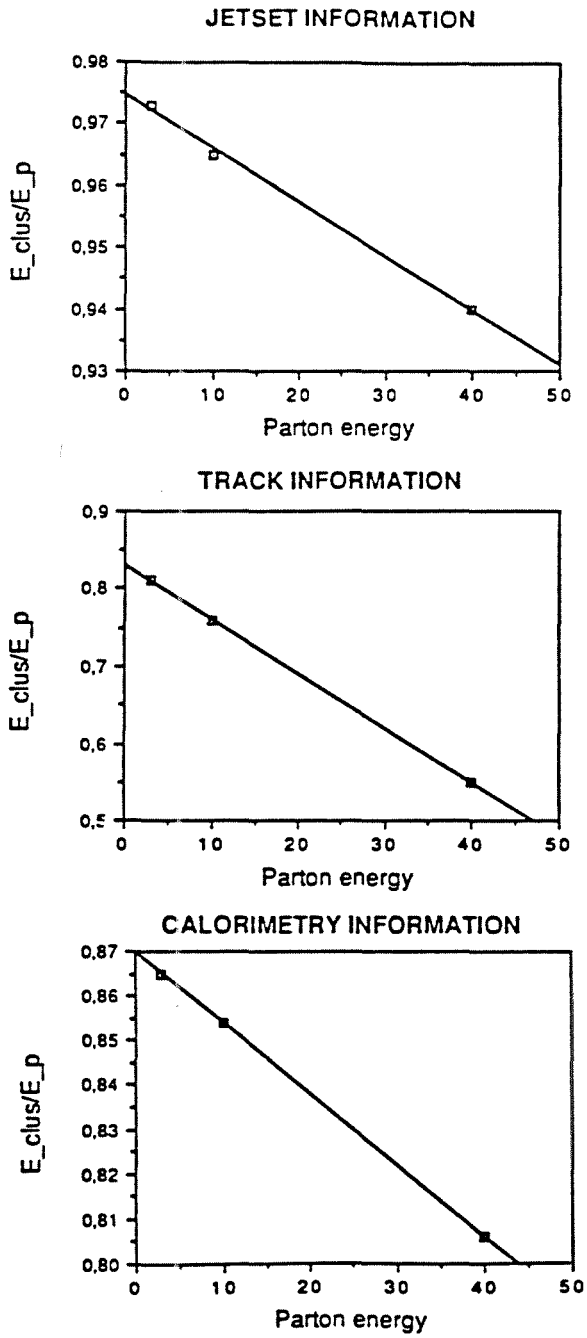


Figure 6.2: The jet energy reconstruction efficiencies.

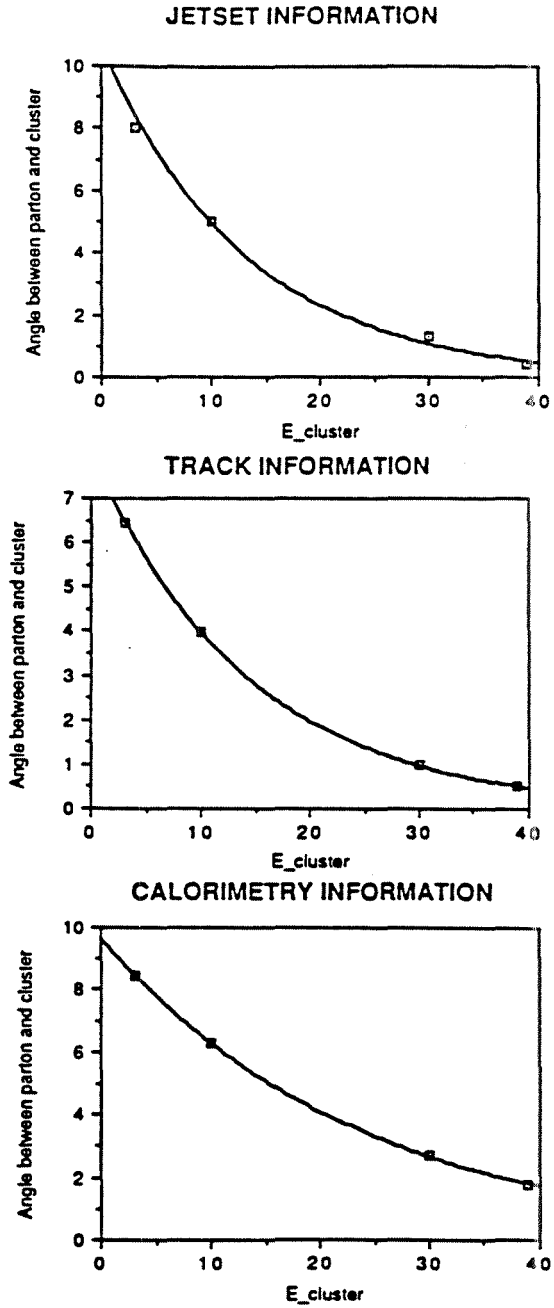


Figure 6.3: The angle between the LUCCLUS cluster axis and original parton direction.

Conclusions

From our analysis we conclude that the track and calorimetric energy deposition information of DELPHI provide highly complementary sets of data to be utilized in jet reconstruction with high efficiency. Slightly better energy reconstruction and direction information could be obtained by combining the two sets of data, but there is a danger of double-counting particle energies.

One should, of course, remember that the present analysis should be taken as a test of the FASTSIM package – the track information does not contain the secondary interactions, for example.

Our next step is to refine our missing energy-momentum analysis in order to complete our analysis of the tools available for evaluating various signatures of the new physics in terms of the event topology.

Chapter 7

The Muon

A separate study was carried out in order to evaluate the backgrounds and inefficiencies in identifying muons with DELPHI ([7]). The geometric efficiency of identifying a muon with the momentum larger than 3.0 GeV/c was found to be 94%, and an overlap probability with the accompanying hadrons was calculated to be 0.6% per muon in a $b\bar{b}$ -event. The muon detection efficiency of HCAL is shown in Fig. 7.1. The background muons can be produced by a) energetic non-interacting hadrons (0.1-2% per an incident hadron), b) pion or kaon decays (0.1-1% per an incident pion/kaon), c) by the hadron cascades (0.01-0.3% per an incident pion/kaon). The total background rates per incident pion or kaon are plotted in Fig. 7.2.

These false muon signals can be suppressed by using the particle identification information and by evaluating the transverse momentum of the muon candidate with respect to the jet axis. It is the correlated track and muon chamber information in combination with the segmented charge information of the HCAL that leads to the high muon identification efficiency of DELPHI.

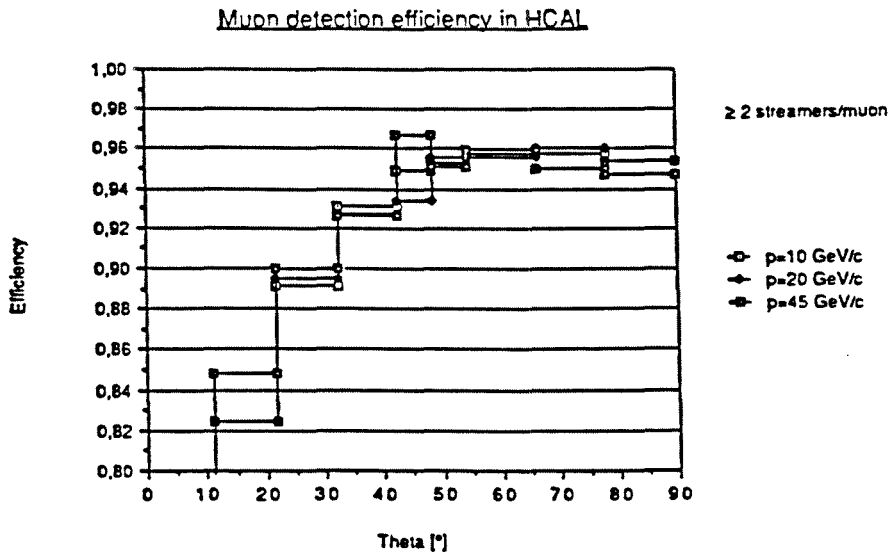
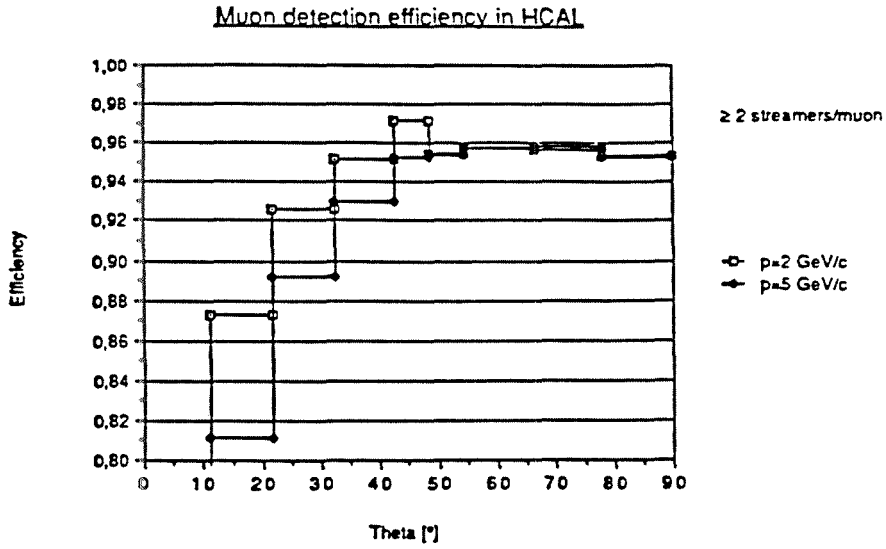


Figure 7.1: Muon detection efficiency in HCAL: a) for momenta 2 and 5 GeV/c, b) 10 – 45 GeV/c.

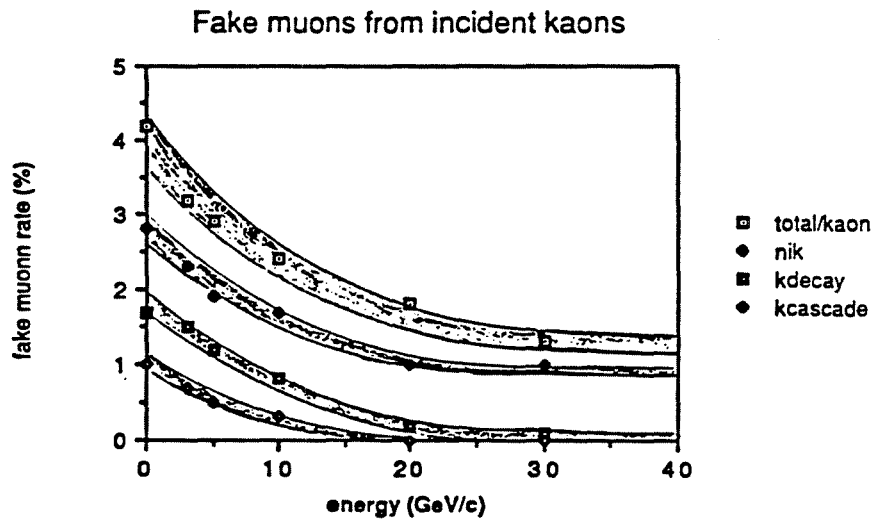
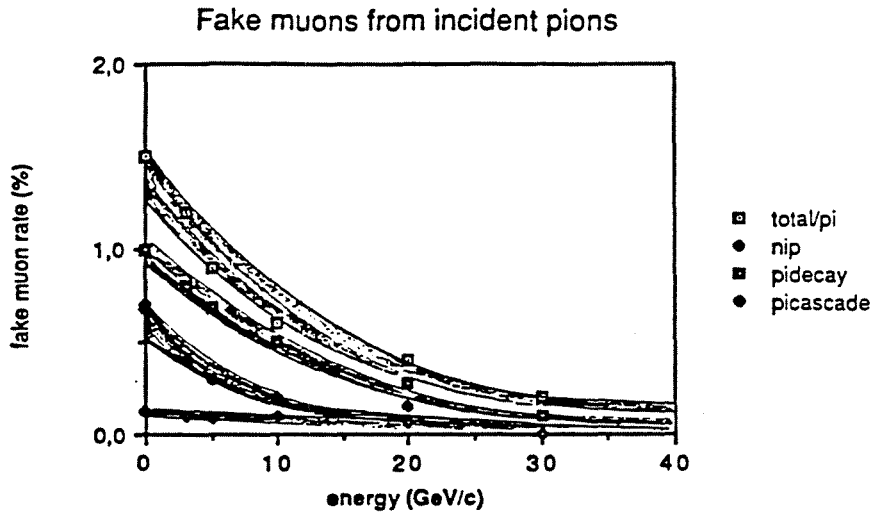


Figure 7.2: Parametrizations for the total number of fake muons generated by incident a) pions b) kaons.

Chapter 8

Example: Supersymmetric Processes

Supersymmetric processes provide us with an example of exotic events, which can be analyzed by using the tagging tools presented in this report. Supersymmetric events usually contain a considerable amount of missing energy due to the unobservable decay products of the produced supersymmetric particles. The events exhibit also acollinear structures for the same reason. Furthermore, isolated muons can be used in order to distinguish between heavy quark and hadron production.

The details of the theoretical assumptions and the cross-sections which have been used in generating the supersymmetric events are described elsewhere [8].

8.1 Selectrons

Selectron pair production was chosen as an example of a leptonic final state. Photino was taken as the lightest supersymmetric particle. Hence, the produced selectron decays with an extremely short lifetime to an electron and a photino. The scalar nature of the selectron distributes the decay products isotropically. Because the re-interaction cross-section of the photino is very small, the final

state consists of an acollinear electron pair. Obviously, there is a large amount of missing energy, carried away by the photinos.

The final state could be imitated by the radiative events, in which an electron pair is accompanied by a radiative photon which remains undetected. The cross-section for these events is strongly peaked in the forward direction due to the t-channel photon exchange. However, a polar angle cut is not enough to reduce this background, but a combined cut using the acollinearity and the missing transverse energy is sufficient to clearly separate the signal.

There is also a background contribution of tau-events, where both tau's decay into electrons and neutrinos. However, the electrons follow very strictly the direction of the tau parent because of the large kinetic energy of the tau. Therefore, the acollinearity cut pushes this background very low.

The present lower limit for selectron mass from JADE, if both types of selectrons have an equal mass and the photino is massless, is $25.2 \text{ GeV}/c^2$ (95 % confidence level) [9]. If the selectrons have different masses, the corresponding lower limit is $21.8 \text{ GeV}/c^2$.

The ASP experiment sets the lower limit to $51 \text{ GeV}/c^2$ (90 % confidence level) for massless photino and degenerate selectron mass states [10]. For non-degenerate masses the lower limit is $42 \text{ GeV}/c^2$. However, if the photino is heavier than $13 \text{ GeV}/c^2$, the mass of the selectron can be anything.

8.1.1 Analysis

The events were generated with the DELSIM events generators, and the detector parametrizations were those of the FASTSIM simulation package [1]. The following parameters of the standard model were used:

- $\sin^2\theta_W = 0.226$
- $M_Z = 92.5 \text{ GeV}/c^2$, $\Gamma_Z = 2.844 \text{ GeV}/c^2$
- $E_{beam} = 46 \text{ GeV}$

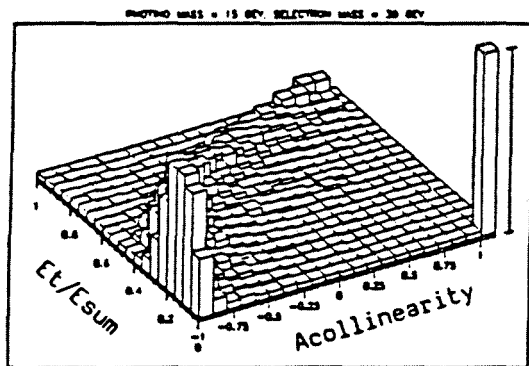
and the following mass values for the supersymmetric partners of $e/\gamma/Z^0$:

- $m_{\tilde{\gamma}} = 15 \text{ GeV}/c^2$
- $m_{\tilde{e}} = 30, 40, 45 \text{ GeV}/c^2$
- $m_{\tilde{Z}} = 60 \text{ GeV}/c^2$

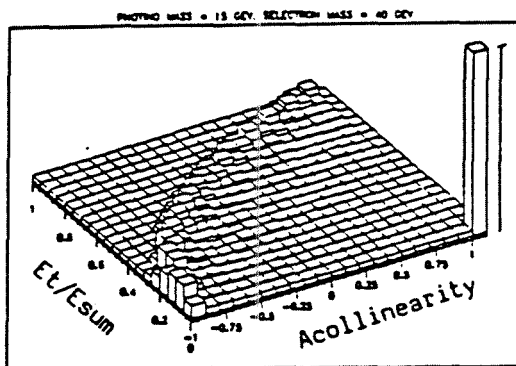
The analysis was performed in two stages. In the first stage, the events were selected which contained only two electrons and nothing else in the final state ("electron cuts" in Table 8.1). Selection criteria required two tracks, both identified as electrons and both pointing to a cluster in the electromagnetic calorimeters, and no energy deposition in the hadron calorimeter (except in the 40° region) or in the SAT. If the cluster was detected in the HPC, a further check was made that the object was not identified as a mip or a hadronic cluster.

The second stage selections aimed at separating the supersymmetric signal from the background with the aid of acollinearity and transverse energy sum ("susy cuts" in Table 8.1). The cosine of the space angle between the two electrons was required to be more than -0.8, and E_t/E_{sum} (absolute value of the vector sum of transverse energies per total energy) more than 0.15.

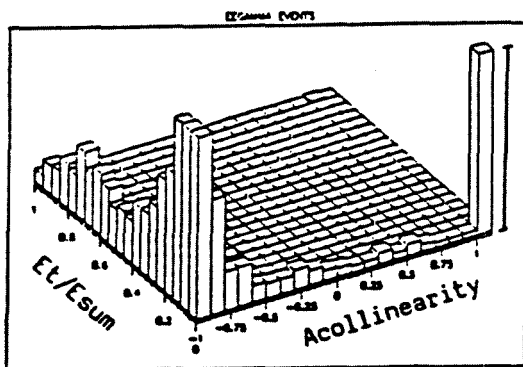
The final results are presented in Table 8.1. The header "ecal" refers to quantities (energy, space angle) measured in the electromagnetic calorimeters, and "track" to a combined measurement of the tracking detectors. The calorimetric measurement seems to be better in this case due to the better energy resolution, when high-energy electron tracks are considered. An example of the effectivity of the first stage selection criteria is shown in Figure 8.1.



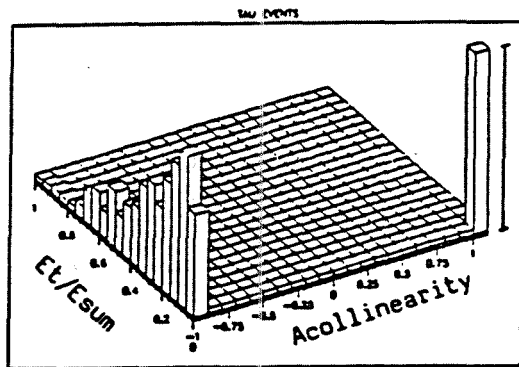
EEAL



EEAL



EEAL



EEAL

Figure 8.1: E_t/E_{sum} vs. acollinearity in selectron final states and in background events

event type	gener. events	electron cuts	susy cuts	
			ecal	track
\bar{e}^+e^-				
$m_{\tilde{e}} = 30 \text{ GeV}/c^2$	34471	22408	16008	16022
$m_{\tilde{e}} = 40 \text{ GeV}/c^2$	9612	6325	5214	5212
$m_{\tilde{e}} = 45 \text{ GeV}/c^2$	715	465	411	416
$e^+e^-\gamma$	1853460	135664	37	185
$\tau^+\tau^-$	171200	5958	0	0

Table 8.1: Number of selectron pairs and background events per 100 pb^{-1}

8.2 Squarks

Photino (i.e. one of the mass states of the SUSY neutralinos) is taken as the LSP in the minimal supersymmetric extension (SUSY $N = 1$), as in Ch. 8.1. The otherwise dominating gluino decay channel is suppressed by the assumption $m_{\tilde{g}} > m_{\tilde{q}}$. All squark masses of six flavours are assumed degenerate. The current experimental limits do not set rigorous constraints on the squark mass, if the condition of zero mass photino is released. At LEP I the phase space of pair production allows squark masses up to 40-45 GeV/c^2 studied.

The photino decays with $m_{\tilde{q}} > m_{\tilde{\tau}}$ result in a characteristic experimental signature of very large missing energy. The heavier the squark is the more spherically the photinos will be distributed. The observed quark jets do not exhibit the back-to-back nature usual for background events and a considerable fraction of the events are observed as monojet events i.e. as events with a single jet cluster and nothing in the opposite hemisphere. The rates of this specific SUSY channel are summarized in Table 8.2.

$m_{\tilde{q}} [GeV/c^2]$	$\sigma_{\text{signal}} [nbarn] (*)$			$\# \text{ events} \cdot 10^3 (**)$		
	$\bar{u}\bar{u}$	$\bar{d}\bar{d}$	$3(\bar{u}\bar{u} + \bar{d}\bar{d})$	$\bar{u}\bar{u}$	$\bar{d}\bar{d}$	$3(\bar{u}\bar{u} + \bar{d}\bar{d})$
10	2.7	3.5	18.7	274	350	1871
20	2.1	2.7	14.5	212	271	1451
30	1.2	1.6	8.4	122	156	836
40	0.3	0.4	1.9	28	36	194

Table 8.2: Cross sections and event rates for the squark-antisquark pair production in the LEP Ring at the Z^0 pole.

(*): in all calculations the following parameters of the Standard Model are used: $\sin^2 \theta_W = 0.22$, $M_Z = 90 GeV/c^2$, $\Gamma_Z = 2.64 GeV/c^2$. The photino mass is chosen to be 1 GeV/c^2 , unless noted otherwise.

(**): corresponding to the integrated luminosity of $100 pb^{-1}$, equivalent to 116 days of running the LEP at full efficiency with the luminosity of $10^{31} cm^{-2} s^{-1}$

The conventional hadronic final states $e^+e^- \rightarrow q\bar{q}$, q : d, u, s, c, b are considered as the reference background, in which the missing energy emerge from the weak decays and detector inefficiencies. The

total production cross-section for 5 standard quark flavours is $34.5nb$, which corresponds to $3447 \cdot 10^3$ events per $100pb^{-1}$.

The missing energy distributions of the signal and the comparison with the standard $q\bar{q}$ background are plotted in Figure 8.2. It can be seen that the missing energy signal is imbedded in the tail of the background distribution. The geometrical cuts described in Chapter 5 can be applied to eliminate the fraction originating in the detector inefficiencies but the remaining background is still considerable - especially when the squark mass approaches the limit of the phase space.

In Figure 8.3 the sphericity distribution and in Figure 8.4 the thrust and the oblateness distributions are plotted for $\tilde{q}\tilde{q}$ -events ($m_{\tilde{q}} = 40 GeV/c^2$ and $m_{\tilde{\gamma}} = 20 GeV/c^2$) and for background events together with the signal. The signal events are more spherical than the background events, but the small number of $\tilde{q}\tilde{q}$ -events prevents us from using this property as a tagging method.

An efficient tagging method is found by studying the acollinearity of the events. In Figure 8.5 the acollinearity is plotted against the variable $P_{T,visible}/E_{visible}$ for the signal and the background events. Taking into account events with $P_{T,visible}/E_{visible} \geq 0.3$ and acollinearity $\geq 60^\circ$ the signal can be distinguished from the background. The acollinearity reveals the considerable fraction of monojets in the signal rate. The rate of observed monojets in calorimeters (defined by acollinearity = 180°) is 52000 events per $100pb^{-1}$ (27% of the original sample), when $m_{\tilde{q}} = 40 GeV/c^2$ and $m_{\tilde{\gamma}} = 20 GeV/c^2$. The underlying background rate due to $q\bar{q}$ -events is less than 0.5 %. The background rates are higher, when only the track information is utilized. This may originate from geometrical effects and neutral leading particles. However, the FASTSIM parametrizations may also increase the background rate artificially.

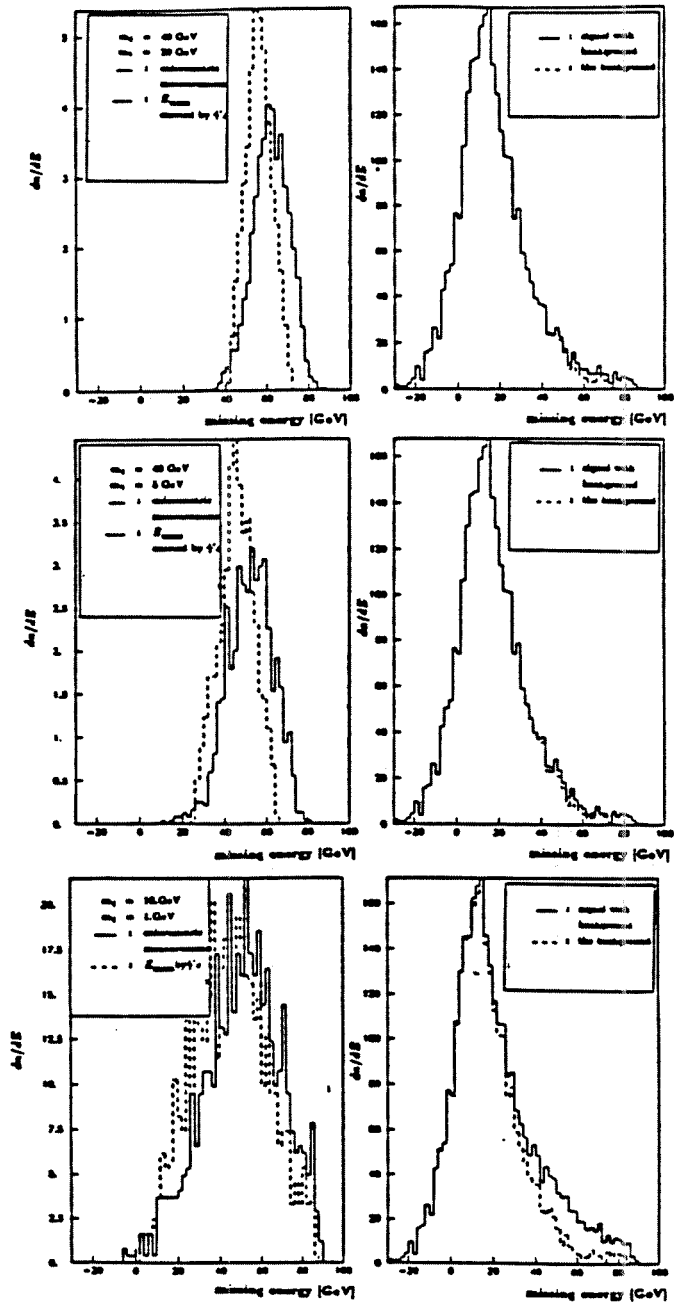


Figure 8.2: Calorimetric missing energy in the squark-photino channel and the comparison with the background.

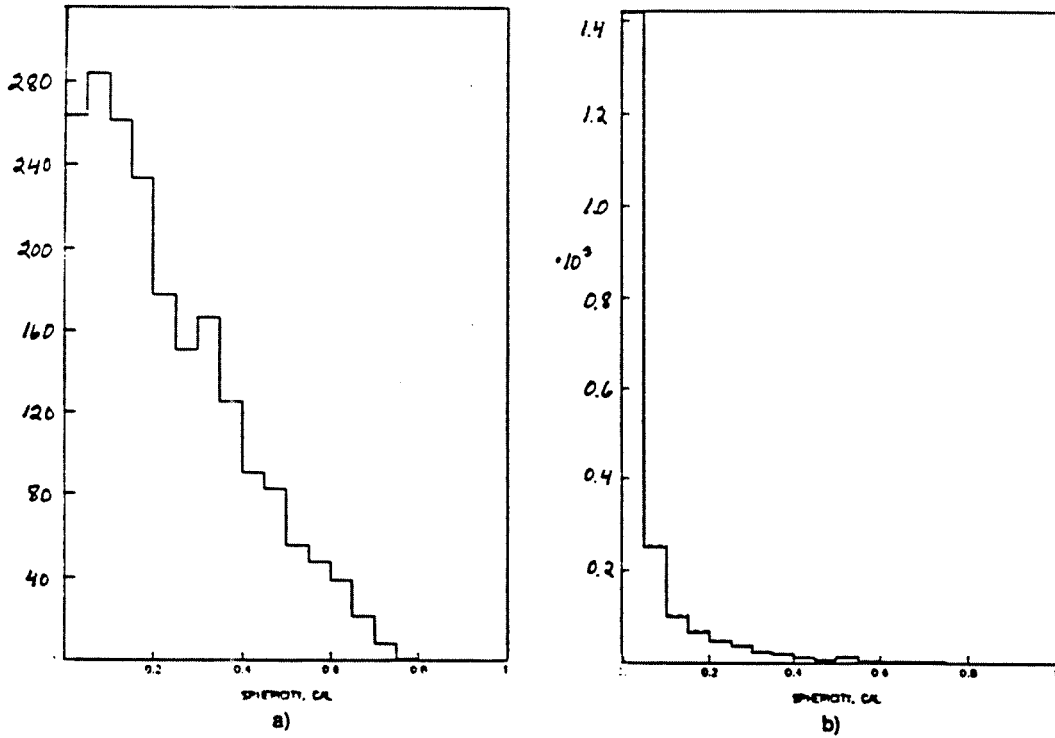


Figure 8.3: Sphericity distribution from calorimetry information a) $q\bar{q}$ -events b) background events (solid line) and background+signal events (dashed line).
 ($m_{\bar{q}} = 40 \text{ GeV}/c^2$ and $m_{\tilde{\tau}} = 20 \text{ GeV}/c^2$)

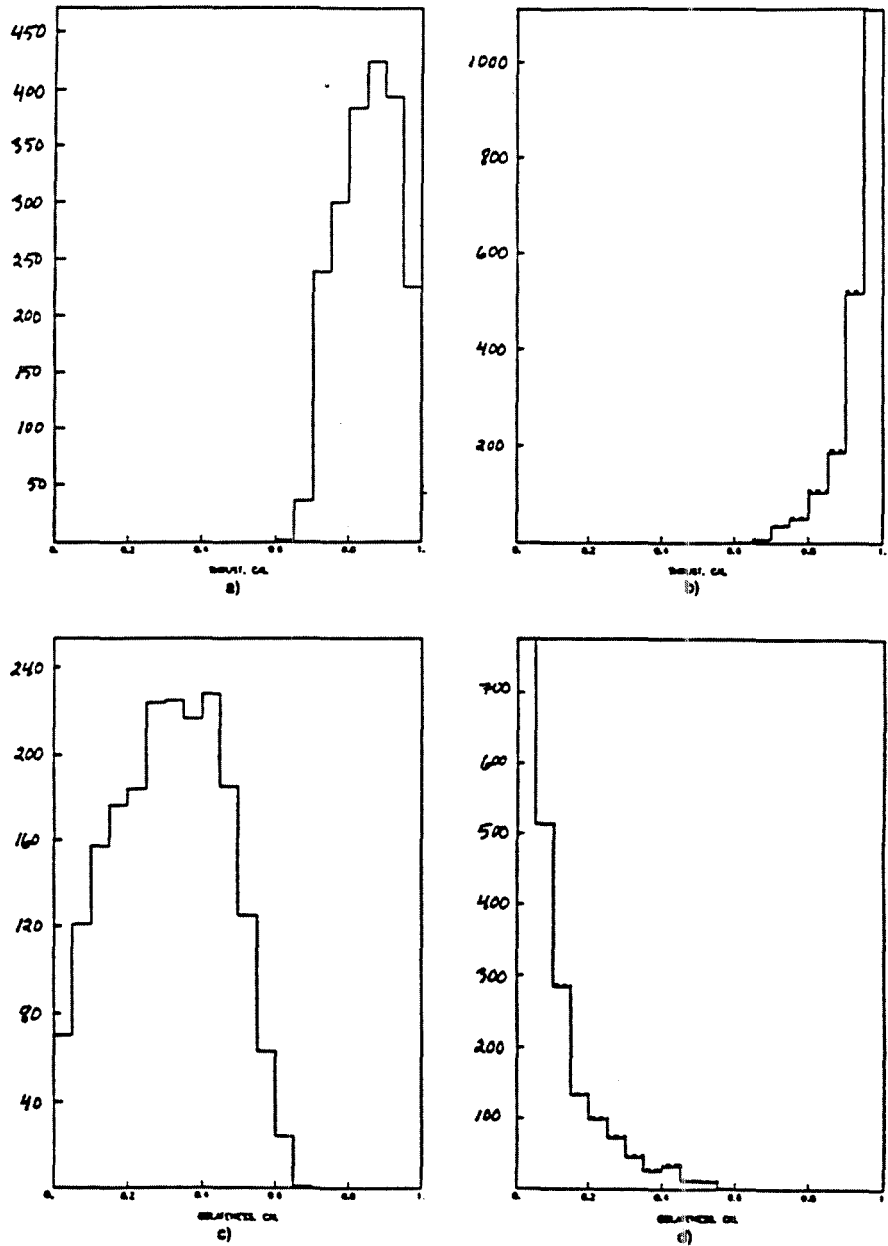


Figure 8.4: Thrust and oblateness distributions from calorimetry information a) $q\bar{q}$ -events b) background events (solid line) and background+signal events (dashed line).
 $(m_{\bar{q}} = 40 \text{ GeV}/c^2 \text{ and } m_{\bar{\gamma}} = 20 \text{ GeV}/c^2)$

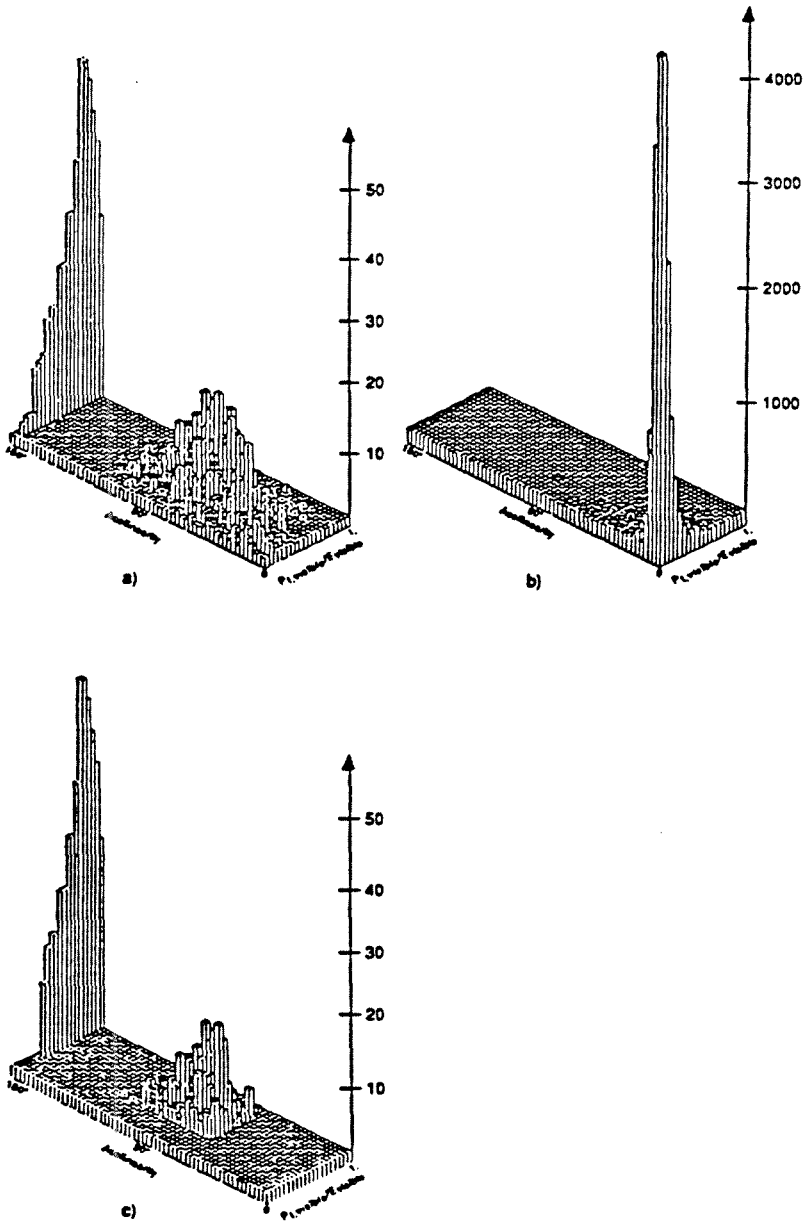


Figure 8.5: Acollinearity vs $P_{T,visible}/E_{visible}$ for a) $\bar{q}q$ -events b) background events c) signal+background events with cuts $P_{T,visible}/E_{visible} \geq 0.3$ and acollinearity $\geq 60^\circ$.
 ($m_{\bar{q}} = 40 \text{ GeV}/c^2$ and $m_{\bar{\gamma}} = 20 \text{ GeV}/c^2$)

Chapter 9

Conclusions

In this report we have documented the analysis and development work done in order to prepare the necessary instruments for fast physics feasibility studies on a selected class of topics.

Although our principal aim has been to concentrate on a set of observables characterizing the topologies of new physics processes, the tools made available within the framework of FASTSIM will certainly prove useful in any standard physics study.

Chapter 10

Acknowledgements

We would like to thank Fabrizio Bianchi and Paola Folegati for contributing in our work. We are also indebted to François Richard for constructive criticism in the course of the analysis.

Bibliography

- [1] FASTSIM Version 3.1; see also J. Cuevas et al., Fast Simulation for Delphi Reference Manual, Version 3.0, Delphi 87-27 Prog-72 Rev. (1988)
- [2] E. Farhi, Phys. Rev. Lett. 39 (1977) 1587
- [3] J. D. Bjorken, S. J. Brodsky, Phys. Rev. D1 (1970) 1416
- [4] S. Brandt, Ch. Peyrou, R. Sosnowski, A Wroblewski, Phys. Lett. 12 (1964) 57
- [5] T. Sjöstrand, LU TP 82-7
- [6] T. Barklow, in Proceedings of the Second Mark II Workshop on SLC Physics, SLAC 306
- [7] P. Laurikainen and R. Orava, Backgrounds and inefficiencies in the muon identification with Delphi, Delphi note in preparation
- [8] F. Bianchi, P. Eerola, P. Folegati, K. Huitu, R. Orava, Susy at LEP, Delphi 85-67 Phys-7 (1985)
- [9] W. Bartel et al., (JADE Collaboration), Phys. Lett. 152B, 385 (1985)
- [10] G. Bartha et al., Search for Anomalous Single Photon Production at PEP, SLAC-PUB-3817 (1985)

RESEARCH INSTITUTE FOR HIGH ENERGY PHYSICS

REPORT SERIES

HU - SEFT - 1990 - 07

The Results of the Combined Beam Test of
the DELPHI Hadron Calorimeter, the
Forward Electromagnetic Calorimeter and
the Barrel Muon Chambers, (π^+ , e^+ Runs)

H. Herr, A. M. Wetherell, G. Zumerle
CERN

G. D. Alekseev, V. M. Golovatyuk, R. B. Kadyrov, N. Khovansky,
G. V. Mitselmakher, J. Ridky, G. Shelkov, V. Timofeev,
E. N. Tsyganov, V. Vrba
JINR Dubna

P. Eerola, R. Keränen, R. Lauhakangas, J. Pyhtä,
R. Orava, M. Voutilainen
University of Helsinki

I. Lippi, M. Mazzucato
INFN Padova

C. Bosio, E. Graziani
INFN Sanita

E. Chernyaev, P. V. Chliapnikov, A. B. Fenyuk, V. V. Lapin,
V. I. Nikolaenko, S. A. Gumenyuk, V. F. Obraztsov, A. M. Zaitsev
IHEP Serpukhov

SEFT

ISSN 0788-3587

UNIVERSITY OF HELSINKI
RESEARCH INSTITUTE FOR HIGH ENERGY PHYSICS
SILTAVUORENPENGER 20 C • SF - 00170 HELSINKI • FINLAND

Abstract

The responses of the DELPHI Hadron Calorimeter (HCAL) and the DELPHI Forward Electromagnetic Calorimeter (FEMC) are investigated in the beam test setup which realizes the actual foreseen DELPHI geometry and data acquisition system. Samples of pion and positron data in the momentum interval $10 - 60 \text{ GeV}/c$ are collected from which the responses of the HCAL, the FEMC and their combined response are analyzed. For the bare HCAL, the response to hadrons is linear in the considered momentum interval. The energy signal ratio of pions and electrons (π/e) is equal to 0.7. The hadronic energy resolution does not scale with $1/\sqrt{E}$ and the mechanisms affecting the energy resolution are studied. Calibration constants are defined for the FEMC and the HCAL separately and the combined response to hadrons is analyzed. Electron separation from pions is studied by using the FEMC and the combined information.

1 Introduction

During July and August 1988, modules of the DELPHI Endcap Hadron Calorimeter (HCAL), the Forward Electromagnetic Calorimeter (FEMC) and the Barrel Muon Detector (MUB) were tested in the H6 beam in the North Area at CERN (Figure 1). In the present report the results concerning the combined analysis of the pion and positron data using the HCAL and the FEMC are considered. The results of the muon runs together with a detailed description of the MUB are presented in the separate paper [1].

2 The Apparatus

2.1 Hadron Calorimeter

The DELPHI HCAL [2] is an iron sampling calorimeter, with limited streamer mode detectors. It consists of a barrel part with 24 modules and two endcaps with 12 sectors. The geometry of the detector is shown in Figure 2 a). The sector number 5 from the end-cap face C (positive z -hemisphere in the standard DELPHI coordinates) was used in this experiment (Figure 2b)). In DELPHI the inner and outer parts of the HCAL sectors are self-supporting, so special flanges were designed to connect the parts together for this experiment.

The detector elements are eight-cell (cell size $9 \times 9 \text{ mm}^2$) plastic streamer tubes with a graphite cathode. Each detector plane is covered with a capacitive copper clad read-out board which is subdivided into pads. Corresponding pads of four sequential planes (seven for the first layer) are connected in the signal read-out and form projective read-out towers. The geometry of one of the detector planes in the end-plug part of the module which was actually used is shown in Figure 2b). The detectors are parallel to the outer edge of the calorimeter for even planes end to the inner edge for odd ones, resulting in triangular dead spaces at the edges.

The standard gas mixture composed of Argon : Isobutane : CO_2 in the ratio 1 : 3 : 6 and the voltage of 3.9 kV were used in the HCAL. The high voltage and gas flow of the calorimeter was switched on for two months in total and operated very stably. The NA32 and NA12 experiments were also taking data during this period and due to this there was a high muon background flux of 1 particle/ $s \text{ cm}^2$ all over the surface of the calorimeter. In a special run the HCAL module was exposed to a high flux of muons $\sim 10^5$ particles/ $s \text{ m}^2$. During this run the total current in the high voltage system of the HCAL was 50 μA ($2\mu A$ being a nominal value). These

background conditions are well above those expected for DELPHI. No dark current problems (from which the prototypes of the HCAL had suffered) were found in any of these conditions, due to the improved design of the final version of the streamer tubes.

The final DELPHI Hadron Calorimeter front-end electronics [3] was used with the amplification factor of $10 \text{ pC}/\text{ADC-count}$. Because the BCO signal (time of beam crossing over) is needed in the read-out cycle of the HCAL front-end electronics, it was impossible to use an external trigger to start the charge collection (there was a 500 ns unavoidable delay between the external trigger and the actual start of the integration which would lead to a complete loss of signal). This is why a timing configuration, similar to that of the DELPHI cosmic trigger, was used. The resulting scheme is presented in Figure 4 in which the trigger signal and instruction cable delays are taken into account. The cycle was started by sending the start-charge-collection (SCC) instruction randomly. The gate for external trigger was set to $1 \mu\text{s}$ and was initialised about 300 ns before the start of the charge collection. In case there was a trigger, the read-out cycle was started, otherwise the reset instruction was sent which took $4 \mu\text{s}$. So, the HCAL was sensitive only $1/6$ of the full time. The time to collect charge for the trigger and data was $300 - 1000 \text{ ns}$ and $1300 - 2000 \text{ ns}$ respectively from the passage of a particle through the calorimeter. In order to simulate the LEP conditions in an adequate way a very short trigger gate (i.e. a low trigger efficiency) should have been used, but this was impossible because of the low hadron beam intensity. Therefore, the timing used was a reasonable compromise and its effects on the data sample will be discussed in the following chapters.

2.2 The Forward Electromagnetic Calorimeter

The DELPHI Forward Electromagnetic Calorimeter [4] consists of two 5 m diameter disks with a total of 9064 lead glass blocks in form of truncated pyramids, dealigned for (-3°) towards the interaction point. For this test, the module #432 was used. It contained 80 lead glass blocks arranged in a rectangular 8×10 matrix. It was positioned in such a way to have the beam hitting one of the central counters with the direction parallel to the block axis.

The standard electronics chain [5] was used for the read-out giving an average noise per counter equivalent to 17 MeV of deposited electromagnetic energy.

2.3 The data acquisition system

The data was transferred from the front-end electronics to FASTBUS crates. The structure of the system is shown in Figure 5.

The interface module FRC which can receive data from 8 front-end crates was used in the HCAL. The data was transferred through a special auxiliary bus to another FASTBUS card, the HFB which is a ring buffer and it can have up to four events in memory. The next stage of the data acquisition is the FIP (Fast Intersegment Processor), which uses the 68020 processor and the OS-9 operating system. When the FIP has read an event it sends a message to the LES (Local Event Supervisor, in the GPM processor) which reads the data as a master. The FASTBUS system was interfaced with a μ VAX-II through a CFI module. In the VAX each run was stored on the disk and consequently copied on the tape.

3 The test beam

The experiment was carried out in the H6 tertiary test beam of CERN North Area. The beam was tuned to the momenta 10, 20, 40, 60 GeV/c with $\Delta p/p = 1\%$. The momentum of the H6 secondary beam was fixed to 200 GeV/c .

The tertiary pion flux varied from 10 pions/burst for the 10 GeV/c beam to 100 pions/burst for 60 GeV/c (burst length 1.4 s). The muon contamination was high: it was of the order of 50% of the hadron flux over the area of $15 \times 15 \text{ cm}^2$ at the high momenta and increased to 200% for 10 GeV/c . Therefore the value of 10 GeV/c was a difficult point and practically the lowest possible for the H6 beam. The positron flux was significantly higher than the hadron one, 50 positrons/burst at 10 GeV/c and 300 positrons/burst at 60 GeV/c .

The beam trigger included coincidence of two scintillators ($10 \times 10 \text{ cm}^2$ and $2 \times 2 \text{ cm}^2$) in front of the FEMC and two CEDARs (differential Cherenkov counters) 90 m upstream. For pion runs the CEDARs were tuned for the pion selection, and in addition a lead plate of 4 mm in thickness was used to suppress the positron background. For the positron runs the lead plate was removed and the CEDARs were tuned accordingly. The dark points marked 1,2,3,4 on Figure 3 correspond to the beam image at the entrance of the layers 1,2,3,4 of the HCAL. The beam was not perpendicular to the HCAL surface ($\cos \theta = 0.4$) in order to reproduce the DELPHI projective geometry.

4 Summary of the data samples

The data can be subdivided into two parts: the 'bare HCAL data', during which there was no FEMC in the beam, and 'the combined data', during which the FEMC was upstream of HCAL. Both sets of data consist of runs with π^+ (e^+) momenta 10, 20, 40 and 60 GeV/c . In addition to this data, separate runs were taken with a different current in the vertically bending magnet in front of the test area, in order to scan the HCAL module in ϕ direction. The FEMC was not in the beam during these runs. The summary of runs is presented in Table 1.

The data processing consisted of the decoding of the information and tests of the data format. The search and the rejection of the repeated events was performed. This was necessary, because this experiment was the first one where the DELPHI data acquisition system was tested. The percentage of 'bad' events was 3-5 %.

As it was already mentioned, the samples contained significant muon background which had to be rejected at the analysis level. For this purpose the information from the Muon Detector was used to veto the event - that is, the events with one good penetrating track were rejected. In addition, internal HCAL criteria (a muon like signal in 3 out of 4 superlayers) were used to suppress further the muon background.

5 The response of the HCAL

5.1 Hadronic response

Figure 6 presents the distributions of the response of the HCAL to 10, 20, 40 and 60 GeV/c pions. The energy dependence is presented in Figure 7. A linear fit $ADC = \alpha \times P + \beta$ gives $\alpha = 5.04 \pm 0.32$, $\beta = 1.61 \pm 9.1$ with $\chi^2 = 0.55$, (2 D.O.F). The linear response is in contradiction with the results reported in the prototype tests [6,7]. The most probable explanation is the different gas mixture Argon:Isobutane: $CO_2 = 1 : 3 : 6$ instead of Argon:Isobutane=1:3 which results in a smaller streamer charge and in smaller dead zones around the streamer.

The measured energy resolutions are summarized in Table 2a). The resolution expected for a hadron calorimeter with the 5 cm iron slots is [8] $\sigma(E)/E \simeq 0.9/E^{1/2} [GeV^{1/2}]$ which was confirmed by the HCAL prototype data. The following aspects can explain the worse resolution found in the present experiment:

1. Detector effects: The beam entered in the HCAL in the area of

distributed dead regions due to the streamer tube configuration at the edge of the module (Figure 3). Thus, the sampling of active detector layers was effectively reduced. Secondly, the charge diffusion (i.e. the phenomenon of longitudinal spread of the streamer charge on the cathodes onto several neighbouring pads which was observed in the end-cap module. see discussion in [1]) possibly affected the resolution. For the high momentum data, the leak of energy outside the calorimeter could play a role.

These effects were carefully studied by the DELSIM32 Monte Carlo simulation program [9] which takes into account dead zones as well as other known effects: the electronics threshold, the charge diffusion etc. The result is shown in Table 2b). The deviation from the naive $\sigma(E)/E = 0.9/E^{1/2} [GeV^{1/2}]$ prediction is distinguishable. In order to check the simulation, the resolution for a barrel point having no dead zones was determined and the results are presented in Table 2c). There is a good agreement with the $\sim 0.9/E^{1/2}$ dependence in the range that has been tested by the prototypes (3 – 10 GeV/c). In order to test further the simulation program, the experimental longitudinal profiles of 20 GeV/c pion induced showers were compared with the Monte Carlo prediction (Figure 8). The comparison is absolute, that is, the relative normalization was not tuned.

As it is seen from Tables 2 a)-c), the simulation gives qualitative explanation of the data (worsening of the resolution and its deviation from $\sim 1/E^{1/2}$ dependence), but there is still a discrepancy of about 20%.

2. There is a specific effect present in the HFM experiment which can affect the resolution: Because of the non existence of the BCO signal for the read-out cycle of the HCAL front-end electronics, a cosmic-type random-start trigger was used (see Figure 4). The charge integration was started 300 ns after the beginning of the pretrigger gate (see the dashed area in Figure 4), thus some fraction of charge might be lost for the 'early' particles. The effect was estimated using the muon runs in [1]). It can reach 20% level.
3. Worth mentioning is also the variation of the distance between the foil which covers the detector plane from the side, opposite to the pads and the detector plane. According to [10], a variation of ~ 1 mm, which is quite possible, can lead to the 10% variation in response.

In summary, we achieved a qualitative explanation of the lower resolution seen in this test. The main effects are specific to the HFM experimental arrangement and they vanish in the region below 10 GeV.

5.2 The calibration of the HCAL

Because the channel-to-channel variations in the HCAL response (due to the dead zones etc.) can be responsible for the smearing of the signal, there was a hope to improve the resolution of the HCAL by using a calibration procedure. The most simple way would be to use muons for this purpose. For example, one can select the events, where a muon crosses the center of the given tower, and use the inverse of the average charge in the tower as the calibration coefficient. However, our numerous attempts to calibrate the HCAL by using the muons failed. The main reason for this is the charge diffusion phenomenon together with relatively high thresholds in the front-end electronics. The charge diffusion implies that the average charge in the central tower, under conditions described above, is about 15 pC instead of 50 pC in the absence of the diffusion. On the other hand, the uncertainty in the front-end threshold is about 10 pC, thus it is impossible to distinguish the threshold variation effect from the difference of the response of channels to the deposited energy. This is, in fact, the most serious problem which has been discovered during the test and which can effect the performance of the HCAL during the real data taking.

The most straightforward way to improve the situation would be to increase the sensitivity of the front-end electronics (a factor of 2 would be enough) and to adjust accurately the pedestals with potentiometers. As this is not realistic for the first data taking periods of the LEP, it is also possible to measure on-line the front-end thresholds for all the channels (the ADC-writing level signal can be used for this purpose). By using a random trigger and by moving the writing level one can define the point where the pedestal noise appears in a given channel.

As the muon calibration turned out to be impossible, we tried the direct hadron calibration. The idea was to minimize the functional $\sum_i \left(\sum_k (c_k A_k^i - E_{\text{beam}})^2 \right)$ where i is an event number, k is a tower index, A_k^i is the charge in the tower k in the event i ; c_k is a calibration coefficient. The procedure is rather complicated, because the total number of towers involved in the showers is $\sim 80 - 90$. Two technically different approaches were used: a) minimization using the MINUIT program [11] and b) the use of an iterative procedure. Figure 9 gives the distribution of the coefficients. The improvement in the resolution of HCAL can be seen by comparing

Table 2a) and Table 3.

5.3 The response of the HCAL to positrons

The collected samples of positron data make it possible to study the HCAL response to positrons. This is important, because in some DELPHI regions HCAL is the only calorimeter. The ratio π/e is measured to be 0.707 and 0.730 for 10 GeV/c and 20 GeV/c, respectively (see Figure 7). So the calorimeter is undercompensated. The energy resolution of the HCAL is 28% for 10 – 20 GeV/c positrons.

5.4 Test of the HCAL trigger chain

One of the functions of the HCAL in DELPHI is to provide muon and hadron trigger. For this purpose, the HCAL raw data contains the digitized total analog charge sum for each half-sector. This charge is digitized 1 μ s before the tower data. The scatter plot of the off-line sum of the charge in the sector versus the trigger sum is displayed in Figure 10. The linear behaviour of the analog sum confirms the proper operation of the trigger chain. Moreover, taking into account the pedestal in the analog sum distribution, both off-line and analog charge distributions have the same relative width.

6 The FEMC response to positrons

Processing of the FEMC data consisted of the pedestal subtraction for each cell and the multiplying on the calibration coefficient. Both sets of constants were determined in the separate FEMC calibration in the North Area. However, the amplification and timing of the shaper cards used in this test were different from the ones used in the FEMC calibration runs. The main effect was corrected comparing the electronic test pulses in the two different conditions. The residual miscalibration is of the order of 2-3%. No special effort was done to correct for this effect because the optimization of the energy resolution was outside the scope of this test. In order to eliminate the pedestal fluctuations, the threshold of 20 MeV was introduced for each channel. To minimize the effect of electronics noise, only cells in 3 \times 3 matrix around the cell with maximum signal were taken into account. The total calibrated signal from the FEMC is presented in Figure 11 for 10, 20 and 40 GeV/c positron beam. The energy resolution can be approximated by $\sigma(E)/E = 9\%/E^{1/2} [GeV^{1/2}]$.

7 The combined response of the FEMC and the HCAL

7.1 The combined hadronic response

Satisfactory measurements of the hadron energy in DELPHI can be achieved only using combined information from the hadron calorimeter and the electromagnetic detector. One of the main goals of the HFM test was to demonstrate the possibility of the combined calorimetry. For this purpose, runs of 10, 20 and 40 GeV/c pion beam with a module of the FEMC standing upstream of the HCAL were processed. The data for 40 GeV are presented in Figure 12. Figure 12a) shows the total calibrated signal from the FEMC. The distribution contains two components: punching through pions which populate the peak at low energy, and showering pions which give a broad distribution. The response of the HCAL (with the common calibration coefficient 0.18 GeV/ADC for all towers) is dramatically different from that of the stand-alone runs (see Figure 12b) and Figure 6c)). The biplot Figure 12c) shows reasonable correlation of responses of both detectors. First, the punching through pions exhibit normal showering in the HCAL (the dark vertical band), for the other hadrons a strong linear correlation of the HCAL and the FEMC responses is seen. The cluster in the left down corner corresponds to the muon background. The sum of the responses of the two detectors is shown in Figure 13a). A clear peak is seen together with a muon background, but the average energy is underestimated (34 GeV instead of 40 GeV). In the events with significant energy deposition in the FEMC, the reconstructed energy is obviously underestimated. The response of the HCAL for the showers starting in the FEMC is also small. The estimate of the energy can be improved if the following algorithm is used:

For the 'punching through region' ($E_{\text{FEMC}} < 2 \text{ GeV}$)

$$E_{\text{tot}} = E_{\text{HCAL}} + 2.0 E_{\text{FEMC}} \quad (1)$$

For the 'FEMC absorbing region' ($E_{\text{HCAL}} < 1.5 \text{ GeV}$)

$$E_{\text{tot}} = E_{\text{HCAL}} + 1.9 E_{\text{FEMC}} \quad (2)$$

For the 'combined region'

$$E_{\text{tot}} = 1.25 \times (E_{\text{HCAL}} + E_{\text{FEMC}}) \quad (3)$$

The result is shown in Figure 13b). The resolution determined as $(FWHM/2.36)/\langle E \rangle$ is 32% is better than for the HCAL standing

alone. The average total reconstructed energies as well as the resolution obtained for the other beam momenta are shown in Table 4.

7.2 The combined electron separation from pions

It is well known that there are two parameters, measured by electromagnetic calorimeters, which contribute to the electron identification - the dispersion of the transverse distribution of the shower and the total energy. The quadratic variance $(\sigma_x^2 + \sigma_y^2)^{1/2}$ of the shower space distributions, normalized to the FEMC cell dimension, are presented in Figure 14 for 10 GeV/c positrons and pions. The peak at the zero dispersion for pions corresponds to the punching-through hadrons. With a selection $0.25 < \text{disp} < 0.65$ one can achieve the efficiency of 95% for electrons and the rejection factor of ~ 5.7 against hadrons.

If the momentum of the incoming particle is known independently, for example from the tracking system in the magnetic field, a much better discrimination can be reached. Figure 15 presents the biplot for the shower dispersion versus the total energy in the FEMC for 10 GeV/c positrons and pions. By using the same dispersion selection and by requiring $8 \text{ GeV} < E_{\text{FEMC}} < 11 \text{ GeV}$ for the visible energy in the FEMC, the pion suppression factor can be improved up to ~ 60 .

It is also important to have a good electron-pion separation without the tracking system, for example, from the points of view of the fast event tagging and the 4th level trigger. This is why the possible contribution of the HCAL in electron identification was studied here. Figure 16 shows the distribution of the ratio of the energy deposited in the HCAL to that of the FEMC for positrons and pions which passed the dispersion selection criterium. A condition $E_{\text{HCAL}}/E_{\text{FEMC}} < 0.1$ results in the efficiency of 90% for positrons and gives a combined hadron rejection factor of 35.

Acknowledgements

The successful completion of the HFM experiment resulted from the hard work on the part of many people from the three detector groups and the DELPHI online group.

We would like to thank all of those who took part in the planning and running of the experiment, and in particular pay tribute to the efforts of J.V.Allaby, M.Jonker, Ph. Charpentier, R.Lucock, Ph. Gavillet. The authors are grateful to A. Baroncelli for useful discussions.

References

- [1] E.Veitch et al.. Muon Identification Efficiencies from the HFM Experiment, DELPHI 89-57 PHYS 48, (1989).
- [2] DELPHI Collaboration, DELPHI Technical Proposal, CERN/LEPC/ 83-3.
- [3] E.Gygi and F.Schneider, The read out electronics of the hadron calorimeter of DELPHI, CERN/EP 0023P, 1986.
- [4] P.Checchia et al. Nucl.Inst.Meth. **A275** (1989) 45-58.
- [5] G.Barichello et al. Nucl.Inst.Meth. **A254** (1987) 111-117.
- [6] G.A. Akopdzhanov et al.. Beam Tests of the Delphi Hadron Calorimeter Prototype, IHEP Preprint 86-62, Serpukhov 1986.
- [7] A.Baroncelli et al., Performance of an iron sampling Delphi test hadron calorimeter. INFN-ISS 88/1.
- [8] R. Wigmans, Nucl. Inst. and Meth. **A259** (1987), 389.
- [9] DELPHI Collaboration, DELSIM DELPHI Event Generation and Detector Simulation, DELPHI 89-68 PROG 143, (1989).
- [10] Yu.P.Guz et al., Some features of plastic streamer tube operation, IHEP 86-208, Serpukhov, 1986.
- [11] MINUIT minimization package, CERN Program Library.

Tables

Beam momentum (GeV/c)	Run conditions	#Events
10	π^+ no Femc	896
20	π^+ no Femc	20800
40	π^+ no Femc	12870
60	π^+ no Femc	5280
20	π^+ +100 A 1)	2024
20	π^+ +50 A 1)	2016
20	π^+ +25 A 1)	4000
20	π^+ -25 A 1)	4000
20	π^+ -50 A 1)	4036
10	π^+ Femc	1375
20	π^+ Femc	5046
40	π^+ Femc	6186
10	e^+ Femc	5142
20	e^+ Femc	10309
40	e^+ Femc	10049

1) Vertical beam bending

Table 1: Summary of the data samples.

a)

Beam momentum	$\sigma / \langle \text{ADC} \rangle$	$\sigma / \langle \text{ADC} \rangle E^{1/2}$
10 GeV/c	36 %	1.14
20 GeV/c	30 %	1.34
40 GeV/c	29 %	1.80
60 GeV/c	29 %	2.24

b)

Beam momentum	$\sigma / \langle \text{ADC} \rangle$	$\sigma / \langle \text{ADC} \rangle E^{1/2}$
10 GeV/c	40 %	1.26
20 GeV/c	40 %	1.79
40 GeV/c	38 %	2.40
60 GeV/c	32 %	2.47

c)

Beam momentum	$\sigma / \langle \text{ADC} \rangle$	$\sigma / \langle \text{ADC} \rangle E^{1/2}$
3 GeV/c	56.7 %	.98
5 GeV/c	41.3 %	.98
7 GeV/c	35.1 %	.93
10 GeV/c	32.0 %	1.0

Table 2: a) The energy resolution of the HCAL (raw data).

b) The Monte Carlo predictions for the energy resolution of the HCAL endcap module (dead-zone region).

c) The Monte Carlo predictions for the HCAL barrel, (dead-zones-free region).

Beam momentum	$\sigma / \langle \text{ADC} \rangle$	$\sigma / \langle \text{ADC} \rangle E^{1/2}$
10 GeV/c	38.8 %	1.23
20 GeV/c	30.4 %	1.36
40 GeV/c	27.9 %	1.77
60 GeV/c	24.5 %	1.90

Table 3: The energy resolution of the HCAL, calibrated data.

Beam	E (GeV)	E_c (GeV)	σ / E	$(\sigma / E) \cdot E^{1/2}$
10 GeV/c	7.1	9.5	35 %	1.10
20 GeV/c	16.4	19.2	33 %	1.47
40 GeV/c	35.0	40.7	32 %	2.02

Table 4: The combined resolution of HCAL+FEMC. The 2nd column shows the uncorrected sum of energies in HCAL and in FEMC. E_c is the corrected energy (see the text). Two last columns present the resolution for the corrected energy.

Figure captions

Figure 1. Plan view of the HFM experiment.

Figure 2. a) The Hadron Calorimeter. b) A HCAL endcap sector.

Figure 3. The geometry of a HCAL detector plane. A layer in the end-plug is shown representing the configuration in the even plane; in the odd planes the streamer tubes are parallel with the symmetry axis of the module. The areas outside the rectangular streamer tubes represent the inactive regions. The solid points show the projection of the beam image in the superlayers 1, 2, 3 and 4.

Figure 4. Random start mode for the HCAL front-end electronics. Two cycles are shown: first is an unsuccessful one (no trigger signal within the pretrigger gate), another one is successful.

Figure 5. HFM FASTBUS data acquisition system.

Figure 6. The response of the HCAL to 10, 20, 40, 60 GeV/c pions (for 60 GeV/c also the data with muon background is shown).

Figure 7. Test of the linearity of the HCAL response. The plot gives the most probable values of the uncalibrated HCAL signals as a function of the beam momentum for pions (circles) and positrons (squares).

Figure 8. Longitudinal shower profile for 20 GeV/c pions in the HCAL (shaded histograms). The unshaded histograms correspond to the Monte Carlo predictions.

Figure 9. The distribution of the HCAL calibration coefficients, the total number of coefficients is 119; $\langle c \rangle = 0.19$; $\sigma_c = 0.09$.

Figure 10. The total off-line ADC sum versus the trigger analog sum in the HCAL for 20 GeV/c pions.

Figure 11. The FEMC response to 10, 20 and 40 GeV/c positrons (calibrated data).

Figure 12. a) The response of the FEMC to 40 GeV/c pions, b) The response of the HCAL to 40 GeV/c pions with FEMC upstream, c) The HCAL signal versus the FEMC signal for 40 GeV/c pions.

Figure 13. a) The sum of energy deposited in the FEMC and in the HCAL for 40 GeV/c pion beam. b) The corrected energy (see the text).

Figure 14. $(\sigma_x^2 + \sigma_y^2)^{1/2}$ distribution for 10 GeV/c positrons (a) and pions (b) in the FEMC. The horizontal scale is given in the units of the FEMC cell dimension.

Figure 15. The biplot of shower dispersion vs. the total energy for 10 GeV/c a) positrons b) pions.

Figure 16. The ratio of the energy deposited in the HCAL and in the FEMC for 10 GeV/c a) e^+ b) π^+ , which passed the dispersion selection.

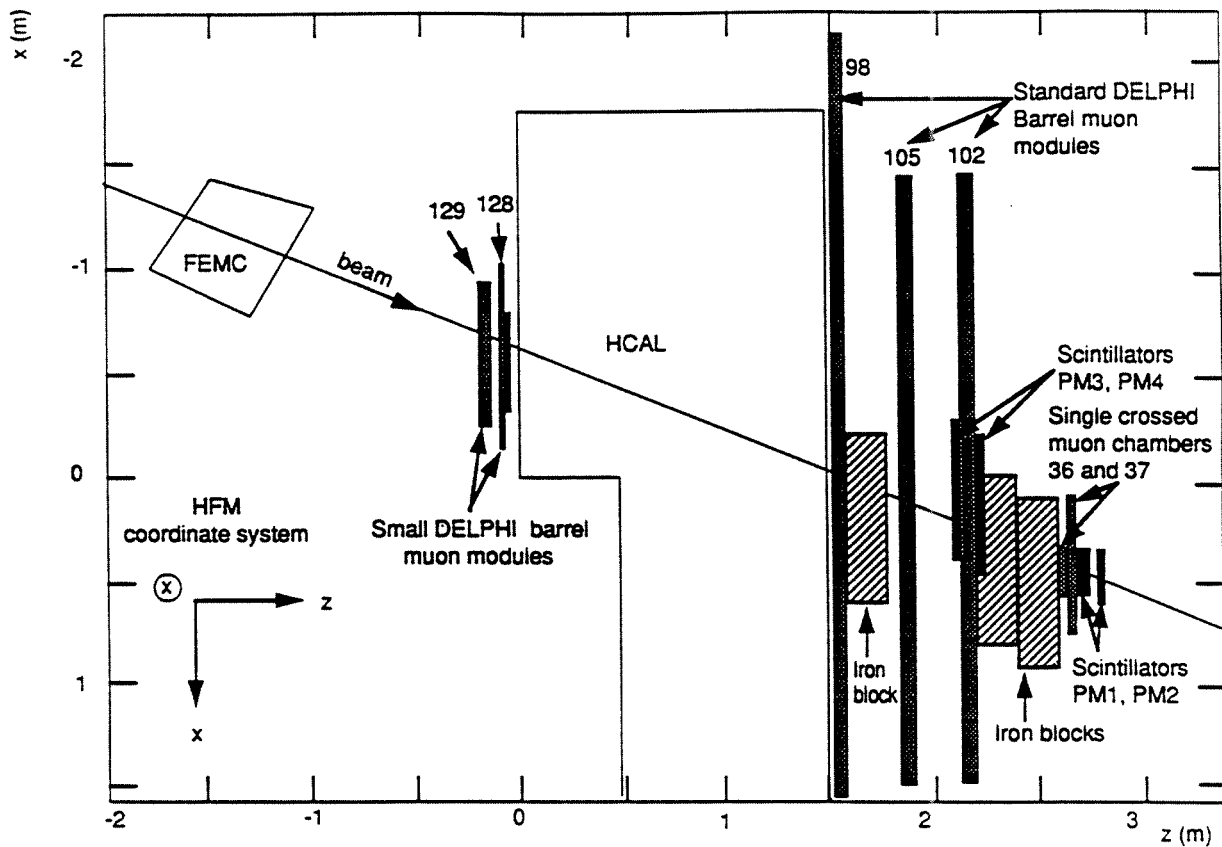


Figure 1:

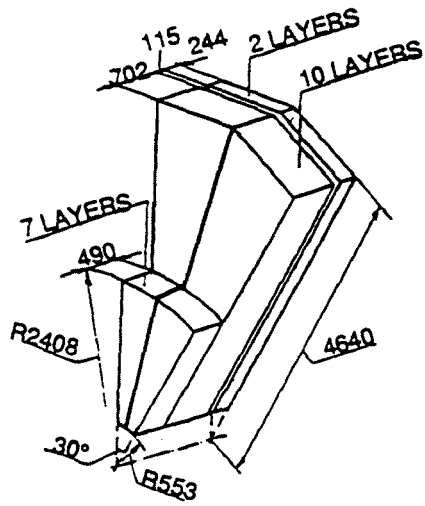
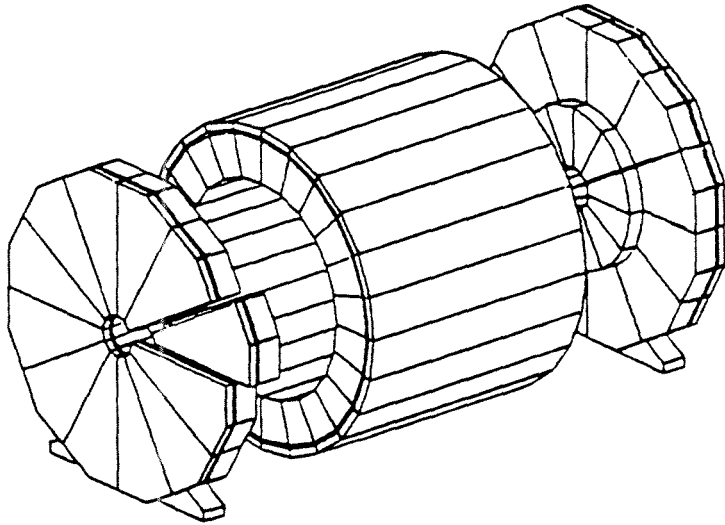


Figure 2:

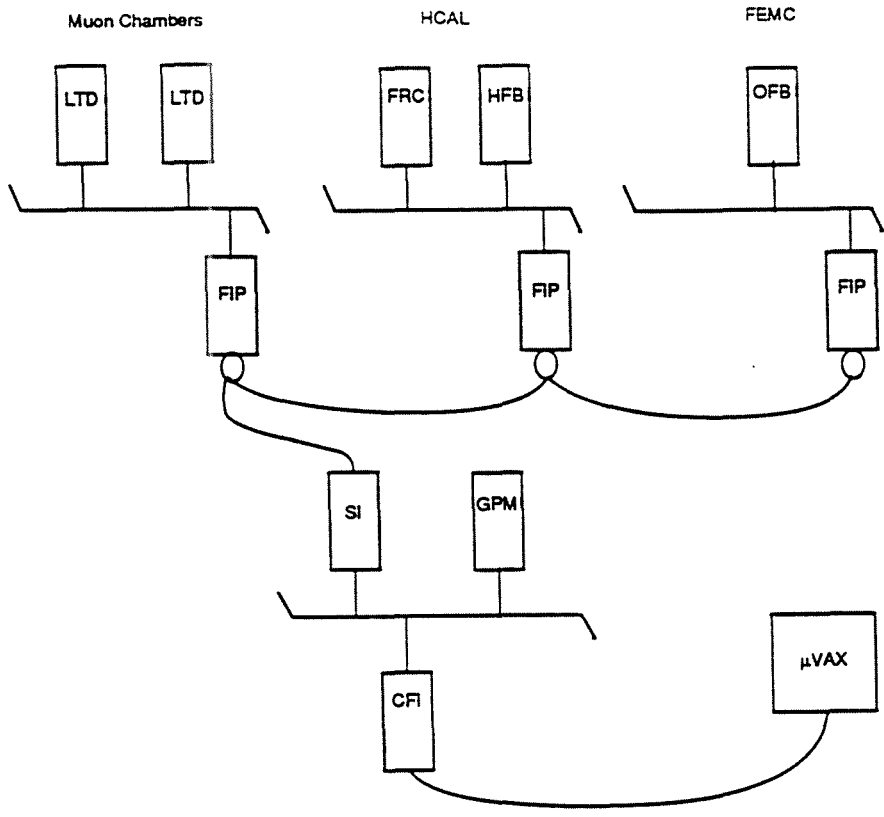


Figure 5:

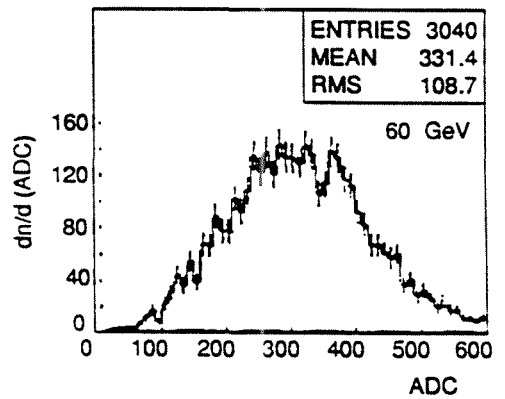
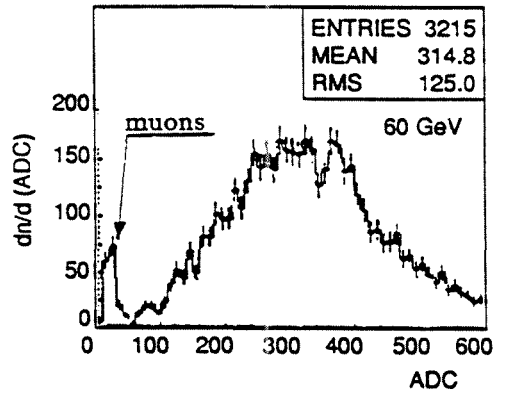
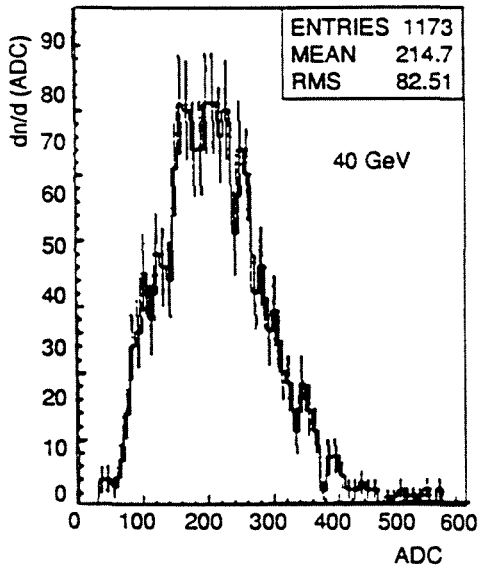
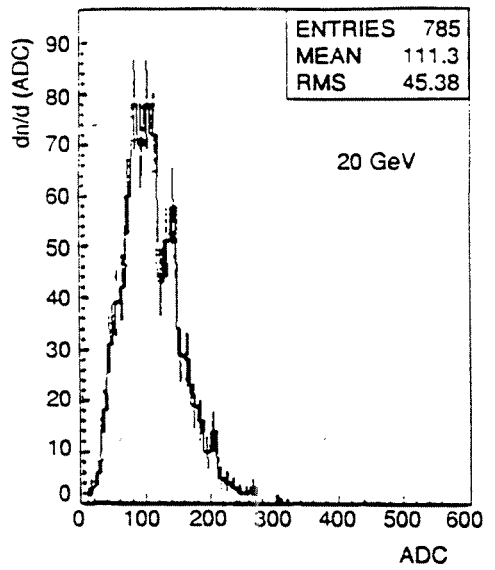
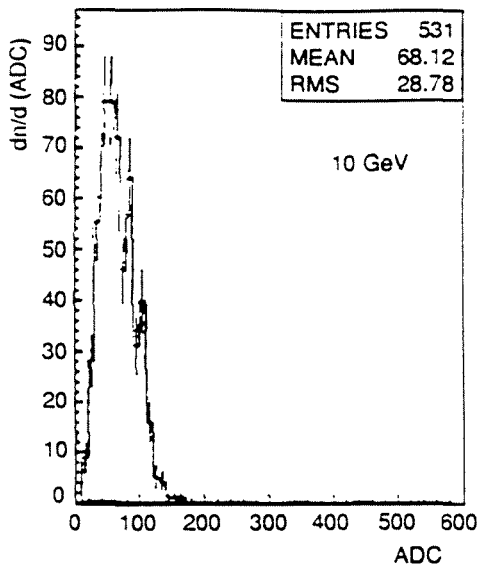


Figure 6:

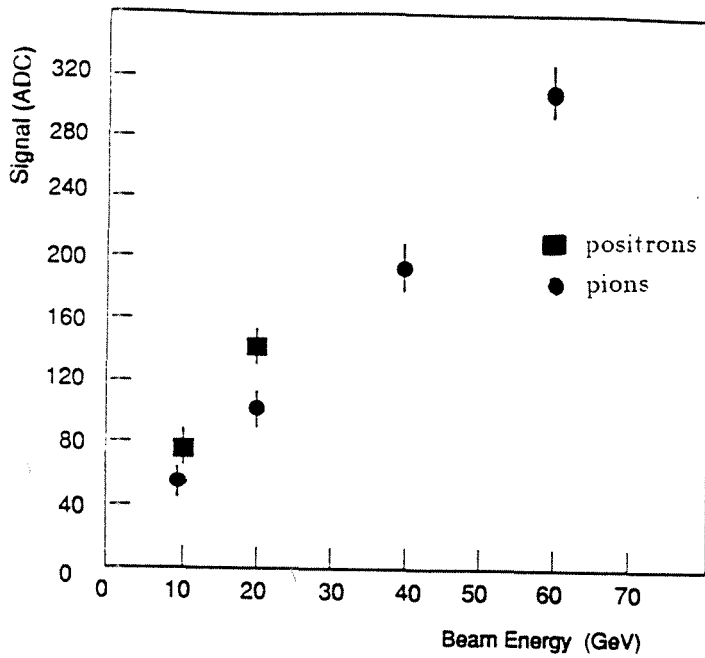


Figure 7:

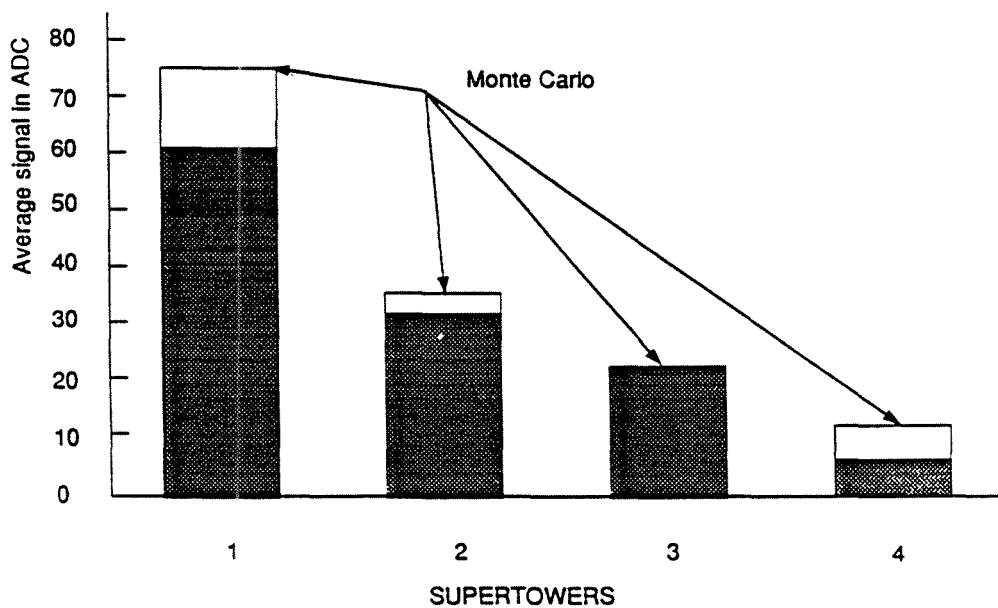


Figure 8:
21

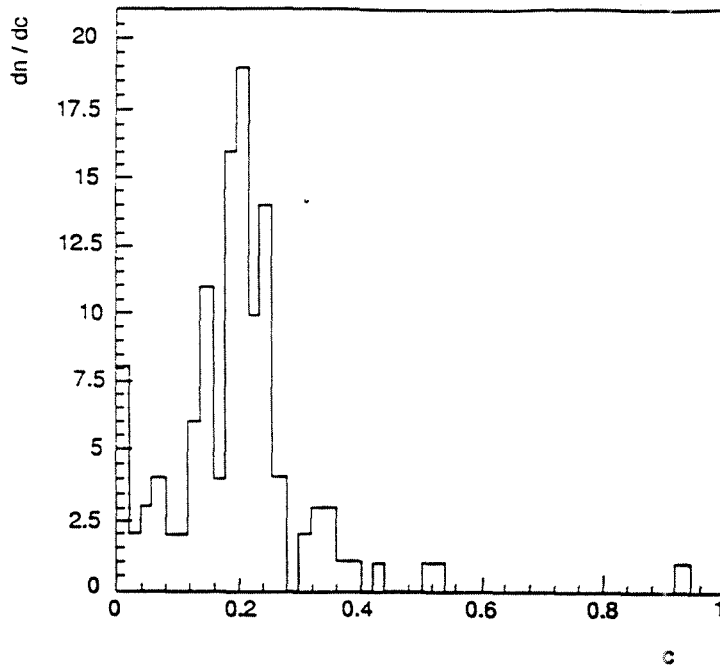


Figure 9:

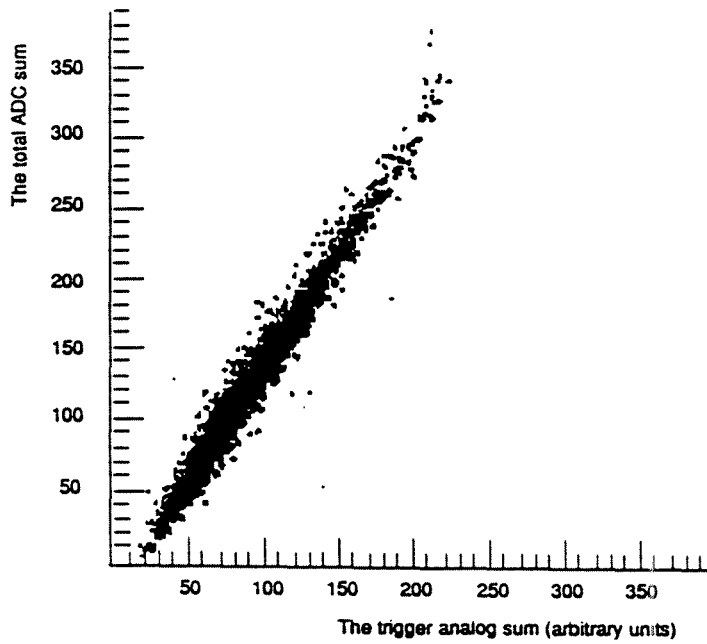


Figure 10:

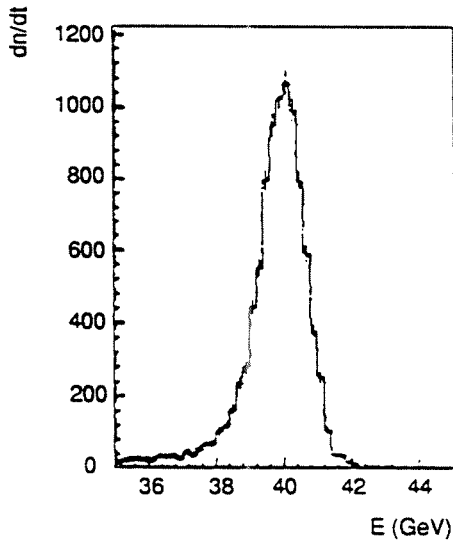
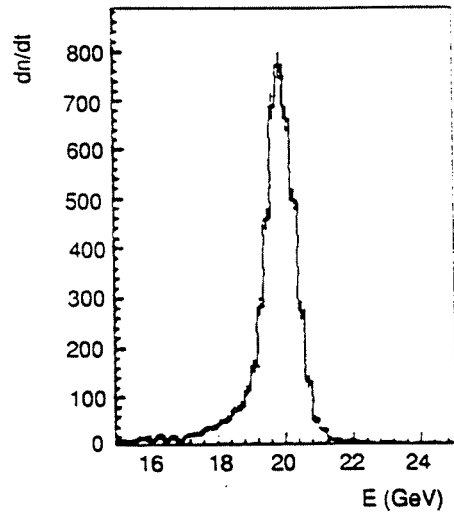
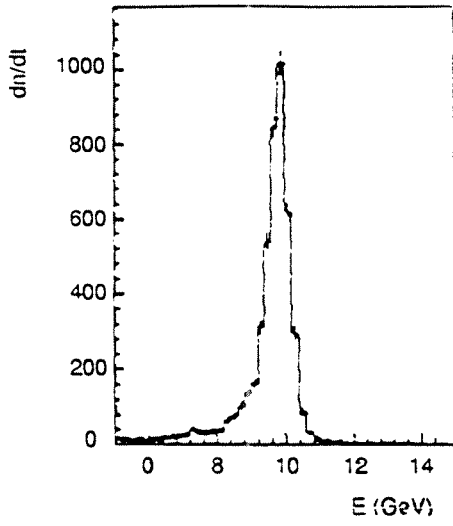


Figure 11:

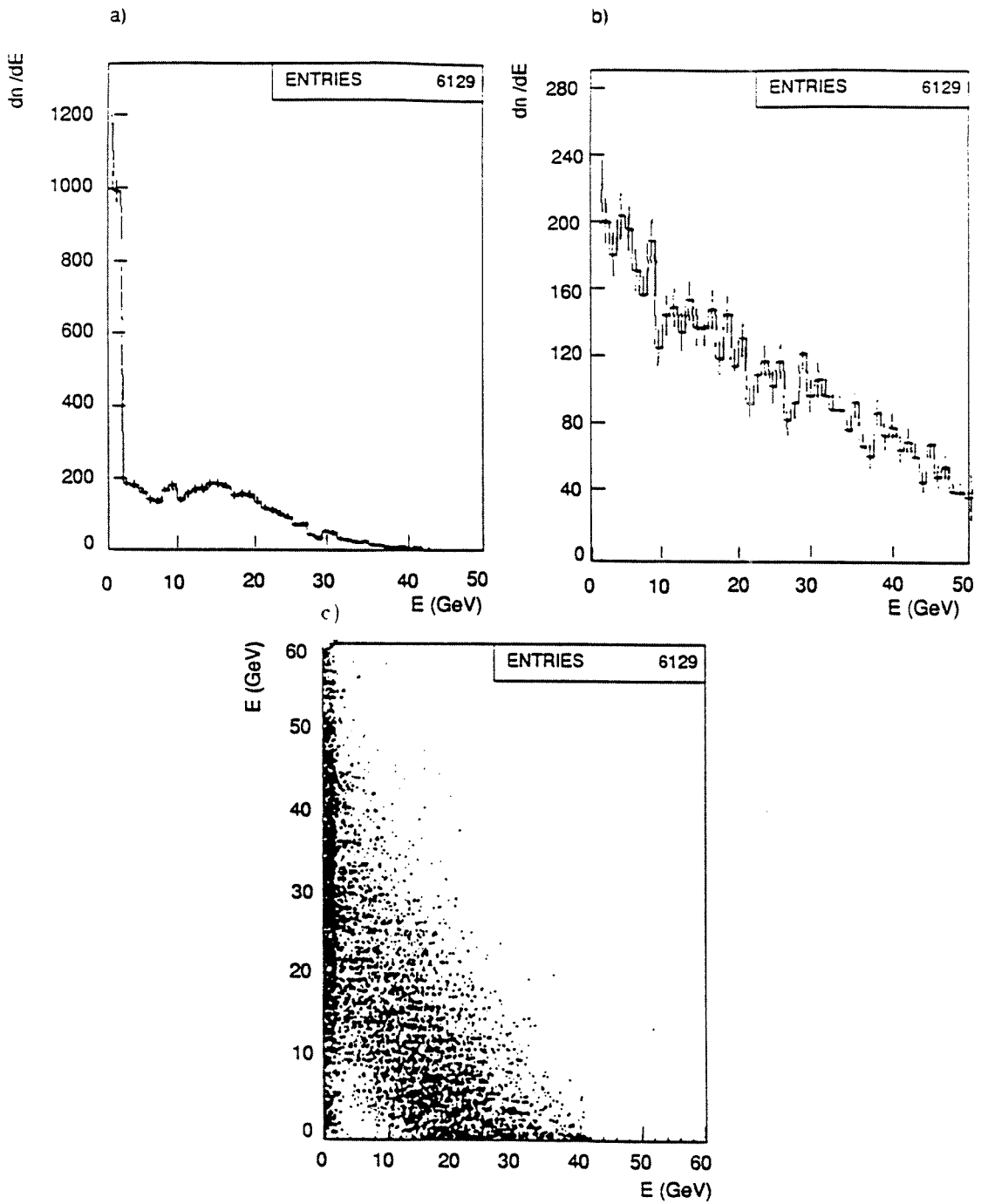


Figure 12:

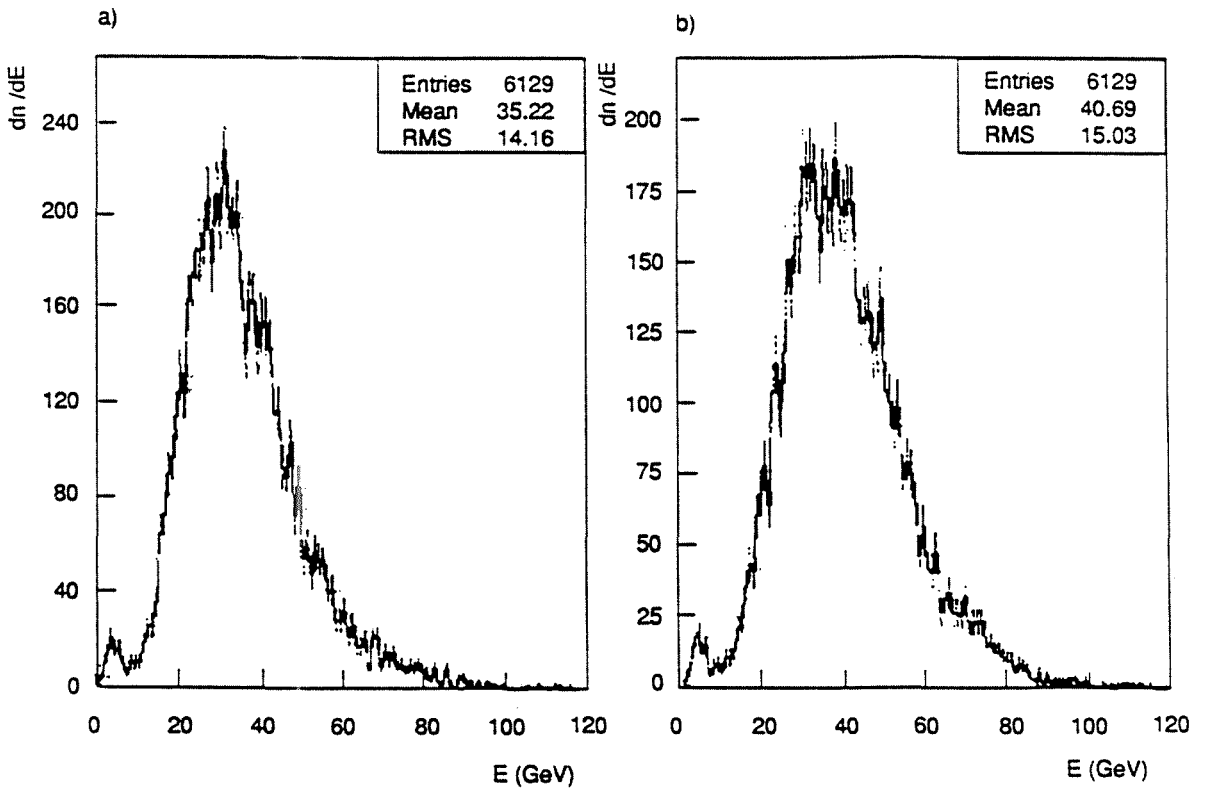


Figure 13:

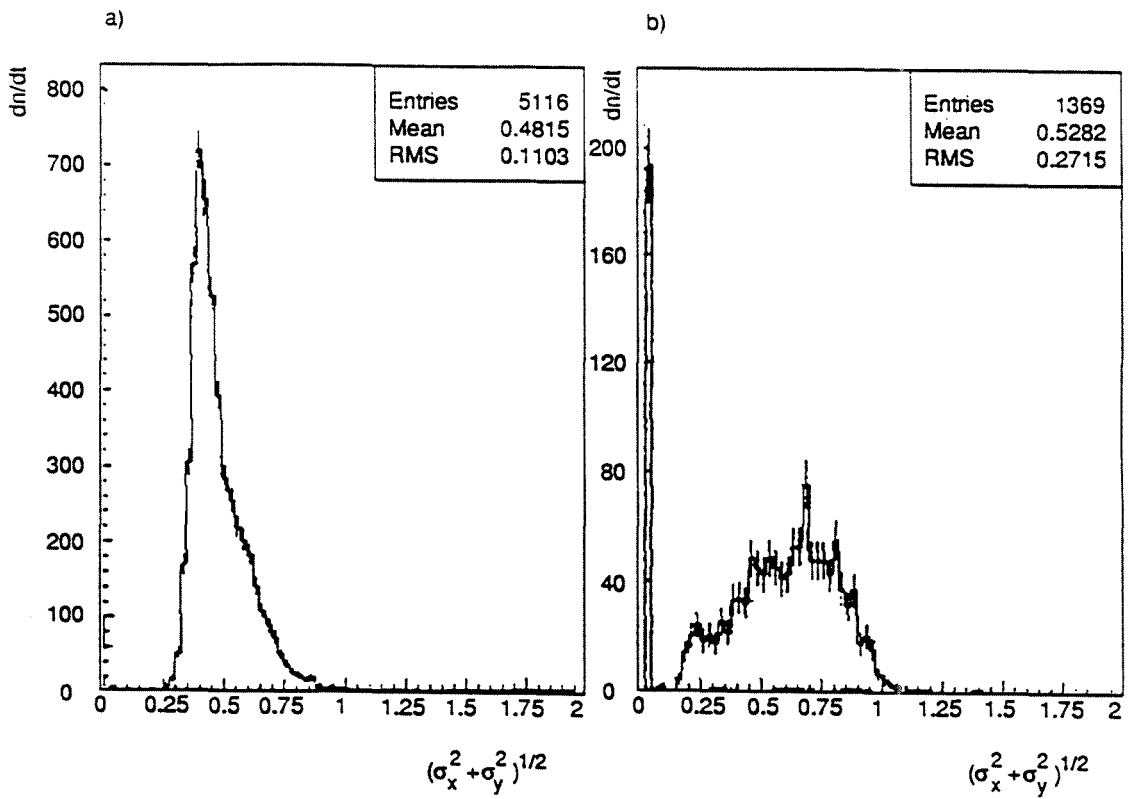


Figure 14:

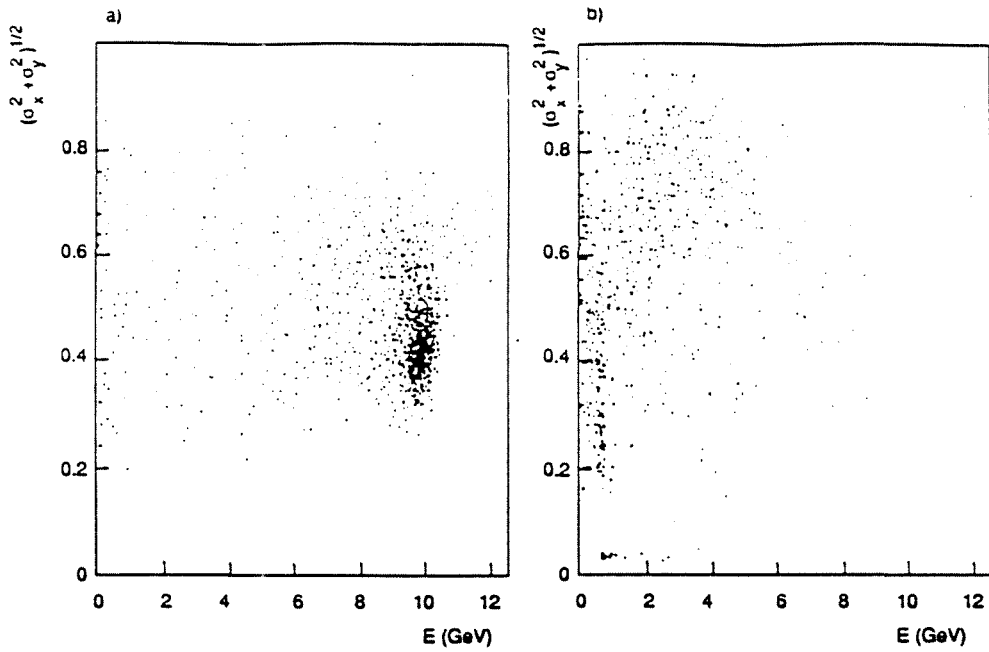


Figure 15:

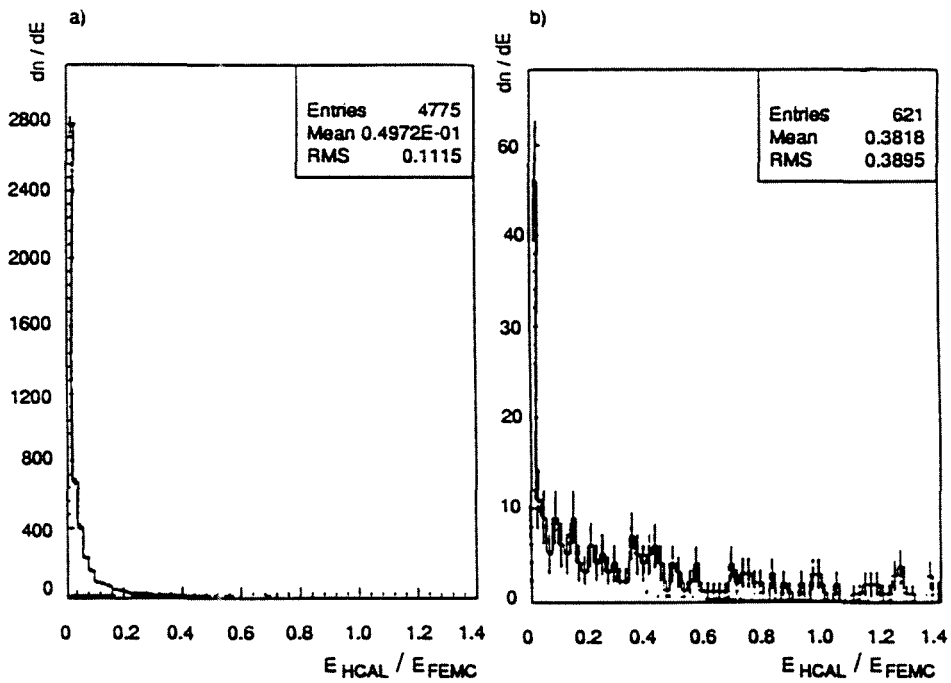


Figure 16:

RESEARCH INSTITUTE FOR HIGH ENERGY PHYSICS

REPORT SERIES

HU - SEFT - 1990 - 06

Evaluation of the Data Analysis Programs of the DELPHI Calorimeters

P. Checchia, R. Keränen, M. Zito

SEFT

ISSN 0788-3587

UNIVERSITY OF HELSINKI
RESEARCH INSTITUTE FOR HIGH ENERGY PHYSICS
SILTAVUORENPENGER 20 C • SF - 00170 HELSINKI • FINLAND

Abstract

The role and some aspects of the development of the data analysis programs in the high energy particle experiments are discussed. A procedure related to the evaluation of the DELPHI calorimeters' data analysis algorithms is introduced and some results of the evaluation work are reported.

1 Introduction

In modern high energy physics experiments particles i.e. their trajectories, energy-momentum vectors and identities are reconstructed by using the information of the digitized electronic signals which are the result of subatomic particles traversing the detectors. The digital data as they come from the fast data acquisition system are directly physically meaningful only at a very rough level (for example, coincidence of signals in various parts of the fiducial detector volume can be used for triggering purposes). The data allow a detailed physical information only when interpreted by a data analysis program which decodes the digitized detector data, calibrates the signals, converts the data given in local detector coordinate systems into the global coordinate system, associates the signals in various channels and detector parts (during which hierarchical internal data structures are created and the final extraction of the meaningful signals from the detector noise is made), and finally calculates the physical quantities of the traversed particles to be stored in a compact format for a more specific analysis.

The complexity of various types of detectors like in the DELPHI experiment at the LEP collider, the long data taking periods and the large data volumes imply that the data analysis program is an extensive modular software product with high requirements on standardization and stability, which comprise the specialized expertise to interpret the data of each detector part optimally. Analogously to the general purpose principle of the detector hardware design, the data analysis program must be developed in such a way that it satisfies simultaneously a multitude of physics topics which are studied in the experiment. In this way computing and analysis resources are considerably saved. In the common frame, the analysis specific to a given physics topic (with the corresponding experimental signature) can then concentrate on the reconstruction of the events in this specific channel, determine the instrumental systematics, and even optimize the reconstruction - which knowledge can again feed back the common data analysis and improve the overall reconstruction quality. The development of such a software product parallelly with the detector hardware and the data acquisition system requires a significant amount of specialized manpower and coordination.

The structure and the development of the data analysis program of the DELPHI experiment, DELANA [1] well reflects these general features. It has a modularity following the hardware composition of the DELPHI detector [2]. The program flow has a two step iterative structure of local pattern recognition algorithms and subsequent global association and

particle track fit stages. It abundantly applies the DELPHI data base, The internal data structures are defined in the TANAGRA package [3] (developed on the dynamical data structure handling package ZEBRA [4]). It is compatible with the DELPHI full simulation program DELSIM [5], and with the DELPHI interactive event viewing package DELGRA [6] which are developed parallelly and have largely supported the development of the data analysis program.

At the stage when the analysis program reaches the level of general structural stability and the actual algorithms, which treat each detector's data, are being integrated in the whole program, the technical tests of the program can be extended to include the performance evaluation of these algorithms. In case of the DELPHI experiment, this stage was reached before the real detector data was available and the data of the full digital simulation program, DELSIM was applied without comparison with the real data. Despite of the apparent danger of possibly unrealistic simulation output, this approach offered unique possibilities for detailed cross checks of the analysis output with the known simulated input and the program performance could be evaluated from the following point of views:

- the spatial resolution of the local pattern reconstruction algorithms: comparison of the position of the reconstructed tracks and showers with the trajectories of the simulated particles,
- the efficiencies of the local pattern reconstruction algorithms,
- the efficiencies of the global association and fitting algorithms: both the shortcomings of the global algorithms themselves and the incompatibilities between the detector specific parts are revealed,
- compatibility of the algorithm updates with the other parts of the program: the quality of the program output is highly fragile due to hierarchial and iterative general structure of the program.

2 DELPHI calorimeter off-line programs

The DELPHI detector contains four calorimetric detector parts. The High Density Projection Chamber (HPC) and the Forward Electromagnetic Calorimeter (FEMC) detect electromagnetic particles and measure their energy over a large solid angle. The Hadron Calorimeter (HCAL) which is geometrically situated outside the electromagnetic calorimeters detects and measures the hadronic particle flow that penetrates through the electromagnetic calorimeters. The Small Angle Tagger (SAT) is dedicated

to detect the electrons and positrons from Bhabha scattering at small angles for luminosity measurement.

Each of these detector modules have separate analysis packages (HPCANA, EMFANA, HACANA and SATANA) which analyze the detector data iteratively in two stages: in the first stage they perform independent pattern recognition (shower search) and calibration after which input of the first stage reconstruction from the other parts of the DELPHI detector consisting of charged particle track information is used to improve the pattern recognition by solving the overlaps, to identify the neutral particles by associating the showers corresponding to the charged particle tracks and to separate hadronic showers from electromagnetic showers as well as to identify muons.

The reconstruction of the electromagnetic and hadronic energy flow and thus the structure of the related analysis programs is complicated by the problematics of the hadronic energy measurement: the electromagnetic calorimeters are not fully transparent to the hadrons but they instead absorb in a widely fluctuating way a part of the hadronic energy flow which is then only partially measured in the HCAL. Due to this, an additional analysis package COMCAL (stands for the combined calorimetry) is included in the DELANA structure. It's task is to associate geometrically the hadronic signals in the electromagnetic calorimeters (minimum ionizing depositions or initiated hadronic showers) with the showers in the HCAL and optimize the combined energy reconstruction. It is vital for a satisfactory total energy reconstruction in the multihadronic final states.

3 Method of the calorimeter off-line program evaluation

We describe here a procedure we have set up for a fast check of the calorimeters off-line programs (HPCANA, HACANA, EMFANA, SATANA, COMCAL) concerning the physical meaningfulness of the outcoming results. We have summarized the information contained in the TANAGRA output of the 1st and 2nd stage calorimeter pattern recognition in a collection of histograms, presenting the distributions of the relevant quantities. For this purpose, we have written a package (EYSCAL) which is called by the standard DELANA steerings and produces in the log file all the histograms we have considered. Using this package one can compare the computed distributions with the expectations or with the results of previous releases of the programs.

The quantities we want to monitor concern the pattern recognition and the energy calibration of the calorimetric showers. We take the information of the reconstructed showers as the TER banks of the TANAGRA structure. Efficiencies and multiplicities are analyzed for various particle types. We compare the TER banks' contents with the reference coordinates of the entering particles given by the simulation (PA vector in the DELSIM simulation). In order to analyze the effect of detector material inside the calorimeters, we produce the distributions for the total sample and for the subsample of events where the incoming particle has produced no secondary interaction before the calorimetry. In Table 1 the most relevant distributions produced by EYSCAL are summarized.

A more detailed description of the EYSCAL package and the usage guide are reviewed in Appendices 1 and 2.

4 Results

Here only the most relevant distributions made by using the development version of DELANA22 are presented (some of the problems found to exist in the frozen version of DELANA21 are solved in the development version). As input for the procedure both single particle and complex physical events were used. We generated raw data for single particle Monte Carlo events (muons, pions and photons at the energy of 1, 3 and 10 GeV respectively, both in the barrel and in the forward region) and we have used the standard samples of multihadronic events (Table 2).

In Figure 1 the energy distributions are shown for the photons of 3 GeV entering the HPC, the FEMC and the SAT ¹ without interacting before the calorimeters. In all cases the peak is centered at the nominal value, and the widths correspond to the expected energy resolutions. The presence of low energy tails is due to the detector cracks.

In Figure 2 the energy distributions are shown for pions entering the HPC, the FEMC and the HCAL. The reconstruction of the COMCAL is shown, too. The punch through particles give the low energy peak in the electromagnetic calorimeters in good agreement with the experimental test results [7,8]. The visible energy in the HCAL is smaller than the nominal values as expected, while the combined calorimetry corrects this by using the energy reconstructed in the electromagnetic calorimeters and gives the right average value.

¹This check is the fastest way to find miscalibrations with respect to the DELSIM output.

The differences between the coordinates of the reconstructed showers and the coordinates of the photons entering in the electromagnetic calorimeters are shown in Figure 3. The values are compatible with the expected ones. The same quantities are plotted in Figure 4 for all the detectors for 10 GeV muons. Here, in the frozen version (dotted curves) we find too large width in the forward hadron calorimeter distributions ($\Delta x, \Delta y$) and a wide and not centered shape in the Δz in the barrel. These two problems have been understood and are solved in the development version. The COMCAL distributions have almost the same widths as the associated electromagnetic calorimeters; this is as expected since the spatial precision in the HCAL does not improve the global result.

In Figure 5 the multiplicity distributions for photons in the HPC and in the FEMC are shown. In the HPC the cracks account for $\approx 10\%$ of the entries so that the low efficiency is not due to the program, while the FEMC has $\sim 100\%$ efficiency (still there can be unfrequent losses due to the cracks).

In Figure 6 shower multiplicity distributions for the noninteracted pions are shown for all the detectors (except for the SAT) and for the COMCAL. It happens quite often that the hadronic interactions give rise to more than one TE bank and consequently the combined calorimetry is inefficient in making the associations.

The next step of the program evaluation is to study the response in the physical multihadronic events, especially the total energy distributions. When writing this note, this analysis is not yet complete and all the observed problems are not fully understood but the detector code authors are working to solve them.

5 Conclusions

A standardized independent evaluation procedure turned out to be very useful in the debugging of the first working versions of the DELANA program. A multitude of problems and bugs in the first stage pattern recognition and energy calibration were pointed out and subsequently solved.

The emphasis of the procedure was at first put in the evaluation of 1st stage pattern recognition routines. The 2nd stage performance was studied in the spirit to look whether they tend to improve the results. More detailed evaluation of the 2nd stage (neutral association) is left to a future work.

References

- [1] DELPHI Collaboration, DELPHI Data Analysis Program (DELANA) User's Guide, DELPHI 89-44 PROG-137, (May 1989), unpublished.
- [2] DELPHI Collaboration, DELPHI Technical Proposal, DELPHI 83-66/1, CERN/LEPC/83-3, (May 1983), unpublished; DELPHI Collaboration, DELPHI Detector, CERN/EF/90-5, CERN-PPE/90-128, 1990, submitted to Nucl. Inst. and Meth.
- [3] D. Bertrand, L. Pape, TANAGRA Track Analysis and Graphics Package, DELPHI 87-95 PROG-98, (June 1988), unpublished.
- [4] R. Brunn, J. Zoll, ZEBRA User Guide, long write-up CERN Computer Centre, Program Library, (January 1987), unpublished.
- [5] DELPHI Collaboration, DELSIM, DELPHI Event Generation and Detector simulation, User's Guide, DELPHI 89-67 PROG-142, (July 1989), unpublished; DELPHI Collaboration, DELSIM, DELPHI Event Generation and Detector simulation, Reference Manual, DELPHI 89-68 PROG-143, (September 1989), unpublished.
- [6] P. Abreu et al., Event Viewing Software, Installation Procedure and User Manual Version 1.00 DELPHI 89-6 PROG-126, (January 1989), unpublished.
- [7] P. Checchia et al., Performance of the Forward Electromagnetic Calorimeter for the end caps of the DELPHI detector, N.I.M. A 275 (1987) 49-58.
- [8] C. Matteuzzi, private communication.

Appendix 1

The EYSCAL package description

EYSCAL is a histogramming package which is implemented in the DELANA program in order to study the performance of the calorimetry data analysis routines. It contains:

1. initialization routines steered by the subroutine EYINI, in which the histograms are booked,
2. histogram filling routines which are called in each event and steered by the subroutine EYSCAL, and
3. end of run routines steered by the subroutine EYEND, in which a short summary of the results is printed out.

The input for the histogramming is taken from

- the TANAGRA structure produced by the 1st or 2nd stage pattern recognition routines of the DELANA calorimeter programs (TER banks), and
- the simulated PA structures in the DELSIM for each detector module.

It should be noted that EYSCAL histogramming is completely independent of the module routines and it does not use any internal data of the pattern recognition routines. The EYSCAL histograms can be filled directly from the existing DELANA output data which contains the TANAGRA and the ZEBRA data thus allowing an independent check.

The EYSCAL package can be applied to the simple topologies described in this report and also to physical events like e^+e^- and multihadronic samples. Basically three kind of histograms are filled:

1. histograms 45101-45199: The reference points of the reconstructed TE's and the PA coordinates of the incoming particles are compared; plots are also given for the differences between the reconstructed energies and the energy of the incoming particles,
2. multiplicity histograms 45201-45299: The numbers of activated/deactivated TE's in each event for all the modules are given, and
3. histograms 45301-45399: The total energy reconstruction in the calorimetry is analyzed.

The first type of histograms help in checking against the geometrical and energy biases in the shower reconstruction. For example, the results show the achieved effective granularity and energy resolution at the single particle level.

Concerning the single particle samples, the multiplicity histograms give information about the efficiencies and about the degree of the shower splittings. Concerning the physical samples the multiplicity histograms describe the general topology of the events.

The third set of histograms shows the energy reconstruction in each calorimeter module and in the COMCAL in complex topologies.

For the first and the second class of histograms the concept of noninteracting incoming particle is useful, because the calorimeter response can be studied either taking into account the secondary interactions before the calorimetry or considering only ideal single particle hits in the calorimetry. This is important especially in the case of electromagnetic calorimeters. Thus, a logical function EYSCLN is defined in EYSCAL, which classifies the events to be a noninteracting ones when:
either

number of of PA's=1 and E of the PA $> 0.9 \times$ initial energy

or, for pion (in order not to exclude events with neutron backscattering)
when

at least one PA is a pion and $E_{\pi} > 0.98 \times$ initial energy

The first type histograms (PA comparison) are filled only for the noninteracted particles in order to avoid ambiguities. Note that these histograms are meaningful in the single particle samples only. For the others all the relevant histograms are filled for the noninteracted and all events.

Furthermore, in order to evaluate the performance of the combined calorimetry, all the histograms containing information about the local pattern recognition are duplicated separately for the activated and for all (deactivated and activated) TER-banks in each calorimeter.

Eventually, more than 70 histograms are filled during the run and they cover systematically all the individual calorimeters as well as the combined calorimetry. In order to have a useful statistical treatment and a compact output, all the histograms are automatically printed out by DELANA with the following HBOOK options:

HIDOPT (0,'STAT')

HIDOPT (0,'INTE')

HIDOPT (0,'NPHI')

HIDOPT (0,'YES')

The released version of the EYSCAL package is available in VXCERN::DISK\$DELPHI3:[EVENTS.CAL]EYSCAL.CAR and it is compiled using the PATCHY cards

+USE,SCAL.

+USE,*EYSCAL.

+PAM,LUN=12,T=C,A.DISK\$DELPHI3:[EVENTS.CAL]EYSCAL.CAR.

An example of the title cards used to run EYSCAL in DELANA is shown in Appendix 2.

Appendix 2

The DELANA22 title cards which steer the filling and printing of the EYSCAL histograms are as follows.

```
=====
C-- Titles for the Calorimetry Checking (select module SCAL)
=====

C-- Select calorimeter checking & statistics package
C--MSTATI 'SCAL'
C-- select comparisons of TE with the simulated PA :
C-- it makes sense only for single particle events !!!
LYSTAS TRUE
C-- single particle energy (GEV)
EYEINI 3.
C-- contains the geometrical region and
C-- type of events encoded in the following way
C-- IYSAGE = 10 * I + J
C-- where I = 1 single particle in Forward direction
C-- " 2 " " Barrel "
C-- " 3 events with particles in the 40 degree hole
C-- " 4 " " everywhere in DELPHI (default)
C-- " 5 single particle in SAT
C--
C-- where J= 1 single particle is Photon
C-- " 2 Pion
C-- " 3 " " Muon
C-- " 4 all kind of events (QQ , e+ e- ...) (default)
IYSAGE 22
C-- select study of energy reconstruction in calorimeters
LYSTAC TRUE
C-- select study of multiplicities " "
LYSTAM TRUE
```

Table captions

Table 1. Summary of the distributions calculated in the EYSCAL package. In addition, a set of distributions giving the total calorimetric energy in the calorimeters defined as $E_{\text{tot}} = \sum_{\text{showers}} E_{\text{active}}^{CCA} + \sum_{\text{HPC,EMF,HCAL}} \sum_{\text{showers}} E_{\text{active}}$ is calculated. (*): distributions calculated for those particles not interacting before the calorimeters, only.

Table 2. Summary of the Monte Carlo simulated data samples. $\theta_{\text{min, max}}$ refer to the polar angle interval in which particles are generated in the origin of the DELPHI detector coordinate system.

Figure captions

Figure 1. Energy reconstruction of a) the HPC, b) the FEMC and c) the SAT for single noninteracted photons (3 GeV). The histograms show the difference between the PA and the TER energy.

Figure 2. Energy reconstruction of a) the HPC, b) the FEMC and c) the HCAL barrel and d) the CCA for single noninteracted pions (10 GeV). The histograms show the difference between the PA and the TER energy.

Figure 3. Position reconstruction in a) the HPC, b) the FEMC and c) the SAT for single noninteracted photons (3 GeV). The histograms show the difference between the PA and the TER position.

Figure 4. Position reconstruction in a) the HPC, b) the FEMC, c) the HCAL barrel and d) the HCAL forward for single noninteracted muons (10 GeV). The histograms show the difference between the PA and the TER position. The dashed distributions have been obtained with DELANA21.

Figure 5. Multiplicity distributions in a) the HPC and b) the FEMC for single noninteracted photons (3 GeV).

Figure 6. Multiplicity distributions in a) the HPC, b) the FEMC, c) the HCAL and d) the CCA for single noninteracted pions (10 GeV).

Tables

Table 1.

detector	$\Delta E = E_{\text{TER}} - E_{\text{PA}}(*)$	$\Delta \bar{r} = \bar{r}_{\text{TER}} - \bar{r}_{\text{PA}}(*)$	shower multiplicity	total energy
SAT	yes	-	-	-
FEMC	yes	$\Delta x, \Delta y$	yes	yes
HPC	yes	$\Delta z, \Delta R\Phi, \Delta\theta, \Delta\phi$	yes	yes
HAF	yes	$\Delta x, \Delta y$	yes	yes
HAB	yes	$\Delta z, \Delta R\Phi$	yes	yes
CCA(f)	yes	$\Delta x, \Delta y$	yes	yes
CCA(b)	yes	$\Delta z, \Delta R\Phi$	yes	yes

Table 2.

file name	particle	energy [GeV]	θ_{min} (deg.)	θ_{max} (deg.)
G3.3_6.DAT	photon	3	3	6
G3.10_35.DAT	photon	3	10	35
E10_10_35.DAT	electron	10	10	35
M10_10_35.DAT	muon	10	10	35
P10_10_35.DAT	pion	10	10	35
G3.45_135.DAT	photon	3	45	135
E10_45_135.DAT	electron	10	45	135
M10_45_135.DAT	muon	10	45	135
P10_45_135.DAT	pion	10	45	135

Figures

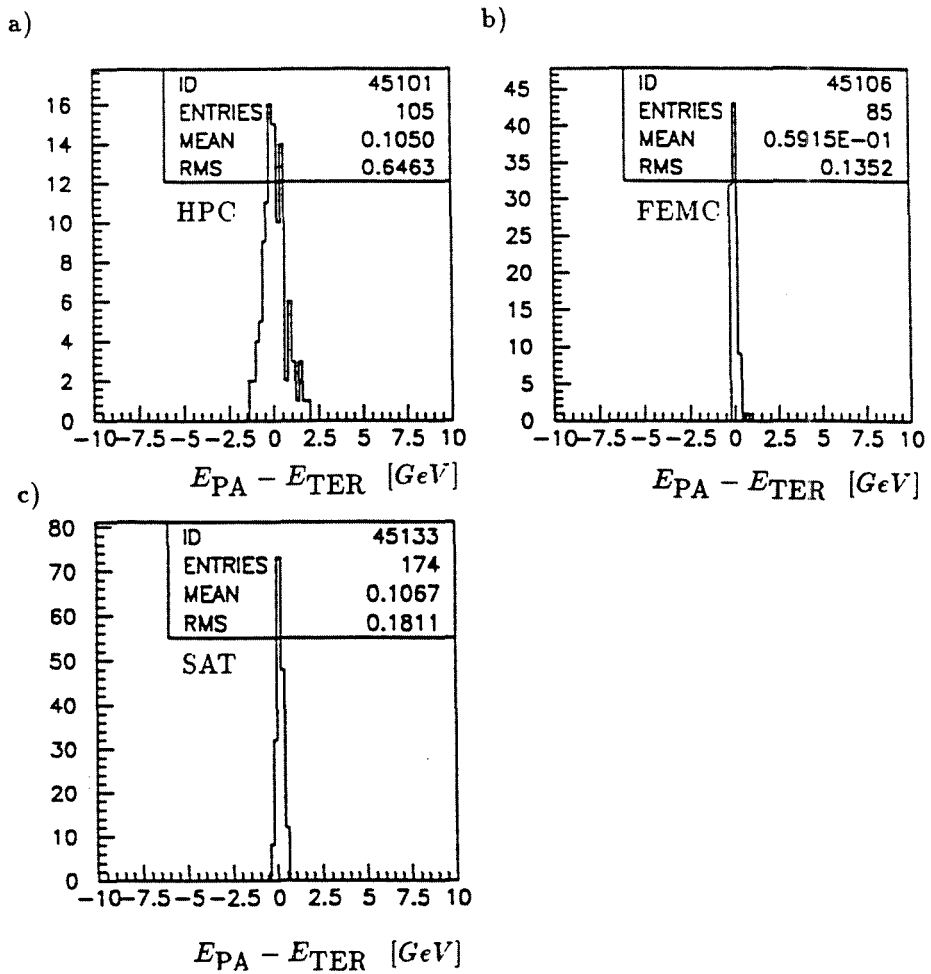
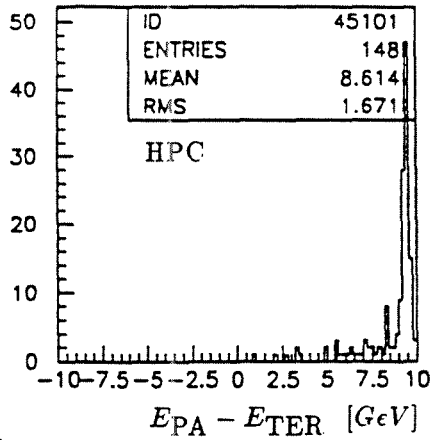
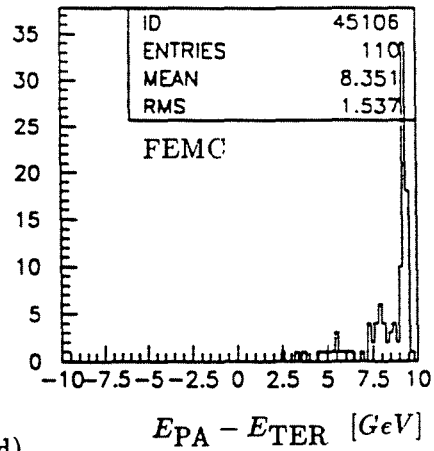


Figure 1

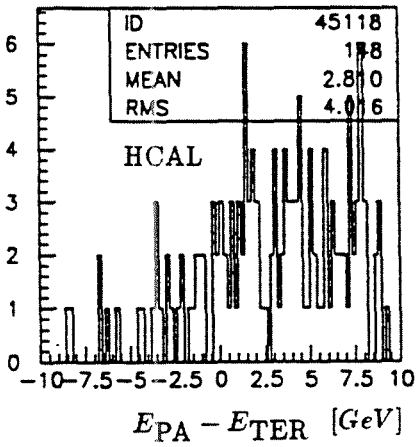
a)



b)



c)



d)

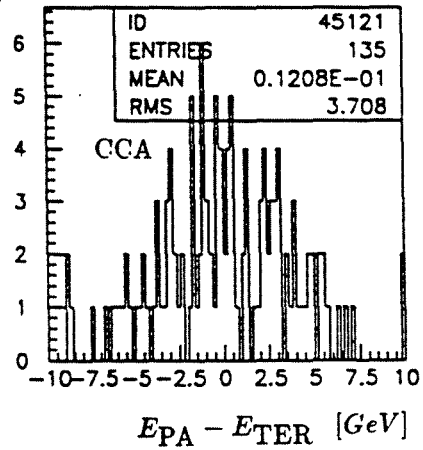


Figure 2.

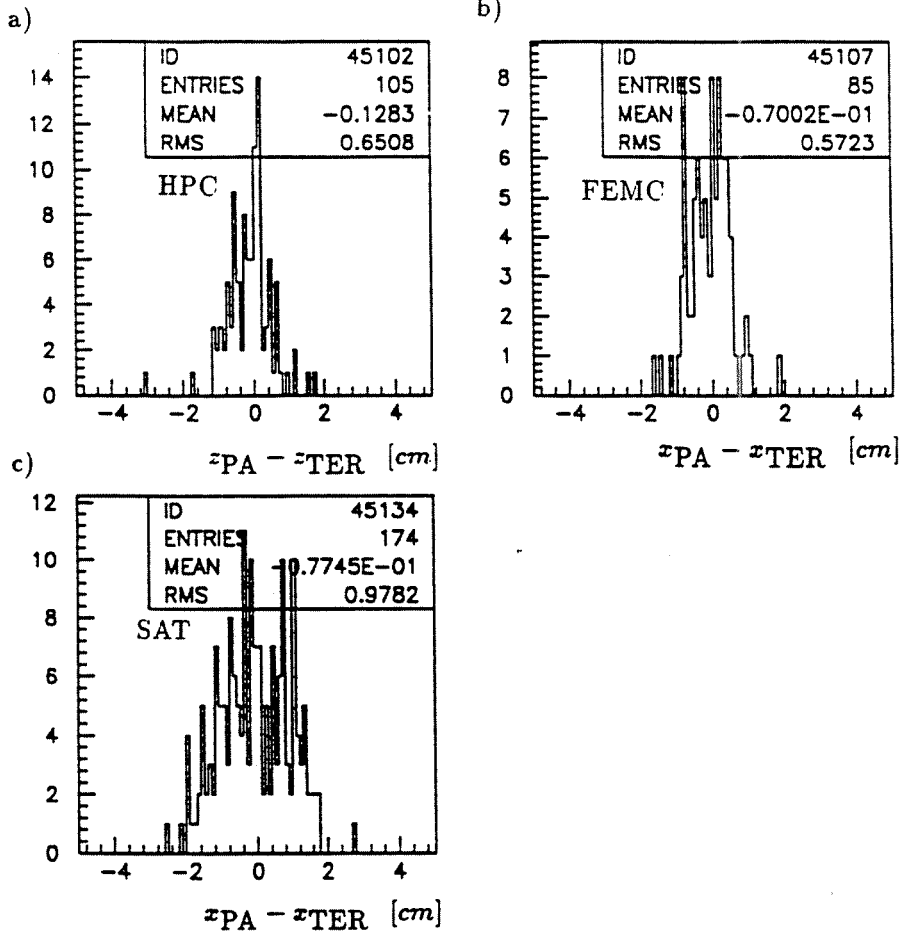


Figure 3.

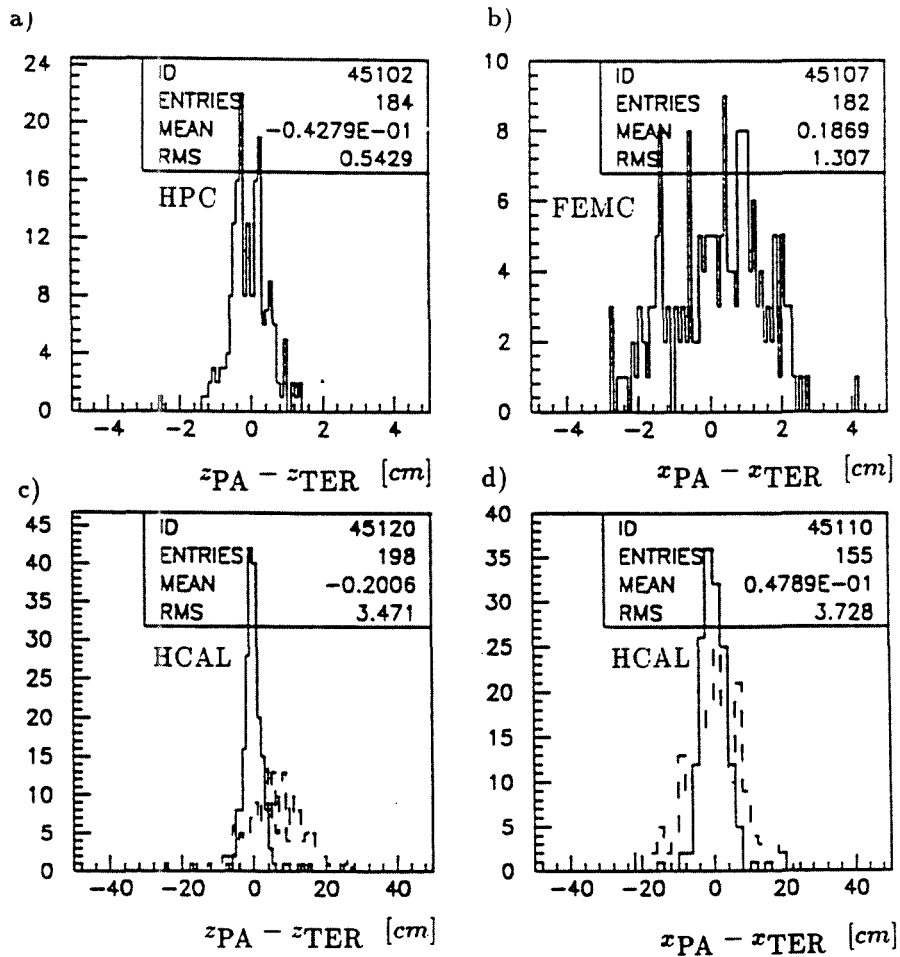


Figure 4.

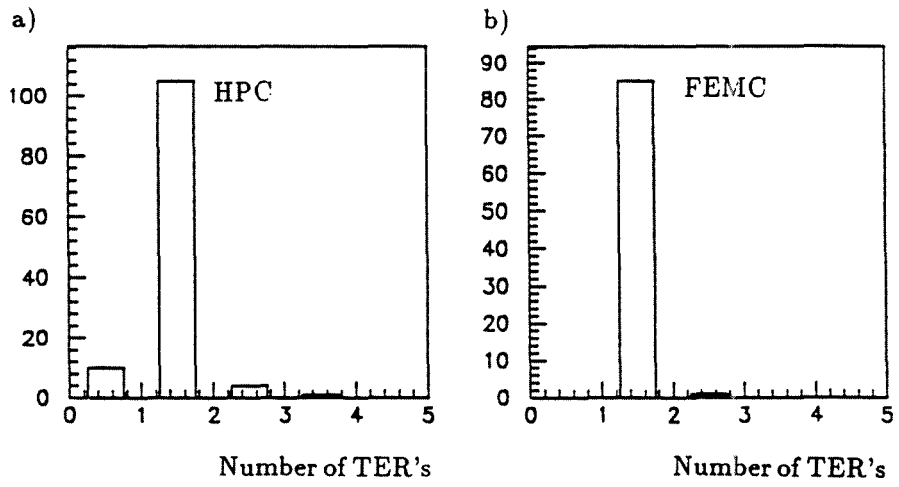


Figure 5.

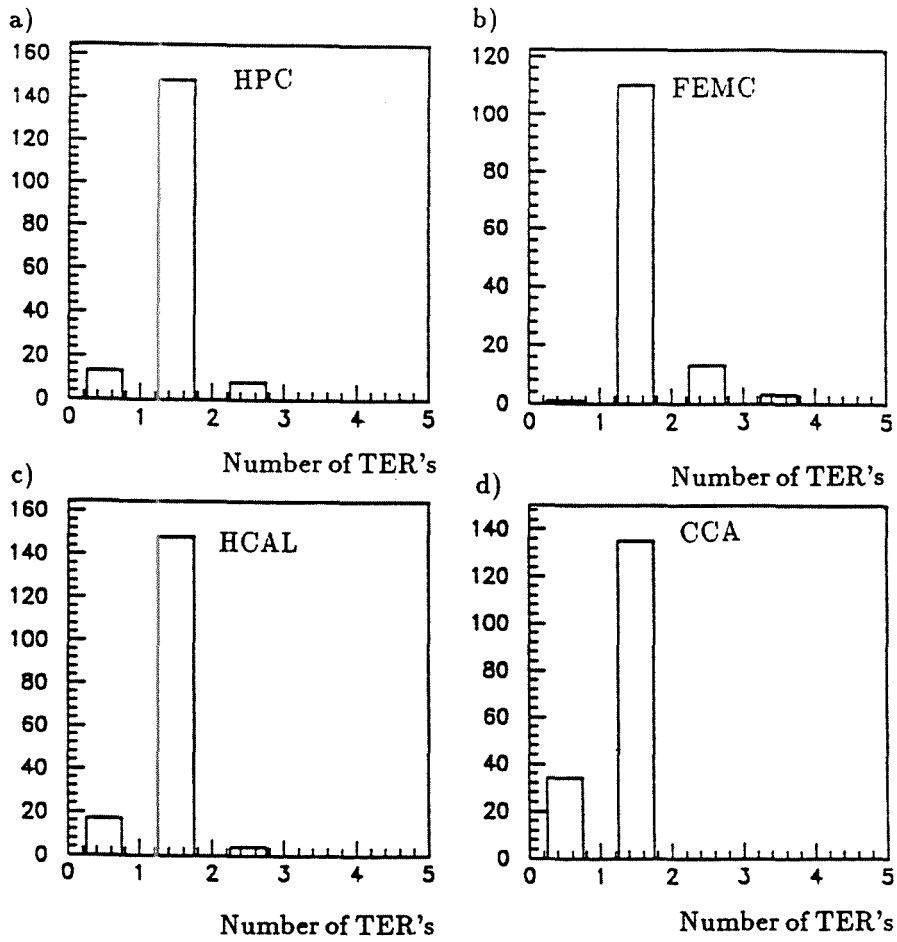


Figure 6.



RESEARCH INSTITUTE FOR HIGH ENERGY PHYSICS

REPORT SERIES

HU - SEFT - 1990 - 08

Analysis of Cosmic Muons in the DELPHI Hadron Calorimeter During the LEP Pilot Run

Reino Keränen and Timo Jokitalo

SEFT

ISSN 0788-3587

UNIVERSITY OF HELSINKI
RESEARCH INSTITUTE FOR HIGH ENERGY PHYSICS
SILTAVUORENPENGER 20 C • SF - 00170 HELSINKI • FINLAND

Abstract

Cosmic muon detection in the DELPHI Hadron Calorimeter (HCAL) during the LEP pilot run, August 1989, has been analyzed utilizing supplementary information from the tracking detectors in operation at the same time. Despite of the provisional running conditions some basic performance characteristics and data quality of the barrel part of the HCAL could be checked and found to be satisfactory.

1 Introduction

The DELPHI Hadron Calorimeter (HCAL) [1,2] was in operation in the pilot run of the Large Electron Positron Collider (LEP), 13-18 August 1989 and collected both cosmic and beam collision data. The data samples represent more than 10 hours of running time in total, of which a significant fraction was taken in synchronization (the same trigger signal) with the other detectors. Due to the commissioning status of the central data acquisition system, the HCAL data was written separately on the mass storage device, and by using the common trigger information it was possible to glue together off-line the coincident events from the two separate data logger streams of the tracking detectors and the HCAL. This investigation is based on the cosmic muons triggered by the DELPHI scintillator trigger system [3] and recorded in the pilot run central partition (data streams from the Inner Detector ID, the Time Projection Chamber TPC, and the Outer Detector OD) [1,2] and the HCAL.

Several aspects of the HCAL performance can be checked with the cosmic data and also some details of the DELANA (DELPHI off-line data-analysis package [4]) pattern recognition can be tested. All these results should be viewed keeping in mind that **the HCAL was not running in the nominal conditions** but with a nonflammable gas mixture (CO_2 (90%) - iC_4H_{10} (8.0%) - Argon(2.0%)) and an operating voltage 3.9 kV which are not optimal for reaching a pure streamer mode. As a result, **the signal size in the HCAL was smaller by a large factor than in the design conditions achieved soon after this data taking period** The efficiencies and the energy calibration obtained in the analysis of the pilot run data are thereby affected

In these temporary conditions one can investigate some of the very basic aspects of the detector performance i.e. check the active regions, check tower geometries (uncertainties due to swapped cables or decoding errors), get estimate for the efficiency and signal distributions and look for time dependent effects (variations of response in the running time). Most of the analysis is constrained by the small statistics, however this analysis is also the basis of our effort to automatize future cosmic candidate selection and analysis with larger statistics.

1.1 Apparatus

The DELPHI HCAL is a gas sampling detector incorporated in the iron magnet yoke. The barrel part covering polar angles between 42.6° - 137.4° and the two end-caps between polar angles of 11.2° - 48.5° and

131.5° – 168.5° form a closed cylinder which covers 98 % of the solid angle (Figure 1). The barrel is constructed of 24 sectors with the inner radius of 318 *cm* and the outer radius 478 *cm* which contain 20 layers of limited streamer mode detectors inserted in 2 *cm* slots between iron plates of 5 *cm* thickness. The end-caps are made in an analogous modularity with 19 sampling layers. The detectors are wire chambers which consist of a plastic cathode coated with conductive graphite varnish (surface resistivity > 50 *kΩ/□*) and eight anode wires. The analogue signal is read out by using copper clad boards which are segmented in pads in the projective geometry with a granularity of ($\Delta\theta = 2.96^\circ$, $\Delta\phi = 3.75^\circ$) in the barrel. The charge integration is made over 5 adjacent pads (a tower) in the barrel with a 8-bit analog-to-digital conversion and a zero suppression. The supertowers containing 4 × 4 towers in a plane are grouped in fast discrimination for triggering purposes.

The TPC which provided the independent information about trajectory of the cosmic particle is a cylindrical multiwire chamber with an inner radius of 30 *cm* and an outer radius of 120 *cm*. It operates in the pressure 1 *atm* and in the solenoidal magnetic field of 1.2 *T* provided by the superconducting coil. It gives 16 space points for polar angles of 40° to 140°; the Kalman filter is used in the track search. Because of the considerably smaller radius of the TPC compared to the radius of the HCAL, the tagged candidates (giving sufficient amount of space points inside the TPC) were well oriented with respect to the projective geometry of the HCAL.

The candidates were triggered by several back-to-back and majority trigger combinations of the two scintillator layers (the Time of Flight counters at the inner edge of the barrel HCAL and the HPC scintillators at the radius of about 220 *cm* [3]).

2 Event sample

The sample of cosmic events was extracted from the central partition runs and the corresponding HCAL runs as show in Table 1. Events were selected by visual scanning and by requiring a reconstructed cosmic track in the TPC in such a way that it could be extrapolated to an active HCAL barrel module. Both the incoming and outgoing tracks into the HCAL were taken into account as independent events. The default DELGRA (the DELPHI interactive graphics package [5]) extrapolation and visual extrapolation were used. As can be seen in Figures 2 and 3, the sample contains mainly vertical tracks crossing the detector and the statistics in

the horizontal barrel modules is very low, as it is expected due to the cosmics angular distribution. A typical event is shown in Figure 4.

3 Signal distribution and comments on calibration

The ADC distribution of the observed cosmic candidates in the HCAL (taken as the original ADC sum of the all the layers associated in the cluster by the HCANA patten recognition) is plotted in Figure 5. We can see that the signal spectra are by a factor of three lower than for the muons observed in the combined beam test of the DELPHI Hadron Calorimeter, the Forward Electromagnetic Calorimeter and the Muon Chambers [6], fully explained by the temporal gas mixture.

Due to the temporal gas mixture no reliable hadron calibration of the HCAL was available. The collected cosmic data sample can be used to achieve a rough estimate of the pilot HCAL calibration. The estimate is deduced by comparing results from the 1988 HFM experiment with these pilot run data, as follows.

The digitation of the analog signals was made with the same amplification in both runs and the ADC counts can be used as a signal measure. In the HFM test, the average ADC signal of the halo muons was 29 ADC counts passing through 20 layers of the HCAL endcap module. In the same runs a hadron calibration of 170 MeV / 1 ADC was obtained. From this scale one can deduce an estimate for the HCAL pilot run hadron calibration multiplying the HFM hadron coefficient by the ratio of the muon signal in the HFM experiment vs. in the pilot run. The ratio is equal to 3.2.

Thus an estimate for the hadron calibration is $530 \text{ MeV} / 1 \text{ ADC}$ usable for the pilot run hadronic events. The uncertainties in this estimate are large and difficult to estimate arising from the unknown effects for example, due to differences in the barrel and endcap geometry and differences in signal readout timing.

4 Efficiency study with estimation of geometrical, time dependent and other systematics

Of the selected 297 cosmic candidate events, in 190 cases (64 %) there is a HCAL signal which can be associated with the trajectory. The fraction has a statistical error of 8.2 (3 %, the binomial variance of the sample).

Systematic errors are estimated to arise from the following sources: 1) bias in the selection based on the visual scanning, 2) wrongly synchronized data streams, 3) time dependent effects in the detector, 4) various effects due to the momentum and angular distribution of the tagged cosmic candidates: a) low momentum cosmic tracks (anomalous energy loss or curvature in the high magnetic field), b) nonprojective direction of the particle trajectory, c) lower statistics in the horizontal barrel direction.

The systematic error due to the misselection in the visual scanning is estimated to be 15 candidates (5 %) based on the number of candidates which satisfy the selection criteria marginally. Similarly we conclude by cross-checking the subsequent triggers that there is no significant systematic bias due to wrongly synchronized data streams.

By dividing the sample in three time intervals (hrs 23.00-24.00, 01.00-02.00, and 02.00-03.00, 17-18 August 1989) efficiencies are $57 \% \pm 8 \%$ (stat.) $65 \% \pm 4 \%$ (stat.) $67 \% \pm 5 \%$ (stat.) respectively. The averages of the ADC sums of the observed candidates during these intervals are 10.7 ± 2 , 8.5 ± 0.7 , 9.0 ± 1 . By looking at these time interval efficiencies, the chronological distribution of the cosmic candidates (Figure 6) and the signal spectra in the time intervals, we observe that the HCAL was triggered in a stable way and signals were recorded with a constant efficiency.

There are geometry dependent tendencies in the observed cosmic efficiency as seen in Figure 7 in which the efficiency is plotted for each module in phi (both hemispheres in z i.e. the faces A and C used together, the bins 1 and 24 correspond to the uppermost modules). Such a behaviour is not apparent in the signal spectra divided geometrically in hemispheres as seen in Figures 8 - 11. The experimental arrangement and the limited statistics do not allow to disentangle possible systematic effects due to the cosmic distribution from unexpected true effects in the detector performance. We assign 22 % systematic uncertainty (calculated as the root mean square of the module efficiencies) in the overall detection efficiency due to the possible systematic effects in the geometrical distribution of the candidates.

We summarize the overall efficiency determined from the cosmic sample to be

$$\text{HCAL efficiency} = 64\% \pm 3\% \text{ stat.} \pm 22\% \text{ syst.} \quad (1)$$

where the systematic uncertainty arises essentially from the poorly understood geometrical effects.

5 Two-candidate correlations and first look on the local off-line muon identification efficiency

Systematic effects in the efficiency can be evaluated also by studying the correlations between the observation of two cosmic candidates in a single trigger (incoming and outgoing track). Ideally there should be no correlation between them.

The analysis was done as follows. The subsample of triggers which have both incoming and outgoing candidate in the active barrel module of the HCAL was extracted. There are 103 such triggers, from which we can build up a contingency Table 2. To test the hypothesis of correlation we use the χ^2 test [8] with a test variable

$$z_{\chi^2} = \sum_{i=1}^2 \sum_{j=1}^2 \frac{(n_{ij} - g_{ij})^2}{g_{ij}} \quad (2)$$

$$n_{ij} = \text{observed triggers in line } i \text{ and in column } j \quad (3)$$

$$g_{ij} = \text{expected triggers in line } i \text{ and in column } j \quad (4)$$

The overall efficiency of 69.9% of this subsample was used in calculating g_{ij} as seen in Table 3, and

$$z_{\chi^2} < \chi_{\beta}^2(1) \quad (5)$$

in the case of noncorrelating observations at a confidence level β . The test variable z_{χ^2} gives 35.20 for the sample under study and at the 99.9% confidence level ($\chi_{99.9\%}^2(1) = 10.8$) observations of the incoming and the outgoing cosmic track in the HCAL were positively correlated.

The correlation between bi-track efficiencies cannot be explained by the lower streamer spectra alone. The wrongly synchronized data streams could produce such a correlation but this possibility is excluded. As in the HFM experiment [6,7], one is tempted to consider the possible sensitivity

of the signal readout on the trigger timing aspects. Namely, the observed correlation can be explained by the varying signal integration time due to the random arrival of the cosmic track during the $1.5 \mu s$ gate.

The efficiency quoted above measures the basic hardware efficiency ("anything seen") i.e. nothing is required from the spatial signal shape for correct muon identification. It is natural to ask how well the DELPHI offline analysis is able to interpret the seen cosmic candidates as muons. This was checked by running the HCANA (Hadron Calorimeter off-line pattern recognition and calibration package) version used in the pilot run analysis on the cosmic data sample. The 1st level pattern recognition finds 67 muons which should be compared to the 190 visible signals. Not all of the signals can be expected to be reconstructed as identified muons, and a realistic identification power should be extracted with a more detailed investigation.

6 Conclusions

During the runs considered, the HCAL, the detectors in the central partition and their data acquisition chains were running in synchronization in stable conditions.

The data sample allowed us to check against any major cabling error in the barrel HCAL. At the super tower level the detector was active, i.e. there are no unexpected dead regions. The overall efficiency is not ideal, but is explained by the temporary gas mixture.

In conclusion, the data indicates that the HCAL signal readout timing must be accurate within less than few hundred nanoseconds in order to exclude additional fluctuations in the measured signal. Similarly, cosmic triggers can be fully exploited in the HCAL efficiency and calibration studies only when taken with a sufficiently narrow trigger gate.

A rough estimate for the pilot HCAL hadron calibration is achieved which is a factor of three higher than the default calibration in DELANA (based on the HFM data and Monte Carlo simulation). The estimate carries large systematic uncertainties due to geometrical effects.

References

- [1] DELPHI Collaboration, DELPHI Technical Proposal, DELPHI 83-66/1, CERN/LEPC/83-3, May 1983, unpublished.

- [2] DELPHI Collaboration, DELPHI Detector, CERN/EF/90-5, CERN-PPE/90-128, 1990, submitted to Nucl. Inst. and Meth.
- [3] P. Aarnio et al., Measurement of the Mass and the Width of the Z^0 Particle from Multihadronic Final States Produced in e^+e^- Annihilations, Phys. Lett. **231B** (1989) 539.
- [4] DELPHI Collaboration, DELPHI Data Analysis Program (DELANA) User's Guide, DELPHI 89-44 PROG-137, (May 1989), unpublished.
- [5] P. Abreu et al., Event Viewing Software, Installation Procedure and User Manual Version 1.00 DELPHI 89-6 PROG-126, (January 1989), unpublished.
- [6] H. Herr et al., The Results of the Combined Beam Test of the DELPHI Hadron Calorimeter, the Forward Electromagnetic Calorimeter and the Barrel Muon Chambers (π^+ , e^+ runs), HU-SEFT-90-7 (1990).
- [7] E. Veitch et al., Muon identification efficiencies from the HFM experiment, DELPHI 89-57 PHYS 48, July 1989, unpublished.
- [8] W. Ledermann, Handbook of Applicable Mathematics, Vol 6, Part A, page 376, John Wiley & Sons, 1984.

List of Tables

1	Summary of the used cosmic data samples.	9
2	Correlation between the observation of the incoming and outgoing cosmic.	9
3	Correlation between the observation of the incoming and outgoing cosmic.	9

List of Figures

1	The DELPHI Hadron Calorimeter	10
2	Selected cosmic candidates	11
3	Seen cosmics in the HCAL	11
4	Example event.	12
5	ADC distribution	13
6	Chronological distribution	14
7	Efficiency	15
8	ADC distribution in the upper hemisphere of the HCAL . .	16
9	ADC distribution in the lower hemisphere of the HCAL . .	16
10	ADC distribution in the backward z hemisphere of the HCAL	17
11	ADC distribution in the forward z hemisphere of the HCAL	17

run number in central partition	run number in HCAL run	time of the first event	time of the last event	number of triggers
383	54	23:11:59	23:41:12	482
385	56	00:45:32	02:29:34	1943

Table 1: Summary of the cosmic data samples taken 17-18 August 1989.

	1st not seen	1st seen
2nd not seen	22	9
2nd seen	9	63

Table 2: Correlation between the observation of the incoming and outgoing cosmic. The candidate pair was ordered randomly as track-1 and track-2. The upper left corner gives the amount of triggers in which none of the hits were seen, lower right corner gives the triggers in which both of them were seen, the rest are the triggers in which either of the track was seen.

	1st not seen	1st seen
2nd not seen	9	22
2nd seen	22	50

Table 3: Expected observations based on the hypothesis of noncorrelation in Table 2.

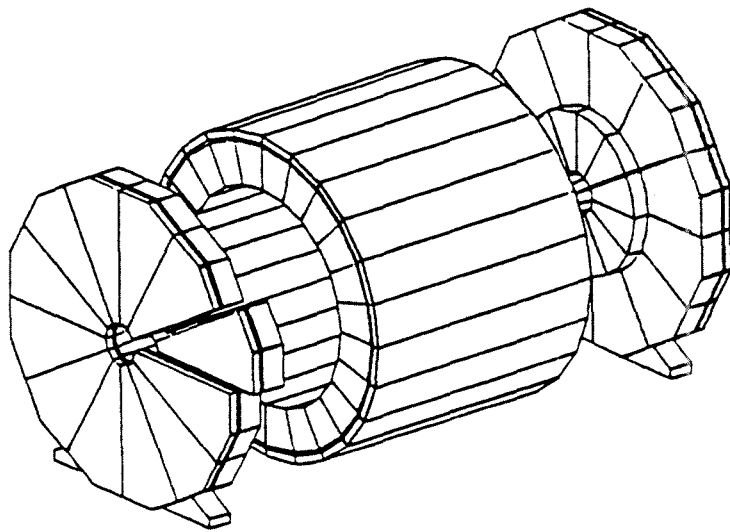


Figure 1: General view of the DELPHI Hadron Calorimeter. The two end-caps are shifted along the beam to allow better visibility and an end-cap module is artificially drawn as separated from the main structure. The diameter of the barrel cylinder is 9.5 m and the length of the cylinder in the closed position is 10 m .

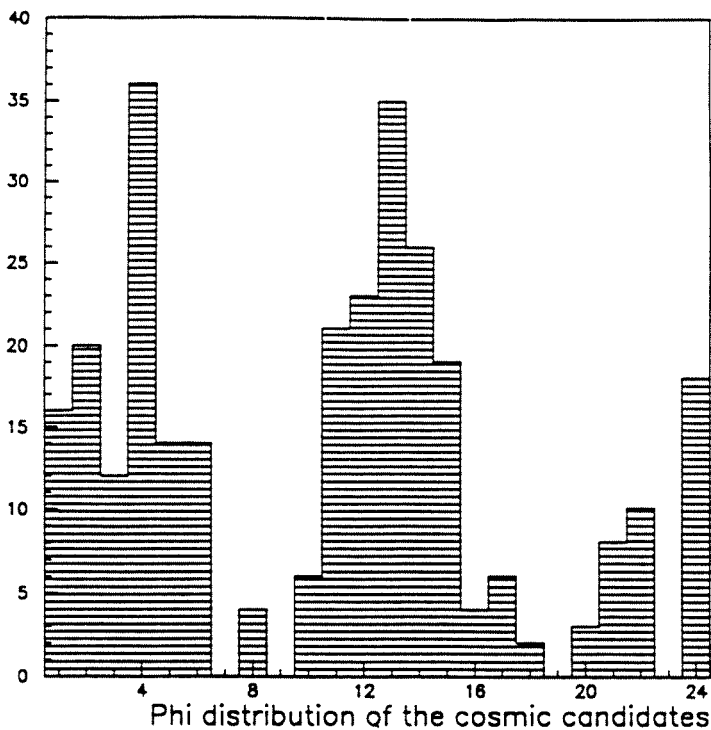


Figure 2: Geometrical distribution of the selected cosmic candidates (297 in total) as a function of sector index (both hemispheres in z summed up).

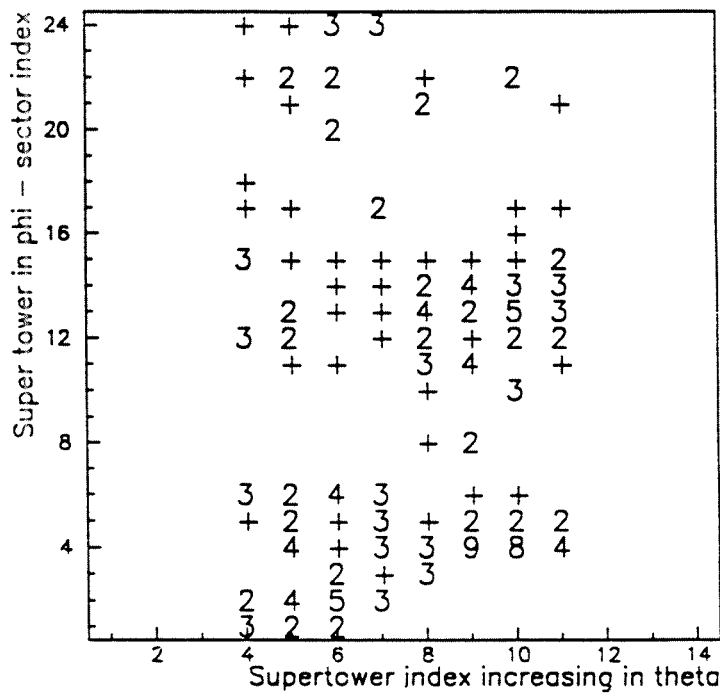


Figure 3: Distribution of the observed cosmic candidates in the HCAL (190 in total) as a function of super tower indices - index in ϕ chosen as the module numbers.

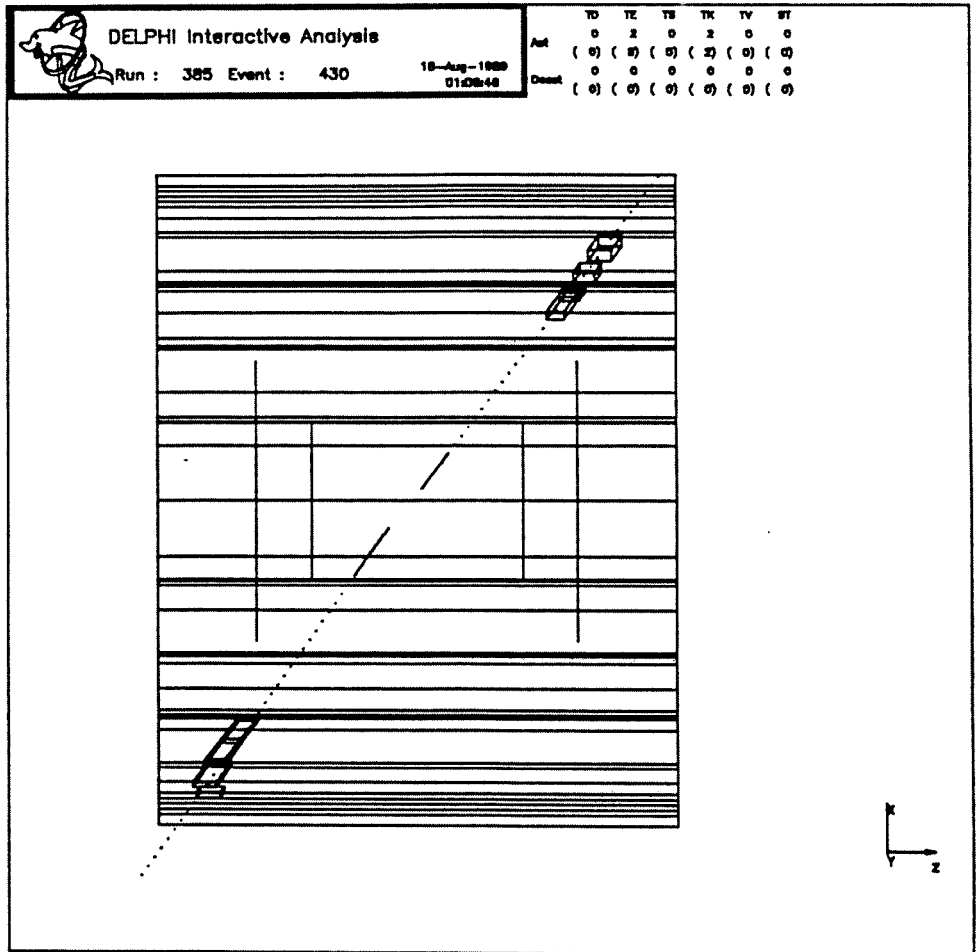


Figure 4: Example event.

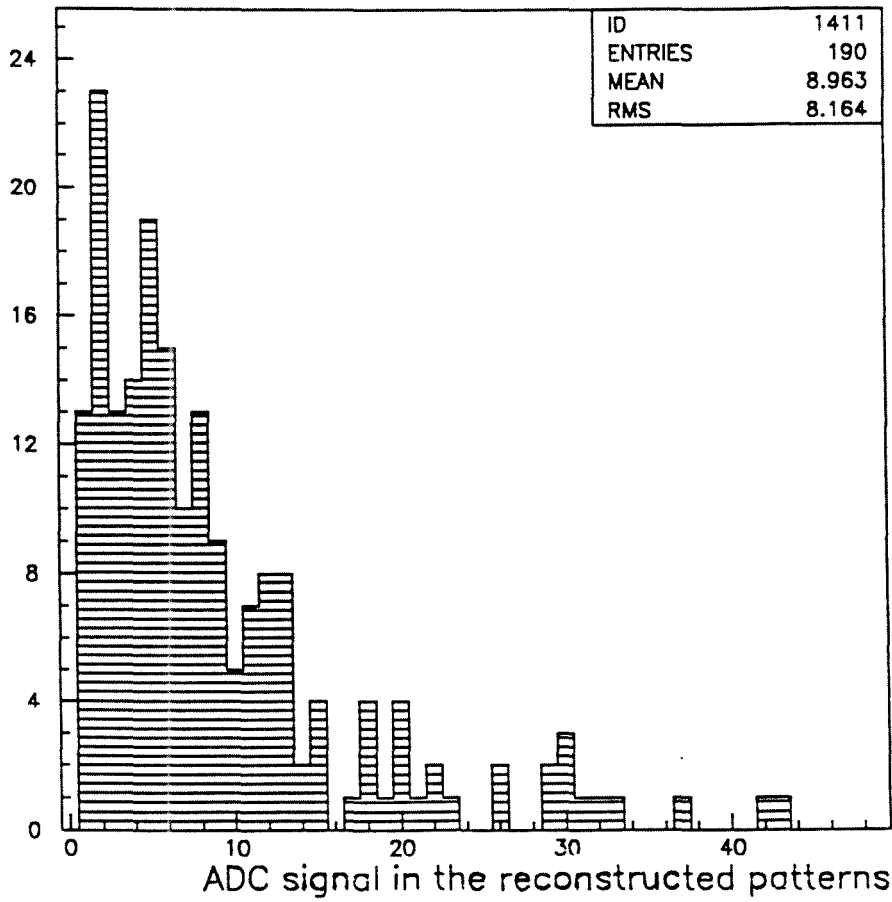


Figure 5: ADC distribution of the observed cosmics in the HCAL.

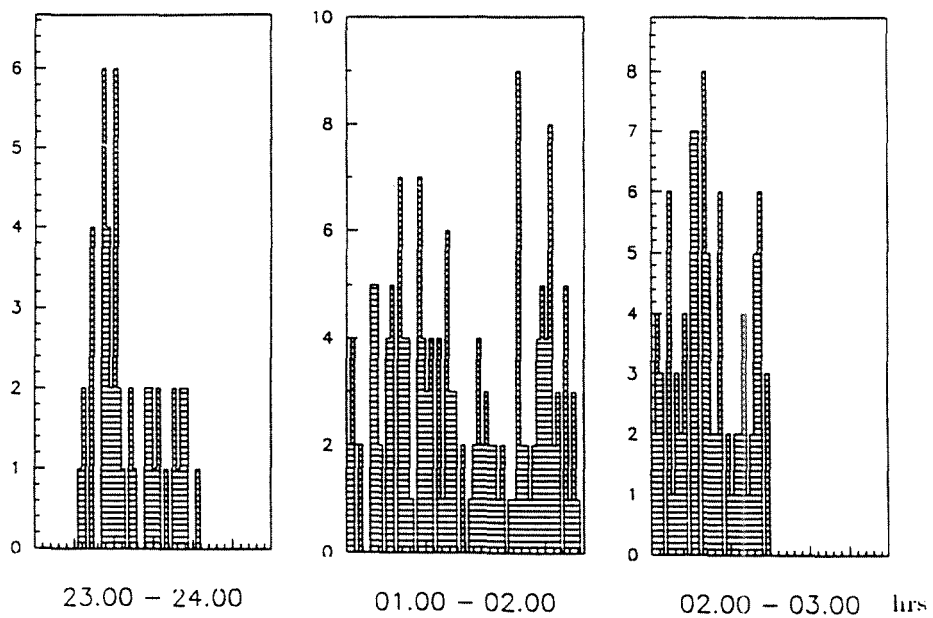


Figure 6: Chronological distribution of the cosmic candidates.

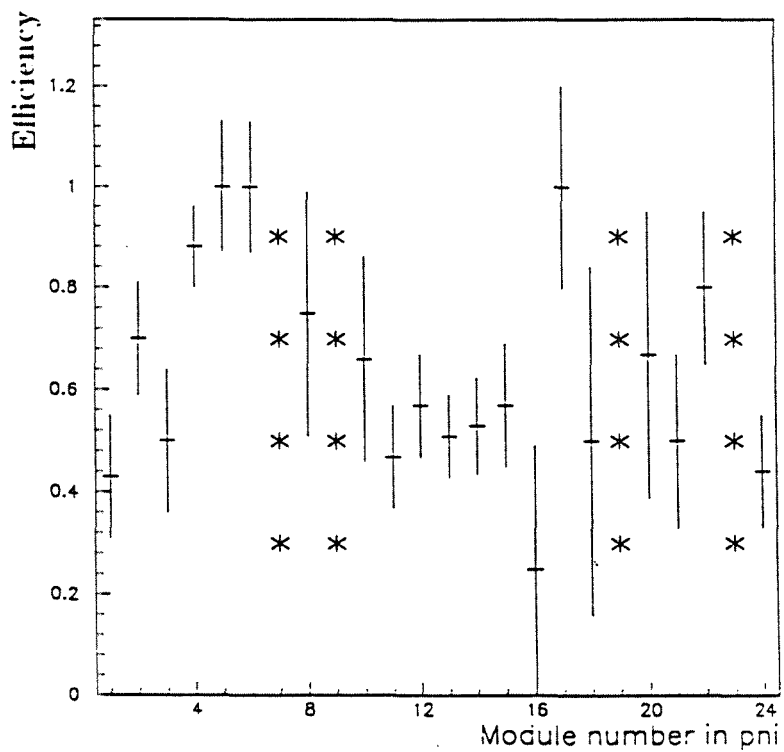


Figure 7: Efficiency as a function of sector index. Both hemispheres in z summed up. The stars refer to the modules with too low statistics.

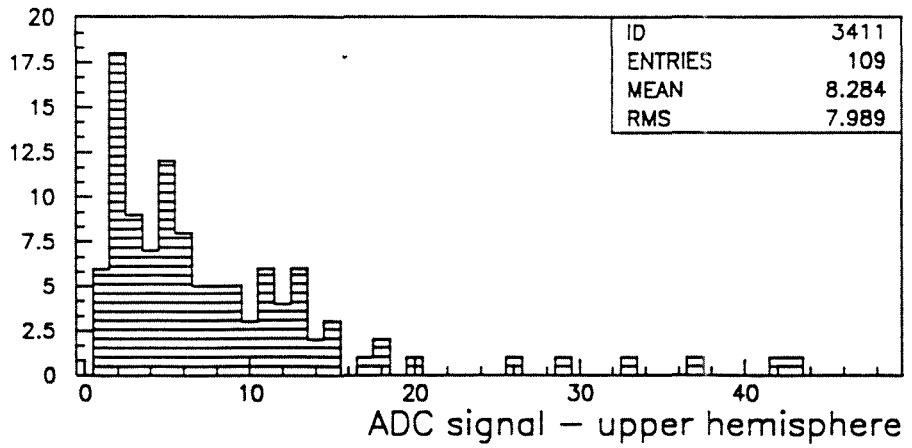


Figure 8: ADC distribution of the seen cosmics in the upper hemisphere of the HCAL.

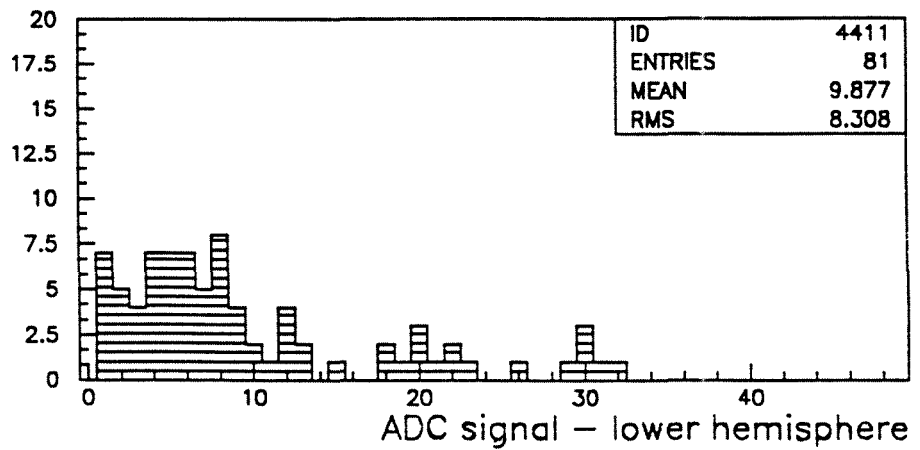


Figure 9: ADC distribution of the observed cosmics in the lower hemisphere of the HCAL.

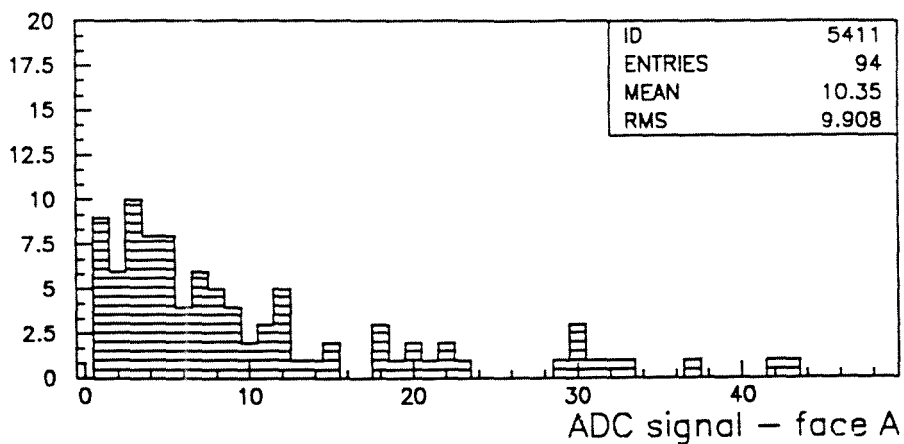


Figure 10: ADC distribution of the observed cosmics in the backward z hemisphere of the HCAL.

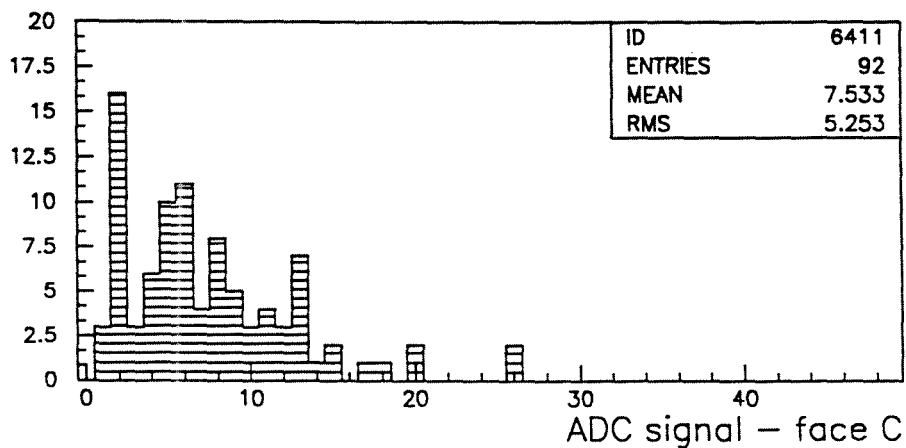


Figure 11: ADC distribution of the observed cosmics in the forward z hemisphere of the HCAL.

